nagra.

ARBEITSBERICHT NAB 22-47

Reference porewaters for SGT Stage 3 of the Opalinus Clay for the siting regions Jura Ost (JO), Nördlich Lägern (NL) and Zürich Nordost (ZNO)

March 2023

U. Mäder, P. Wersin

Nagra | National Cooperative for the Disposal of Radioactive Waste
Hardstrasse 73 | 5430 Wettingen | Switzerland
+41 56 437 11 11 | info@nagra.ch | nagra.ch

nagra.

ARBEITSBERICHT NAB 22-47

Reference porewaters for SGT Stage 3 of the Opalinus Clay for the siting regions Jura Ost (JO), Nördlich Lägern (NL) and Zürich Nordost (ZNO)

March 2023

U. Mäder[1] & P. Wersin[2]

[1] Rock-Water Consulting, Boll, Switzerland

[2] Rock-Water Interaction, Geological Sciences, University of Bern, Switzerland

KEYWORDS
Porewater, porewater chemistry, Opalinus Clay, porewater model

Nagra | National Cooperative for the Disposal of Radioactive Waste
Hardstrasse 73 | 5430 Wettingen | Switzerland
+41 56 437 11 11 | info@nagra.ch | nagra.ch

Nagra Arbeitsberichte ("Working Reports") present the results of work in progress that have not necessarily been subject to a comprehensive review. They are intended to provide rapid dissemination of current information.
This report was prepared on behalf of Nagra. The viewpoints presented and conclusions reached are those of the author(s) and do not necessarily represent those of Nagra.

April 2023: Corrigendum
Correction of the titles of Fig. 4-5 and Tab. 5-6.

Abstract

The scope of this report is to define a reference porewater composition for the host rock Opalinus Clay in the three siting regions Jura Ost (JO), Nördlich Lägern (NL) and ZNO (Zürich Nordost) as a constraint for deriving bentonite porewater compositions, sorption coefficients and solubility limits for radionuclides used in performance assessment calculations. This work is performed in the context of the Sectoral Plan, Stage 3 (SGT Etappe 3), that provides an in-depth evaluation of the three regions remaining from the pre-selection process of Stage 2.

A single composition for a reference porewater for the Opalinus Clay is defined for the siting region Zürich Nordost (ZNO) and Nördlich-Lägern (NL), abbreviated ZNO-NL. A reference porewater of lower salinity is defined for Opalinus Clay of the region Jura Ost (JO). These reference porewaters are based on data derived from the recent deep drilling boreholes Trüllikon-1-1 (TRU1-1, 2019/2020), Marthalen-1-1 (MAR1-1, 2020), Bülach-1-1 (BUL1-1, 2019), Stadel-3-1 (STA3-1, 2021), Stadel-2-1 (STA2-1, 2021), Bachs-1-1 (BAC1-1, 2022), Bözberg-1-1 (BOZ1-1, 2020) and Bözberg-2-1 (BOZ2-1, 2021) as well as from the geoscientific boreholes drilled in Benken (1998/1999) and Schlattingen (Schlattingen-1, 2011), and some few older boreholes (only partial information), all penetrating the Mesozoic strata and ending in Permo-Carboniferous sediments or basement rocks. The regions are therefore well constrained in terms of expected salinities and salinity gradients.

The borehole geochemical depth profiles for ZNO-NL share a similar stratigraphy of the clay-rich confining units, a salinity maximum at the top of Opalinus Clay and/or at the base of the overlaying clayey strata, and a small decrease towards the base of Opalinus Clay (in boreholes BUL1-1, STA3-1 and BAC1-1 no or only minor impact of a Keuper aquifer). Common is also the presence of a bounding aquifer in the Malm, but an aquifer of low salinity in the Keuper is only consistently present in the ZNO region. A Keuper aquifer is lacking at BUL1-1 and STA3-1 and is bearing similar or only moderately reduced salinities at STA2-1 and BAC1-1 in the NL region, where steeply decreasing chloride concentrations in the Staffelegg Formation are lacking. Chloride concentrations in the Opalinus Clay for ZNO are similar at the TRU1-1 and MAR1-1 locations, and somewhat lower at the Benken location, with an overall range of approximately 6'500 – 10'000◦mg/L for the most saline parts. Chloride concentrations for NL are highest at BUL1-1 (11'500 – 14'000◦mg/L, depending on the method), but cover a range of 6'000 – 10'700 mg/L for STA3-1, STA2-1 and BAC1-1. There is a distinct and systematic difference between chlorinities obtained by porewater squeezing and advective displacement, the latter being more saline by approximately 10 – 25%. These two independent methods sample directly porewater aliquots from core samples and form one of the pillars for defining the reference porewater compositions.

The borehole geochemical depth profiles for JO feature distinctly less saline porewaters compared to ZNO-NL. BOZ1-1 located in the southern part of JO has chloride concentrations near 3'000◦mg/L in the Opalinus Clay and upwards (no aquifer sampled), and it is decreasing to 1'000◦mg/L at the position of the Keuper aquifer (visible as a modest dip in water stable isotope composition, but too low hydraulic conductivity for sampling). The profile at BOZ2-1 in the northern part is bound by distinct aquifers in the Hauptrogenstein and the Keuper, with maximum chloride concentrations approaching 2'000◦mg/L at the top of the Opalinus Clay and decreasing towards the bounding aquifers. The systematic difference between chlorinities from squeezing and advective displacement (the latter being more saline) is present but distinctly smaller compared to data form the ZNO-NL regions.

The geochemical model for the reference porewaters is very similar to a previous model (SGT Etappe 2) with fixed chloride and sulphate concentrations, a prescribed partial pressure of CO_2, a measured exchanger composition (as initial estimate) and multiple mineral saturation constraints.

An average chloride concentration of 8'500 mg/L is adopted for the reference porewater (Tab. 5-5) for the ZNO-NL regions, and a sulphate concentration of 2'250 mg/L constrained by advective displacement experiments and squeezing experiments. A partial pressure of CO_2 of $10^{-2.2}$ bar is imposed as expert judgement on multiple lines of evidence, and the obtained model pH is 7.1. The reference porewater for JO is derived in an analogous fashion but it is distinctly less saline and more sulphatic relative to chloride, with an imposed chloride concentration of 3'000 mg/L, and a sulphate concentration of 2'600 mg/L (Tab. 5-6). A partial pressure of CO_2 of $10^{-2.2}$ bar is imposed as expert judgment, and the obtained model pH is 7.3.

Redox condition and some minor and trace components (F, Si, Al, Fe, Ba, Mn) are constrained by mineral saturation of stoichiometric end-member phases (fluorite, quartz, kaolinite, pyrite, siderite, barite, rhodochrosite). While calcite, dolomite, pyrite, quartz, kaolinite (and possibly fluorite) are ubiquitously present and reasonable choices as equilibrium phases, siderite, barite, and rhodochrosite are proxies, and are observed as solid-solutions rather than end-member phases. The concentrations of Fe, Ba and Mn may therefore be overestimated in this model and are likely just an upper limit for concentrations. Celestite is used in the model as a solubility constraint for Sr concentration, but it is not inferred to be necessarily present as a controlling phase. It is not ubiquitously present in Opalinus Clay (confirmed as traces in some samples, searched for but not found in many others), but it is at/very near saturation or slight supersaturated in squeezing and advective displacement aliquots.

The calculated redox potentials (ZNO-NL: −2.76 pε [−163 mV Eh_{SHE}] at pH = 7.07; JO: −3.06 pε [−181 mV Eh_{SHE}] at pH = 7.34) are based on the given sulphate activity and mutual pyrite – siderite equilibrium. Because of the siderite equilibrium, this is also tied to the carbonate system (calcite – dolomite – alkalinity – P_{CO2} – pH). The redox potential is therefore shifting with pH and is not an independent quantity.

Uncertainties related to the partial pressure of CO_2, mainly based on previous work, are such that a variation of a log-unit from $10^{-1.8}$ bar to $10^{-2.8}$ bar result in a pH range from 6.9 to 7.4 (for ZNO-NL), and correlated shifts in alkalinity (Tab. 5-5, Tab. 5-6), with other components undergoing little change. This uncertainty, including the correlated parameters, is addressed for ZNO-NL and JO with two porewater variants calculated with a P_{CO2} of −1.8 and −2.8 log-bar units. Apart from well-constrained chloride concentrations, it is not possible to provide exact bounds on uncertainties of other components because the uncertainty range of the underpinning measurements is not accurately known (complex laboratory procedures and known/suspected experimental artefacts). A substantial uncertainty related to sulphate concentration arises from seemingly contradictory constraints (measurements of aqueous extracts vs. advective displacement and squeezing), and this is addressed with a more sulphate-rich porewater variant (with approximately twice the sulphate concentration), and accordingly lower concentrations of Ca, Mg and Sr in order not to be supersaturated with respect to gypsum/anhydrite and/or celestite.

The reference porewaters were requested for a temperature of 25 °C for subsequent radionuclide solubility and speciation calculations. The use of the latest version of the PSI Chemical Thermodynamic Database 2020 (Hummel & Thoenen 2023) was a pre-requisite, but comparative calculations to commonly used older versions and the PHREEQC database are also performed and show only small differences for most components. The potential effects of temperature on the porewater composition are addressed in a separate section. Similarly, an alternative modelling approach using a combination of selected hydrous silicates as equilibrium phases in lieu of a prescribed partial pressure of CO_2 is also presented.

Table of Contents

List of Tables

List of Figures

List of Acronyms

AD	Advective displacement experiment or method
AqEx	Aqueous extracts
BRGM	French Geological Survey (Bureau de Recherches Géologiques et Minières)
Cc	Calcite
CEA	Atomic Energy Commission
CIEMAT	Centre for Energy, Environmental and Technological Research (Centro de Investigaciones Energéticas, Medioambientales y Tecnológicas) in Spain
COx	Callovo-Oxfordian argillite
DI	Through-diffusion experiment or method
Do	Dolomite
GW	Groundwater
HAA	High-level radioactive waste
JO	Jura Ost region
LLNL	Lawrence Livermore National Laboratory
OPA	Opalinus Clay
NAB	Nagra Work Report (Nagra Arbeitsbericht)
NL	Nördlich Lägern region
NTB	Nagra Technical Report
PSI	Paul Scherrer Institut
PW	Porewater
SGT	Sectoral Plan for Deep Geological Repositories
SMA	Low/intermediate-level radioactive waste
SQ	Squeezing experiment or method
TBO	Deep drilling project, deep borehole, 'Tiefbohrung'
TDB	Thermodynamic database
UniBE	University of Bern
ZNO	Zürich Nordost region

1 Scope of this report

The scope of this report is to define – to the best of our current knowledge and scientific understanding – a reference porewater composition for the host-rock Opalinus Clay Formation in the three siting regions ZNO (Zürich Nordost), Nördlich Lägern (NL) and Jura Ost (JO) (Fig. 1-1) as a constraint for deriving bentonite porewater compositions, sorption coefficients and solubility limits for radionuclides used in performance assessment calculations. This work is performed in the context of the Sectoral Plan, Stage 3 (SGT Etappe 3), that provides an in-depth evaluation of the three regions remaining from the pre-selection process of Stage 2.

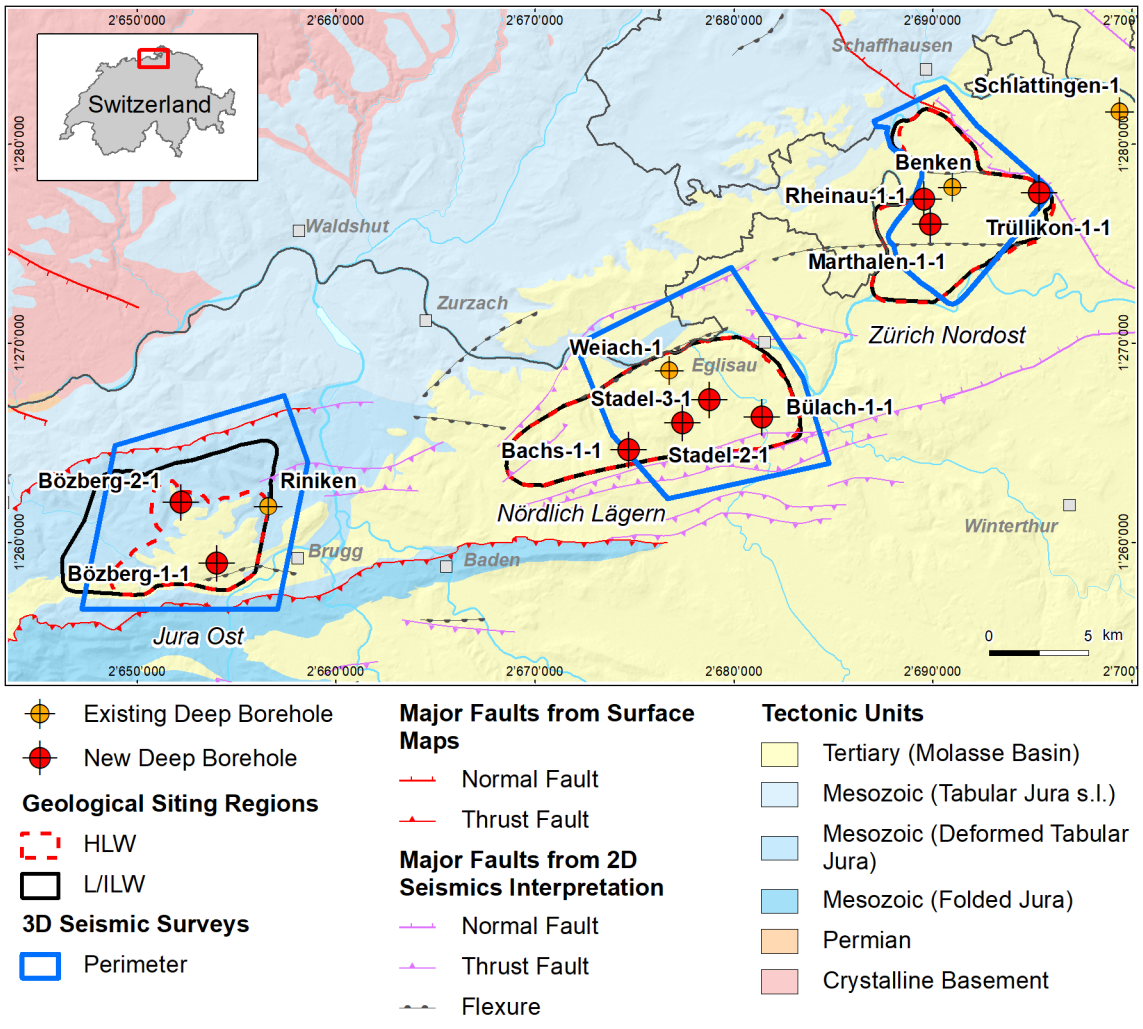

Fig. 1-1: Overview map of the three siting regions with the locations of nine new boreholes and some older boreholes

Field data and experimental data considered – apart from previous work – derive from the completed nine TBO boreholes (eight boreholes were analysed for porewater hydrochemistry) and some relevant older deep boreholes within or very near the three siting regions. The outcomes are thermodynamically modelled porewater compositions that represent a region for Opalinus Clay within observed ranges, including all relevant parameters for the intended purpose. Main compositional uncertainties are addressed by means of some porewater variants that are also fully

modelled. The models, the constraining data, any expert decisions, the data selection process, and few data inconsistencies are discussed in detail. The porewaters are modelled at a reference temperature of 25 °C and 1 bar as stipulated by performance assessment. There is a chapter included that addresses potential temperature effects and some alternative approaches selecting solubility-limiting constraining phases.

A reference porewater for a siting region – as chosen in this report – is not a complete model of the aqueous electrolyte phase contained in the claystone. It focuses on that part of the claystone porosity that contains an electrolyte solution not affected by charged surfaces of clay minerals (so-called 'free porewater'). It is argued that this part of the pore solution is adequate to define activities of the aqueous species that are then used for solubility and sorption calculations for radionuclides. The other part of the pore space contains an electrolyte solution affected by negatively-charged clay mineral surfaces with different species concentrations, but with the same species activities as dictated by the assumption of thermodynamic equilibrium (equal chemical potentials).

A relatively extensive two-year discussion period with representatives from Nagra, PSI and the University of Bern defined the relevant parameters, discussed the approach and constraining data, and tried to satisfy different requirements for the timing of interim results. This had led to some preliminary versions for reference porewaters for Opalinus Clay that were used as input to derive the bentonite porewater compositions after re-saturation (Curti et al. *in prep.*). The compositions are not exactly but nearly the same as the final compositions represented here. During this process, more and more data became available from sample analyses of the progressing deep boreholes, and this led to a somewhat iterative process arriving at the final results presented here. The constraining data from the nine TBO boreholes are largely complete, although not yet fully reported, and there is no indication of emerging data that may invalidate some of the data summaries or comparisons represented here.

2 Introduction

The Opalinus Clay Formation (Opalinuston) was proposed by Nagra (2008) as a potential host rock for high-level (HAA) and low/intermediate-level radioactive waste (SMA) in five siting regions. Nagra (2014) proposed a reduced number of three siting regions to be further investigated. Starting in 2018, Nagra had drilled nine deep boreholes (Tiefbohrungen, TBO) in Northern Switzerland to provide input for site selection and the safety case. The aim of the drilling campaign is to characterise the deep underground of the three remaining siting regions located towards the shallow parts of the Northern Alpine Molasse Basin, including Jura Ost (JO), Nördlich Lägern (NL) and Zürich Nordost (ZNO) (Fig. 1-1).

One important reason for having to know – by measurement or interpretation – the porewater composition of a geological formation is to be able to derive its radionuclide-specific sorption / retardation properties and solubility limits. In general, the sorption properties depend on geochemical parameters, most importantly mineralogy (sorption capacity), pH, ionic strength, redox state, and the speciation of the main dissolved constituents (potential ligands for radionuclides) of the porewater (Bradbury et al. 2008).

Because direct sampling of porewater in sedimentary formations of very low permeability is not feasible or subject to artefacts, the process of deriving a porewater composition requires the integration of analytical data from diverse methods, and a geochemical model to integrate all constraints that are thought to be relevant for controlling the porewater composition. A prime example of such an approach is that developed for Opalinus Clay at the Mont Terri rock laboratory (Pearson et al. 2003).

The efforts (tens of person-years) undertaken for the case of Opalinus Clay comprised numerous laboratories and in situ experiments as well as geochemical modelling and synthesis work. The result was a robust and defendable geochemical model for the porewater composition and its controls via mineral-water interaction and ion-exchange processes. Despite this effort, a number of open issues – or lack of accurate constraints on some parameters – are still persisting and are the subject of on-going research, most recently summarised by Wersin et al. (2020, 2022b).

A preliminary reference porewater composition for the Opalinus Clay and «Brauner Dogger» was defined by Mäder (2009) during an early stage of the Sectoral Plan, based on data available at that time and on earlier reference porewaters (e.g., Pearson 2002), mainly derived from data of the Benken borehole and the Mont Terri rock laboratory. It was more generic in its adaptation and served for all siting regions with Opalinus Clay and «Brauner Dogger» examined at that time. It is not surprising that this preliminary reference porewater resembles the current version in composition and approach. It is, however, with 5'800◦mg/L chloride distinctly less saline than the current version for ZNO and NL, with a chlorinity of 8'500◦mg/L, but more saline compared to the JO region (about 3'000◦mg/L). A high-salinity variant was defined by Mäder (2009) with 22'800◦mg/L chloride for covering uncertainties based on highest chlorinities measured at Mont Russlin, located next to Mont Terri. It is now known that such high salinities are not present in the remaining three siting regions ZNO, NL and JO, with highest chloride concentrations encountered in BUL1-1 of about 11'000 – 14'000◦mg/L in the Opalinus Clay (Mazurek et al. 2021).

Throughout this report we use the term porewater for the variably saline water contained in the porosity of a low-permeability rock, implying that it refers to an undisturbed state. Extraction of porewaters from core samples by means of squeezing or advective displacement yields strictly speaking not porewater samples of the undisturbed state but squeezing aliquots and aliquots from advective displacement. It is possible to deduce information on the state and composition of the in situ porewater from such aliquots considering also artefacts that arise from drilling, unloading, sample conditioning, sample storage, sample preparation, and the methods themselves for different types of analyses.

3 Approach

A simplified porosity concept is adopted for this approach, similar or identical to most previous approaches: the total porewater-filled and connected pore space is subdivided into a sub-volume affected by negatively-charged clay mineral surfaces or interlayers (illite, illite/smectite mixed-layers), and a sub-volume of porewater not affected by electrostatic forces, named 'free porosity' (e.g., Pearson et al. 2003). The porosity affected by electrostatics is given different names in literature and includes diffuse-layer and interlayer volumes (electrolyte associated with clay mineral outer and inner surfaces). These latter volumes contain an excess of cations near the charged surfaces to balance the negative surface charge and are depleted of anions (and associated balancing cations), termed the anion-exclusion effect or ion-exclusion effect. The exclusion is not complete, but governed by the Poisson-Boltzmann relationship at a macroscopic scale, that describes the distribution of ions in the presence of an electrostatic potential, with dependent variables being the electrostatic potential (as a function of the distance from the charged surface and the surface charge density), the ionic strength of the electrolyte, the ionic charge of the ion and its activity coefficient (e.g., Tournassat & Steefel 2019a, b, Appelo et al. 2009). The purely electrostatic treatment may be additionally combined with surface complexation theory to include chemical forces, e.g. by including double-layer or triple-layer features next to the charged surfaces (e.g., Appelo & Wersin 2007). Considering an average electrostatic potential for a sub-volume of pore space leads to the Donnan approximation of the Poisson-Boltzmann relationship, and resembles the simplified concept adopted here, except that the Donnan relationship does not completely exclude anions from the porosity affected by negatively charged surfaces (e.g., Tournassat & Steefel 2019b). This leads to a slight overestimation of the chloride concentrations in the 'free porosity' in our simplified model, to a lesser extent at higher ionic strength where the 'free porosity' fraction is larger, and more so at low ionic strength where the extent of diffuse layers is larger and the 'free porosity' fraction smaller.

This report is only concerned with the 'free porosity' that contains a charge-balanced electrolyte solution (porewater). We use 'free porosity' interchangeably with chloride-accessible porosity when discussing the chloride concentration data. It is a static view, considering a sub-volume of the total pore space but that allows activities of aqueous species, including dissolved gases, to be calculated with accepted geochemical models. The two types of porosities are related by the equilibrium condition stipulating equal chemical potentials for all species in the two sub-volumes, and thus also the composition of the electrostatically affected portion of pore space can be calculated given appropriate thermodynamic and electrostatic models. The main simplifications include therefore that anion-exclusion is treated as complete (e.g., all chloride is contained in the 'free porosity'), and that different types of charged surfaces and its associated pore volumes (outer clay surfaces, interlayer surfaces, edge sites, etc.) are all lumped into a single pore volume, the difference between the total porosity and the 'free porosity'. The total porosity for all rocks treated in this report is set equal to the water-loss porosity derived from the gravimetric water-content measured by drying at 105°°C, a quantity established for virtually all samples examined in the framework of the TBO programme. It is known that this water-loss porosity is very close to the true total water content of a fully saturated sample, and therefore almost all pore space is connected and involved in diffusive transport. The proportion of 'free porosity' is obtained from squeezing and advective displacement experiments as detailed in Sections 4.1.3 (ZNO-NL) and 4.2.3 (JO).

A generic approach to constraining a porewater composition in the 'free porosity' of a low-permeability formation is to fix as many compositional parameters as possible by direct or indirect measurements, and provide substantiated constraints exerted by inferred mineral equilibria and ion exchange equilibria for all remaining parameters. The result is a geochemical model that is consistent with the principles of equilibrium thermodynamics and that fixes the porewater

composition at a particular location or limited region and limited depth range in a formation. The model also explains the relevant mineralogical controls on the porewater composition. By the same token, such a model will also predict, in principle, how the porewater composition is expected to react to external geochemical disturbances or on-going slow diffusion processes, provided transport parameters and relevant reaction rates are implemented. Also required for modelling of mass transfers is the consideration of the electrostatically affected porosity and its ion inventory as outlined above. It should be noted that the term thermodynamic equilibrium refers to the equilibrium between the aqueous electrolyte solution and the selected mineral phases and ion-exchanger, and not to a global minimum in Gibbs free energy of the entire composition of the system (including solid phases).

Such thermodynamic models for porewater composition are established, well constrained and tested for the case of Opalinus Clay (Wersin et al. 2020, Pearson et al. 2003). This is not the case for adjacent units such as the overlying «Brauner Dogger» and the underlying Staffelegg Formation that are part of the clay-rich confining units. For the former unit, the same porewater composition was suggested in previous work (Mäder 2009) based on similarity in mineralogy and hydraulic properties, stratigraphic continuity, and continuity in formation-scale porewater diffusion profiles (chloride, stable isotopes). The geothermal well at Schlattingen and the new TBO programme provided abundant new data that permit a more detailed assessment of porewater composition across the clay-rich sequence of the different siting regions, although in this report the focus is solely on the host-rock Opalinus Clay.

There were several different models proposed in literature (see Wersin et al. 2020 for a recent summary) and there is no consensus on what the most appropriate model might be, although all these models share essential principles but differ in some of the constraints chosen. Models are developed for specific purposes and different purposes may require different models. Differences in models relate mainly to the mineral phases that are selected to impose saturation constraints, and the presence or absence of 'expert decisions' on, for example, choosing the partial pressure of CO_2 as an independently fixed value. By including silicate phases (micas, clay minerals, feldspars) – in combination with carbonates – it is possible to fix the pH internally by mineral equilibria, and thus also the partial pressure of CO_2 (Pearson et al. 2011, Wersin et al. 2020). The 'expert decision' is shifted in these models to picking a subset of silicates, the exact number and simplified compositions dictated by the phase rule that ties the number of constraining mineral equilibria to the number of components of interest in the porewater (e.g., just 2 or 3 silicates out of K-feldspar, plagioclase, muscovite, illite, illite-smectite mixed layers, kaolinite, chlorite, etc.). Introducing silicates as solubility constraints may also impact on how the iron-system is constrained, for example in case of choosing chlorite that is invariably Fe-bearing (Fe^{II} and Fe^{III}), or in case of considering also mixed Fe^{II}/Fe^{III} oxy-hydroxides. The choice of constraining phases is also limited by the availability of thermodynamic data that is commonly only available for end-members of solid solutions, or are based on calorimetric measurements on mineral separates that are inherently associated with substantial uncertainties. There are no measured thermodynamic data available for illite, illite-smectite mixed layers or chlorite from Opalinus Clay.

There is no doubt that silicates do play a geochemical role in porewater composition, particularly during diagenesis, burial of sedimentary basins, the long-term evolution and in buffering slow compositional disturbances, but also some short-term chemically severe impacts such as exposure to hyperalkaline conditions (cement – clay interaction). The long-term evolution (past and future) in particular remains partially obscured by the fact that the natural rock environment obviously represents a disequilibrium state with respect to several minerals present to which the porewater has been exposed to for thousands or hundreds of thousands of years. There is therefore no unique or universally accepted choice of silicates that are supposed to control the porewater composition, in addition to carbonates, any sulphates, or also some sulphides (e.g., pyrite) that are known to be more reactive compared to silicates.

The composition of the clay exchanger can be measured (large data set obtained from the new deep boreholes) and used as a constraint to define a porewater, provided that exchange coefficients are known well-enough that relate the exchanger composition to the porewater composition. There is no agreement in literature on what the exact values of these exchange coefficients should be, and therefore the measured ion-exchanger is used here as a 'soft' constraint to initialise the cation ratios in the porewater that are later adjusted to the imposed mineral saturation constraints.

Due to similar salinities encountered in the ZNO and NL regions, a decision was made to define a common reference porewater composition for these two regions, named ZNO-NL. This is not to say that these two regions necessarily share an identical geochemical evolution for the porewater composition, but simply that the parameters most relevant for use in safety analysis are sufficiently similar in these two regions. This will simplify subsequent work to derive solubility limits and sorption parameters for relevant radionuclide species. A decision was also made to use an averaged salinity (chloride and sulphate concentrations) that represent a region despite the presence of regional gradients (commonly more dilute towards the North / shallower depths), or local depth gradients within the Opalinus Clay (these are rather small). This simplification is justified by recognising that moderate differences in salinity are not leading to significant differences in safety analysis (a few components, like Hg, Ag, Pd that do form chloride complexes may be more sensitive to salinity changes). The distinctly less saline porewaters encountered in the JO region, along with distinctly higher SO_4/Cl ratios compared to ZNO-NL led to a decision to define a specific reference porewater for the JO region, again aiming at an average salinity, despite the presence of moderate regional differences and gradients.

4 Constraining data for the three siting regions

A detailed summary of constraining data is provided in this section, derived mainly from new data obtained from TBO drillcore samples, but also from data of some of the older boreholes. As explained in the previous section, a common reference porewater composition is defined for ZNO and NL, and we denote this with ZNO-NL. The data presentation for ZNO and NL is also amalgamated such that data comparisons are more readily evident. Data included in this summary are:

- Composition of aliquots from squeezing and advective displacement experiments
- Composition of the clay exchanger determined by selective extractions
- Composition from aqueous extracts, and associated water contents, from which the vertical borehole profiles are obtained for conservative components (chloride), providing context for the Opalinus Clay
- Chloride-accessible porosities derived from advective displacement experiments, from squeezing experiments and from through-diffusion experiments (performed at PSI)
- Stable water isotope profiles (only δ^2H shown) further illustrate the context of the data for Opalinus Clay

The above data and its regional and vertical distribution form the justification for the selected reference porewater composition, along with constraints from modelling, as detailed in Chapter 5. There is no attempt made to discuss porewater evolution – the present-day state is used to derive the reference porewater compositions. The observed vertical and lateral composition gradients give some indirect indication about the past dynamics of the system in its geological and hydrological context.

Of the nine new boreholes located within the three siting regions (Fig. 1-1), eight were analysed geochemically and yielded data included in this report. Borehole Rheinau-1-1 located in the ZNO region served other purposes, but a water stable isotope profile was established. Older boreholes are also indicated, and the Schlattingen-1 geothermal well is located towards the NE of the ZNO region.

4.1 ZNO and NL regions (Zürich Nordost, Nördlich Lägern)

The **Zürich Nordost (ZNO) siting region** (Fig. 4-1) belongs tectonically to the autochthonous eastern Tabular Jura. The major tectonic structures in the area are the NW-SE trending Neuhausen Fault to the north-east of the region and the Rafz – Marthalen Flexure. The Neuhausen Fault zone runs parallel to the Bonndorf – Hegau – Bodensee Graben that is known to cut the entire Mesozoic sedimentary stack. The Rafz – Marthalen Flexure is an E-W striking structure in the southern part of the region that is possibly associated with the northern margin of a large Permo-Carboniferous trough.

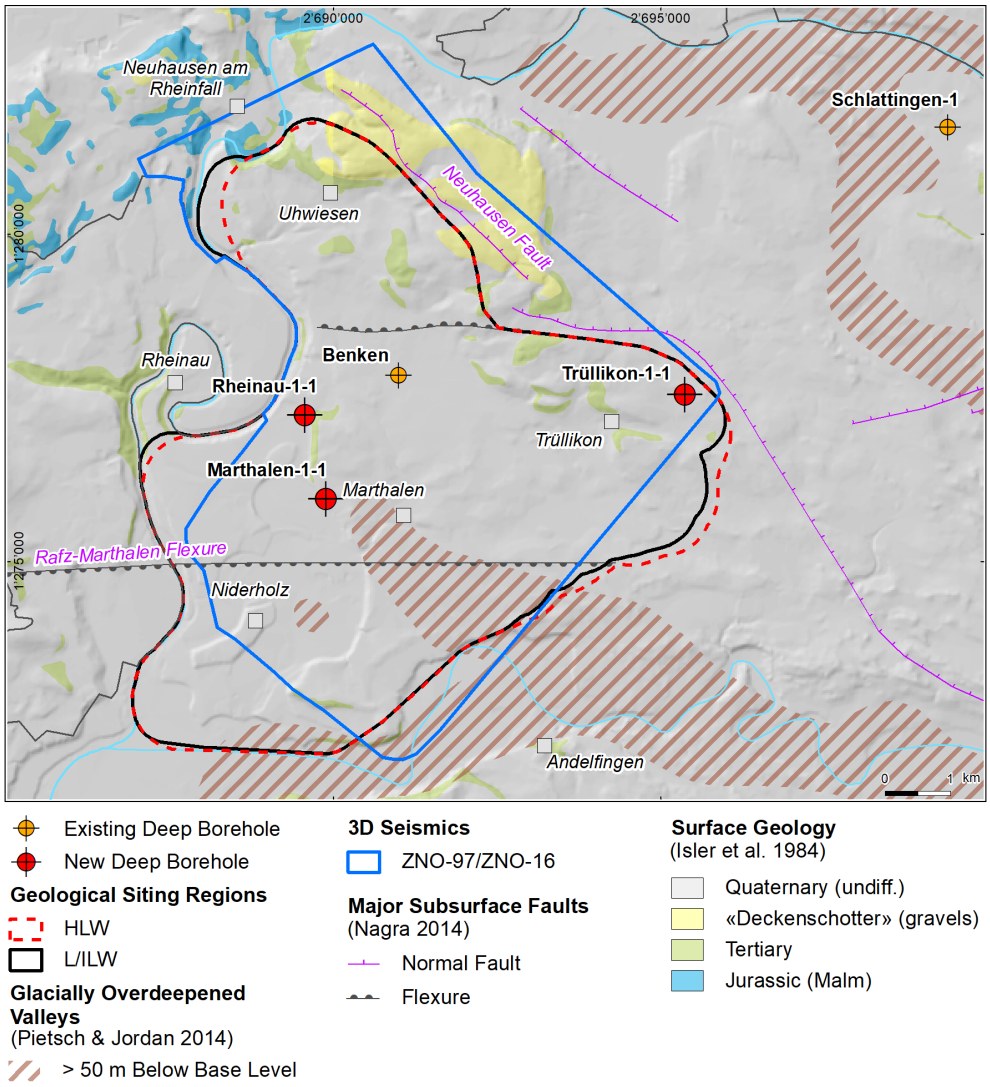

Fig. 4-1: Overview map of the Zürich Nordost (ZNO) siting region

Locations of boreholes are marked near Benken, Marthalen, Trüllikon, Rheinau and Schlattingen further to the NE.

The Trüllikon-1-1 (TRU1-1, 2019) and Marthalen-1-1 (MAR1-1, 2020) boreholes are the second and third boreholes drilled within the framework of the TBO project. Rheinau-1-1 (RHE1-1, 2021) is a special-purpose borehole, with geochemical investigations restricted to a water stable isotope profile, and hydraulic tests limited to the clay-rich tight units. Benken is an earlier exploratory deep borehole drilled in 1998/1999, with a comprehensive but less advanced analytical programme concerning porewater chemistry, compared to the current state-of-the-art. The geothermal well Schlattingen-1 was drilled in 2011 to a depth of 1'508 m, including a sampling and analysis programme that covered the clay-rich confining units from the Effinger Schichten to the Lias underlying the Opalinus Clay. Analytical techniques used for the Schlattingen-1 borehole were comparable to those of the recent TBO boreholes, but the analytical work was done at a lower sampling density.

The four boreholes within the ZNO perimeter reveal a similar lithostratigraphy for the Mesozoic strata, and the clay-rich confining units «Brauner Dogger» to Lias) in particular. The borehole depths are 1'007°m for Benken, 828°m for RHE1-1 (a deflected borehole), 1'099°m for MAR1-1, and 1'310°m for TRU1-1. Permian strata are encountered from 1'038 – 1'094°m in the MAR1-1 borehole (underlain by crystalline basement) and from 1'246 – 1'260°m in the Trüllikon borehole (underlain by crystalline basement), but are not present in the Benken borehole that is located to the North of a WSW-ENE trending large Permo-Carboniferous trough to the South (encountered in earlier exploratory boreholes Riniken and Weiach further to the WSW, in the Schlattingen-1 geothermal well to the ENE, and in four new TBO boreholes, BUL1-1, STA3-1, STA2-1 and BAC1-1 of the NL region to the WSW). The distribution of anhydrite-rich rocks in the Muschelkalk (Zeglingen Formation) and Gipskeuper is also similar in the boreholes, with a main difference being the occurrence of rock salt (Zeglingen Formation, «Salzlager») restricted to the Benken borehole (about 13°m of thickness). The Staffelegg Formation (Lias), underlying the Opalinus Clay, is of a uniform thickness of 40 – 44°m. The Opalinus Clay is intersected at a uniform thickness of 113 – 115°m, and the Formation's depth is shallowest at Benken (539 – 652°m), slightly deeper at Marthalen (590 – 705°m) and deepest at Trüllikon (816 – 928°m). The Dogger above the Opalinus Clay is thickest at Benken (108°m), 84°m at Marthalen and 91°m at Trüllikon. The Malm strata are 230 – 252°m thick in the ZNO region. The region is overlain by 30 – 60°m of Quaternary strata, and 130 – 450°m of Molasse rocks: least at Benken (68 – 199°m depth), slightly thicker at Marthalen (48 – 254°m depth), most extensive at TRU1-1 (24 – 474°m depth). The lithostratigraphic profile from Rheinau is not integrated here as it is a deflected borehole, but the section that was detailed included Opalinus Clay to the Bänkerjoch Formation, and it is identical to the other boreholes.

Further to the NE, across the Neuhausen Fault, at the geothermal well of Schlattingen-1, the Molasse ranges from 53 – 491°m depth, the Malm from 491 – 758°m, and the Opalinus Clay is slightly thicker compared to ZNO, intersected at 831 – 950°m depth, underlain by 53°m of Staffelegg Formation (Lias). The anhydrite-rich rocks of the Muschelkalk contain a thin halite-bearing section (about 5°m of «Salzlager»). Permian strata are encountered from 1'261 – 1'339°m, and the borehole ends at 1'508°m in crystalline basement rocks.

Complete geochemical data are contained in the topical Dossier reports for the TBO boreholes, Aschwanden et al. (2021) for Trüllikon, Mäder et al. (2021) for Marthalen, in a comprehensive report for Benken (Nagra 2001) and a detailed geochemical report by Waber et al. (2003), and in a dedicated report on porewater characterisation for the Schlattingen-1 geothermal well (Wersin et al. 2013). The water stable isotope profile for Rheinau is reported in (Iannotta et al. *in prep.*). Some subsidiary reports are cited where necessary.

The **Nördlich Lägern (NL) siting region** (Fig. 4-2) lies in the Deformed Eastern Tabular Jura between the autochtonous Tabular Jura in the NW and the Folded Jura in the SW. The siting area is delineated by some major tectonic structures, the Siglistorf Anticline and the Eglisau Fault in the north and the Baden – Irchel – Herdern Lineament and the Jura Main Thrust to the south. Tectonically, the Deformed Tabular Jura is compressively overprinted by the alpine forefront.

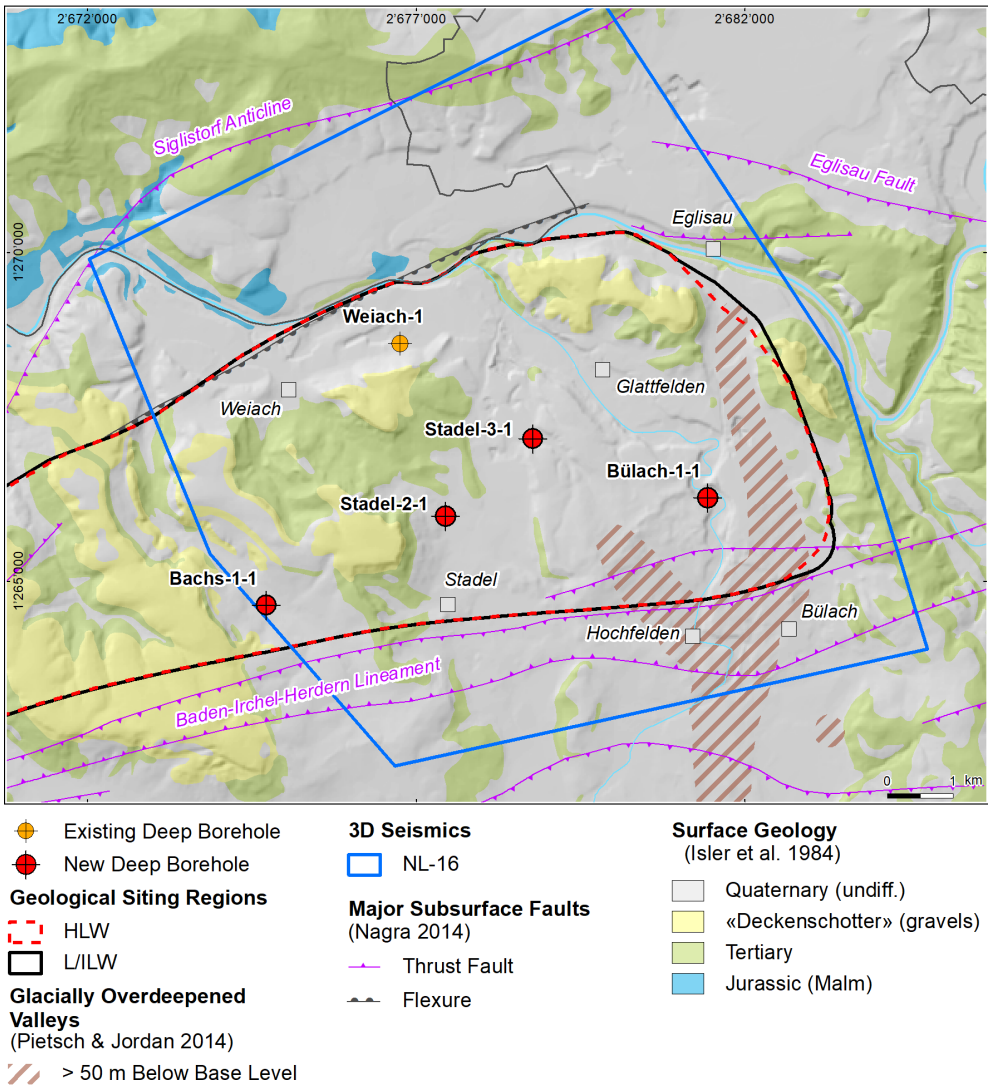

Fig. 4-2: Overview map of the Nördlich Lägern (NL) siting region

Locations of boreholes are marked near Bachs, Stadel and Bülach, and an older borehole near Weiach.

The four new boreholes within the NL perimeter reveal a similar lithostratigraphy for most of the Mesozoic strata. The borehole depths are 1'370°m for BUL1-1, 1'281°m for STA3-1, 1288°m for STA2-1, 1'306°m for BAC1-1, and 2'482°m for the older borehole Weiach-1. Permian strata (Rotliegend) are present in the Weiach borehole (992 – 2'020°m depth, including coal-bearing Carboniferous strata) in the northern part of NL underlain by basement rocks, and in all four new TBO boreholes: BUL1-1 (below 1'320°m), STA3-1 (below 1'226°m), STA2-1 (below 1'237°m) and BAC1-1 (below 1'257°m). The Permian-Carboniferous strata are part of a WSW-ENE trending large Permo-Carboniferous trough deepening towards the South, encountered in earlier exploratory boreholes Riniken and Weiach, the TBO boreholes MAR1-1 and TRU1-1 of the ZNO region, and in the Schlattingen-1 geothermal well further to the ENE. The distribution of anhydrite-rich rocks in the Muschelkalk (Zeglingen Formation) and Gipskeuper is also similar in the boreholes, with a main difference being the occurrence of rock salt (Zeglingen Formation, «Salzlager»): not present in the Weiach borehole, 15°m thick at BUL1-1, 40°m at STA3-1, 28°m at STA2-1 and 35°m at BAC1-1. The Staffelegg Formation (Lias) underlying the Opalinus Clay is of a uniform thickness at all borehole locations of NL, 35 – 38°m. The Opalinus Clay is

intersected at a uniform thickness of 104 – 111°m, and the Formation's depth is shallowest at Weiach-1 (555 – 666°m), deepest at BUL1-1 (892 – 996°m), and somewhat shallower at STA3-1 (779 – 888°m), STA2-1 (800 – 905°m) and BAC1-1 (808 – 915°m). A special feature, not intersected in the other siting regions, is a reef facies («Herrenwis Unit») some 20 – 50°m above the Oaplinus Clay in the Dogger, between the Variansmergel Formation / «Parkinsoni-Württembergica-Schichten» and the Wedelsandstein Formation. This cavernous unit is not present in the Weiach borehole in the northern part of NL, and also not in the western part at BAC1-1 but was encountered in the other three new TBO boreholes (11 – 40°m thickness). The Malm strata range in thickness from 275 – 301°m and comprise units from the Wildegg Formation to the «Felsenkalke» + «Massenkalk». The region is overlain by 14 – 37°m of Quaternary strata, and 149 – 479°m of Molasse rocks, mainly USM: least at Weiach-1 (37 – 186°m depth), and 378 – 468°m of thickness in the four new TBO boreholes, least at STA3-1 (378°m) and most at BUL1-1 (468°m).

Complete geochemical data are contained in the topical Dossier reports for the TBO boreholes, Mazurek et al. (2021) for BUL1-1, Aschwanden et al. (2021) for STA3-1, Zwahlen et al. (*in prep.*) for STA2-1, Gaucher et al. (*in prep.*) for BAC1-1 and Matter et al. (1988) for the older borehole Weiach-1.

4.1.1 Chloride and water stable isotopes in depth profiles for ZNO-NL

4.1.1.1 Chloride and water stable isotopes in depth profiles for ZNO

The porewaters in the ZNO region – at least the central part constrained by the deep boreholes – have evolved to display smooth depth profiles for the clay-rich confining units, as shown by water stable isotope profiles (Fig. 4-3) and the salinity profiles (here shown as chloride concentrations, Fig. 4-4). The chloride concentrations are obtained from aqueous extracts at a known solid-to-liquid ratio and are recalculated to the measured water content and thus represent bulk concentrations rather than those present in the free porosity (see subsequent sections for constraints on the latter quantity, Section 3 for porosity concept). The shapes of the bulk porewater profiles are comparable to those defined by the chloride concentrations in the chloride-accessible porosity ('free porosity') because the chloride-exclusion effect is not very dependent on clay-content in the clayey confining units (see scaled profiles in Section 4.1.2), with some exceptions. In the following, local minima visible in chloride concentration (Fig. 4-4) and water stable isotope profiles (Fig. 4-3) are located at the position of aquifers and represent a shorter-term disturbance in the formation-scale profiles by the aquifer groundwater composition that are different from the older archive of porewater composition preserved across clayey units. All profiles share such evidence for a Keuper aquifer below the confining units and a Malm aquifer above it (not constrained by isotope data in the Benken borehole, but groundwater was sampled; RHE1-1 is only constrained by sampling/data to 20 m above the Opalinus Clay). The hydraulic conductivity of the Keuper aquifer was too low for sampling groundwater in the MAR1-1 borehole, but the water isotope and chloride profiles clearly indicate the influence of a Keuper aquifer. A Malm aquifer was sampled in three boreholes, some 70 – 90°m above the «Brauner Dogger». A common key feature of the chlorinity profiles are very moderate vertical gradients across the «Brauner Dogger» and Opalinus Clay, but very steep gradients in the Staffelegg Formation towards very low chloride concentrations in the region of the Keuper aquifer. The chloride concentration maximum is located at or near the top of the Opalinus Clay, decreasing moderately towards the base of this formation. A similar situation is also encountered at the Schlattingen-1 geothermal borehole where the Muschelkalk aquifer is being exploited, but geochemical data are restricted to a cored section comprising the lower-most Malm, «Brauner Dogger», Opalinus Clay, most of the Lias, but not the region of the Keuper aquifer. There are no chloride concentration data for the Rheinau borehole.

The mineralogy of these units across the region is also comparable, both in terms of clay mineral content and also the types of clay minerals present. The same is true for the carbonate mineralogy, quartz, feldspars, pyrite, and the absence of sulphates detectable by XRD methods. A single occurrence of celestite ($SrSO_4$) was confirmed and analysed by SEM-EDX in one out of two sample studied from Opalinus Clay from the Schlattingen-1 borehole (Wersin et al. 2013). Jenni et al. (2019) examined two samples of Opalinus Clay from Schlattingen by element mapping at high resolution and detected very small amounts of sub-micron size celestite in both samples and a few larger grains in one sample (10 – 20 µm) (sandy facies sample in report Jenni et al. 2019). There is intrinsically more heterogeneity in the «Brauner Dogger» units compared to Opalinus Clay and the Staffelegg Formation. This – and some variation in chloride-accessible porosity fraction – may be a reason why the data becomes 'noisy' in parts of the «Brauner Dogger» units (e.g., «Herrenwis Unit»), and in the uppermost Staffelegg Formation.

Based on these similarities, and the absence of large differences, it is concluded that the ZNO region contains also similar porewaters within the clay-rich confining units, varying within the observed ranges, and extrapolating spatially over at least short distances (potentially limited by regional faults) according to observed gradients between boreholes. Some moderate differences do exist, for example in the sulphate concentrations and SO_4/Cl ratios in particular. More detailed concentration data are presented and discussed below.

Sulphate concentrations as constrained by the direct sampling methods squeezing and advective displacement are presented in Section 4.1.2. Details of aqueous extracts are reported in the Dossier reports by Aschwanden et al. (2021) for TRU1-1, by Mäder et al. (2021) for MAR1-1, by Wersin et al. (2013) and by Waber et al. (2003) for Benken.

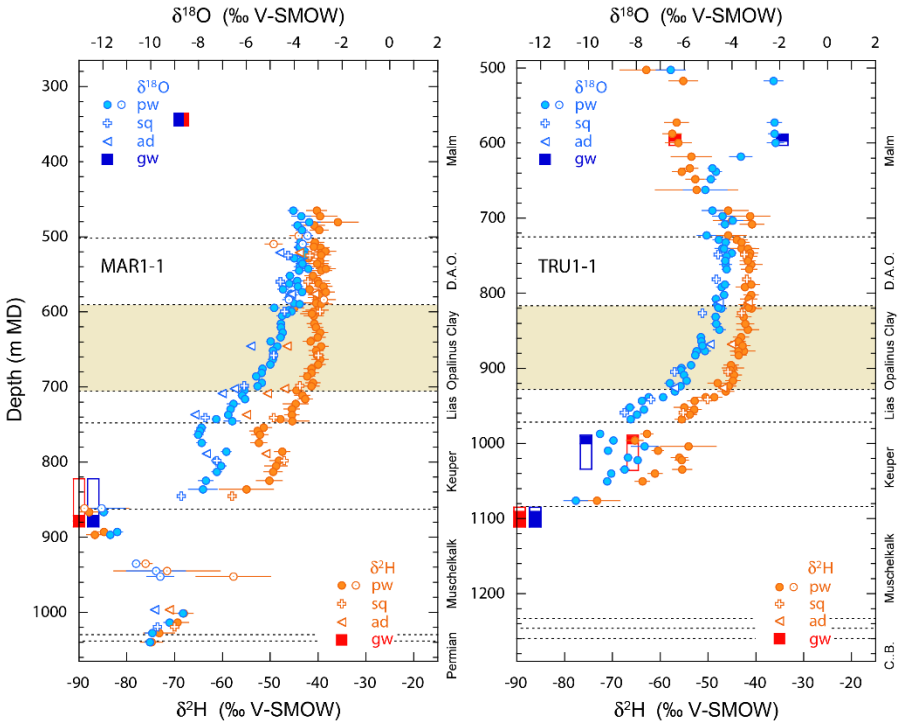

Fig. 4-3: Overview of the pore- and groundwater stable isotope profiles of boreholes MAR1-1 and TRU1-1 in the ZNO region

Modified figure based on Mäder et al. (2021) and Aschwanden et al. (2021). Blue: $\delta^{18}O$, orange: $\delta^{2}H$. Porewater data from isotope diffusive exchange (pw, open symbols are less reliable), squeezing (sq) and advective displacement (ad), as well as groundwater data (gw, open rectangles extend over packer interval, symbols show probable inflow zone). Error bars for porewater data represent propagated analytical errors. D.A.O.: Dogger above Opalinus Clay, C.B.: Crystalline basement.

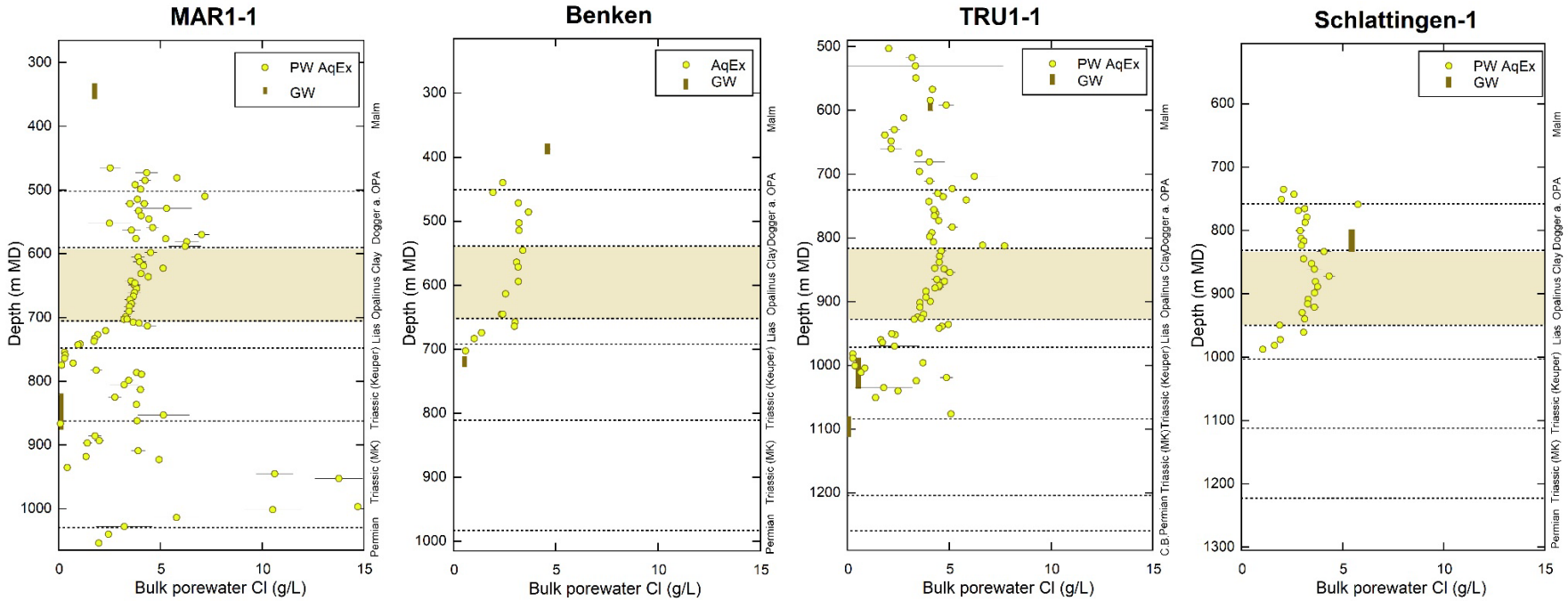

Fig. 4-4: Overview of the chloride concentration profiles (aqueous extracts) for the ZNO siting region

Chloride concentrations are scaled to the bulk water content. Data from boreholes Benken (Nagra 2001, Waber et al. 2003), MAR1-1 (Mäder et al. 2021), TRU1-1 (Aschwanden et al. 2021), and a partial profile for the geothermal well Schlattingen-1 to the NE of ZNO. The profiles are aligned at the level of the Opalinus Clay. Values for aquifers (GW) are provided where known (sampled). Analytical errors are shown vor MAR1-1 and TRU1-1.

4.1.1.2 Chloride and water stable isotopes in depth profiles for NL

The geochemical depth profiles in the NL region, represented by water stable isotope ratios, chloride concentrations and sulphate concentrations, are more varied compared to the ZNO region. The δ^2H profiles (Fig. 4-5, also $\delta^{18}O$) show continuity in the eastern part of NL (BUL1-1, STA3-1) across the Staffelegg and Klettgau Formations, whereas further to the NE a clear signature of a Keuper aquifer is seen in the ZNO region that affects the profiles within the latter formations. A Keuper aquifer was also sampled in the western part of NL (STA2-1, BAC1) and its presence is seen clearly in the depth profile of δ^2H for STA2-1 and BAC1-1 as a local minimum in the lowest part of the Klettgau Formations (STA2-1) or near the top of the Bänkerjoch Formation (BAC1-1). The Keuper aquifer has relatively little apparent effect on the shape of the profile within the Opalinus Clay at STA2-1 but forms a local minimum of a continuously decreasing trend at BAC1-1 extending from the base of the Wutach Formation to the Keuper aquifer. For boreholes BUL1-1 and STA3-1 the water stable isotope profiles drop sharply towards the Muschelkalk aquifer (Fig. 4-5) in the Schinznach Formation, and the same is true for STA2-1 and BAC1-1, but with a region of less negative values between the two aquifers. The isotope ratio profiles are somewhat irregular in the «Brauner Dogger» above the Opalinus Clay, and a Malm aquifer in the «Felsenkalke» + «Massenkalk» is present across all four TBO boreholes of the NL region.

The depth profiles of chloride concentrations (Fig. 4-6, recalculated to the measured water content) show only small gradients across the Opalinus Clay in all four boreholes, with slightly higher concentrations at the top of the formation, except for BAC1-1 where Cl concentrations are uniform. Chloride concentrations drop significantly above the Opalinus Clay in the lower part of the «Brauner Dogger» in the eastern part of NL (BUL1-1, STA3-1), but are rather smooth in the western part (STA2-1, BAC1-1), with some apparent outliers (high chloride) just above and just below the Opalinus Clay (possibly due to large variations in anion-accessible porosity fractions). The decrease in the chloride concentration below the Opalinus Clay seen in STA2-1 is less pronounced compared to ZNO, mainly because the chlorinities in the Keuper aquifer are much higher (4◦g/L) compared to ZNO (<◦1◦g/L). The Cl profile below the Opalinus Clay at BAC1-1 shows a large scatter and it is difficult to define trends across this part of the Keuper. The Keuper aquifer was sampled at STA2-1 and yielded rather high salinities of nearly 10◦g/L. The Cl profile at STA3-1 shows some continuity (along with δ^2H, Fig. 4-5) from OPA across the Staffelegg and Klettgau Formations, but then drops to very low values in the Bänkerjoch Formation. At BUL1-1, where chlorinities are highest in the Opalinus Clay, these also do not drop, but may even be more elevated in parts of the Klettgau Formation, with a rather large uncertainty associated with some samples having very low water contents and a very low clay mineral content (issue of measurement uncertainties and of scaling to Cl-accessible porosity fraction, see below).

The mineralogy of these units across the NL region is comparable, both in terms of clay content and also the types of clay minerals present. The same is true for the carbonate mineralogy, quartz, feldspars, pyrite, and the absence of sulphates detectable by XRD methods. There is intrinsically more heterogeneity in the «Brauner Dogger» units compared to Opalinus Clay and the Staffelegg Formation. This – and some variation in chloride-accessible porosity fraction – may be a reason why the data becomes 'noisy' in parts of the «Brauner Dogger» units, and in the uppermost Staffelegg Formation, and also in clay-poor units further below.

Based on these similarities, and the absence of large differences, it is concluded that the NL region contains also similar porewaters within the clay-rich confining units, varying within the observed ranges, and extrapolating spatially over at least short distances (limited by regional faults) according to observed gradients between boreholes. BUL1-1 shows distinctly higher salinities

compared to STA3-1, STA2-1, BAC1-1, and this is further discussed in Section 4.1.2. The chlorinities at STA3-1, STA2-1, BAC1-1 are similar to those of the ZNO region, and this has led to a decision to define a single reference porewater for ZNO-NL.

Sulphate concentrations as constrained by the direct sampling methods squeezing and advective displacement are presented in Section 4.1.2. Details of aqueous extracts are reported in the Dossier reports by Mazurek ed. (2021) for BUL1-1, Aschwanden et al. (2021) for STA3-1, Zwahlen et al. (*in prep.*) for STA2-1 and Gaucher et al. (*in prep.*) for BAC1-1.

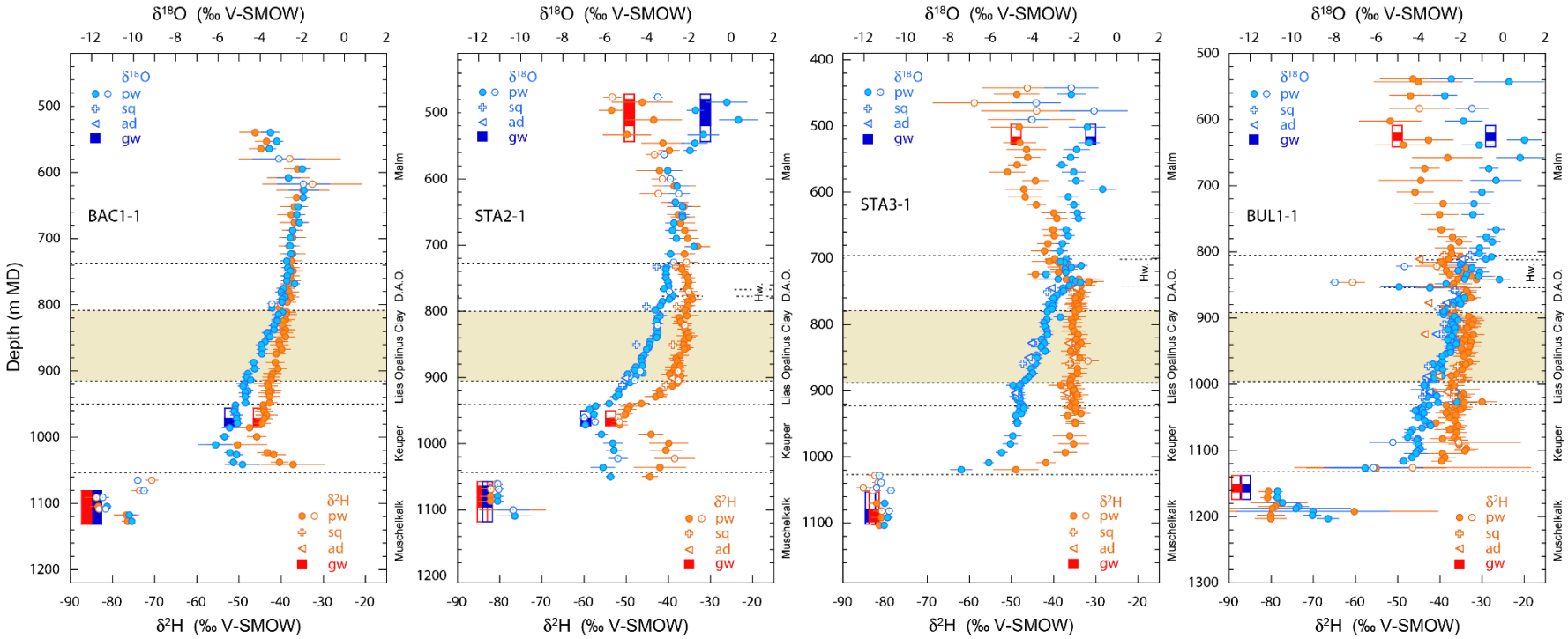

Fig. 4-5: Overview of the pore- and groundwater stable isotope profiles of the NL region

Modified figure based on Gaucher et al. (in prep.), Zwahlen et al. (in prep.), Aschwanden et al. (2022) and Mazurek et al. (2022). Blue: $\delta^{18}O$, orange: $\delta^{2}H$. Porewater data from isotope diffusive exchange (pw, open symbols are less reliable), squeezing (sq) and advective displacement (ad), as well as groundwater data (gw, open rectangles extend over packer interval, symbols show probable inflow zone). Error bars for porewater data represent propagated analytical errors. D.A.O.: Dogger above Opalinus Clay; Hw.: Herrenwis Unit.

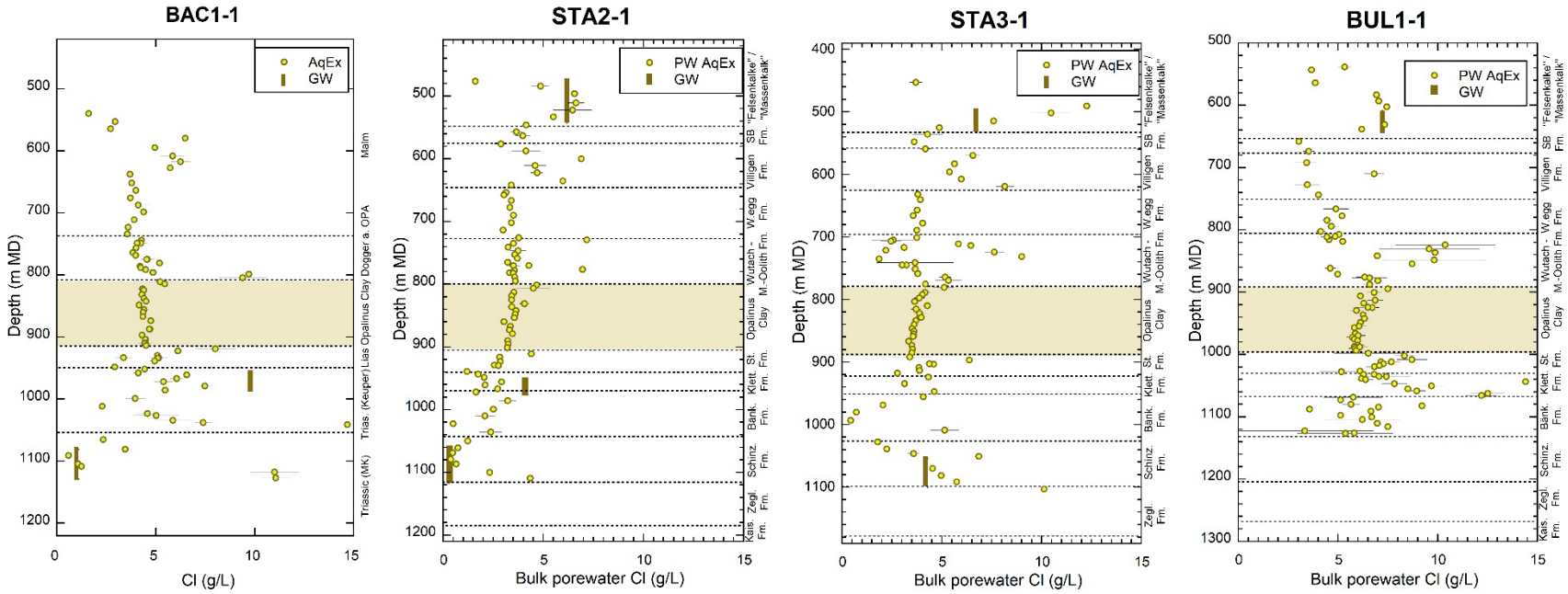

Fig. 4-6: Overview of the chloride concentration profiles (aqueous extracts) of the NL siting region

Data are scaled to bulk water content, from boreholes BUL1-1 (Mazurek et al. 2021), STA3-1 and STA2-1 (Aschwanden et al. 2021, Zwahlen et al. *in prep.*) and BAC1-1 (Gaucher et al. *in prep.*). Values for aquifers (GW) are provided where known (sampled). Error bars reflect the analytical error. SB Fm.: Schwarzbach Formation, St. Fm.: Staffelegg Formation.

4.1.2 Chloride and sulphate concentrations in AD and SQ aliquots from ZNO-NL

In the following, reference is made to two methods for obtaining aliquots of porewater of a core sample, namely porewater squeezing and porewater advective displacement that are detailed in a method report (Waber et al. 2020). Briefly, porewater squeezing applies large uniaxial stresses to a rock sample confined in a cylindrical squeezing cell to compress the rock skeleton and displace a fraction of the porewater outwards to a sampling system. The technique of advective displacement applies a large hydraulic gradient to a confined core sample, using an artificial porewater to displace the in situ porewater to a sampling system. In addition, the method of aqueous extraction (details in Waber et al. 2020) was applied to numerous samples to constrain closely-spaced depth profiles for conservative components (Cl, Br). The latter method yields the bulk inventory that can be recalculated as a concentration in the bulk water or, by additional scaling, in the 'free porosity' (chloride-accessible porosity) (Section 4.1.3).

4.1.2.1 Chloride concentrations in AD and SQ aliquots from ZNO-NL

Chloride concentrations are best constrained by measurements from the so-called direct methods, advective displacement (AD) and squeezing (SQ). Data for Opalinus Clay are available for several samples from all TBO boreholes located in the ZNO and NL regions, but only for two samples from the older Benken borehole by squeezing, and some data (SQ and limited AD) are available from the Schlattingen-1 borehole further to the ENE of ZNO. These two methods are expected to deliver preferentially the most mobile portions of porewater that approximately correspond to a charge-balanced 'free porosity' not affected by negatively charged clay outer surfaces and interlayers of clay minerals (detailed in Chapter 3). Aqueous extracts yield the entire inventory of ions and aqueous complexes, and this can be recalculated to concentrations based on the total water content for conservative components that do not participate in ion-exchange processes or that are not subject to mineral dissolution / precipitation reactions (details in Waber et al. 2020). To calculate concentrations for conservative components like Cl in the 'free porosity' from aqueous extracts requires knowledge of the Cl-accessible porosity fraction, and this factor can be derived from the direct methods (see Section 4.1.3, and Waber et al. 2020). A chloride-accessible porosity can also be evaluated from through-diffusion experiments that were performed for some samples from TRU1-1, and many samples from BUL1-1 (also many from BOZ1-1, JO) (Van Loon & Glaus in prep.). In addition, some estimate of the amount of 'bound water' (pore space affected by charged surfaces) can be made from a quantified clay mineralogical composition and surface properties derived from gas adsorption methods (e.g., BET; e.g., Wersin et al. 2020) but this has not yet been further pursued for this work.

It is evident from all squeezing and advective displacement data for Opalinus Clay from the ZNO and NL regions (Fig. 4-7, data listed in Tab. 4-1 in Section 4.1.3) that there is a systematic and significant difference in chloride concentrations between advective displacement early aliquots and squeezing aliquots (obtained at lowest pressures), with the latter being quite consistently 10 – 25% lower in chloride concentration. This is also true for data from adjacent strata but there it is less evident due to a larger heterogeneity, also in the chloride-accessible porosity fraction (e.g., discussion in Mäder et al. 2021), and the presence of large concentration gradients in the Staffelegg Formation. This difference between the two methods is not surprising given the contrasting mechanisms by which porewater is mobilised from a core sample: by a large hydraulic gradient in case of advective displacement, and by mechanical compaction implying shear movement and deformation of pore space in case of rock squeezing. Given this systematic difference, the two methods are therefore not probing the same pore sub-volume, and/or are differently affected by experimental artefacts, although in case of chloride, artefacts are thought to be small or negligible.

The data derived from the two methods do share communalities and in tandem provide important anchor points for the chloride profiles and on other porewater components, like sulphate.

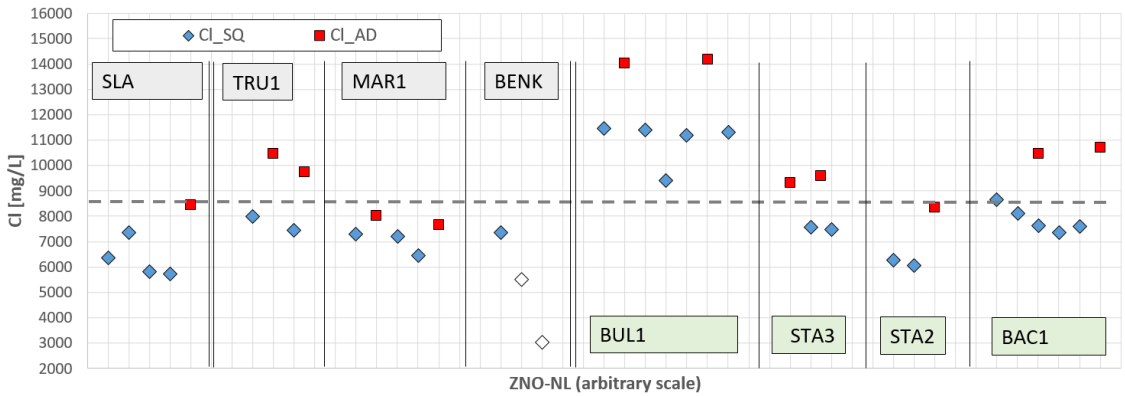

Fig. 4-7: Cl concentrations obtained from squeezing and advective displacement aliquots

For each borehole, data are arranged in sequence according to borehole depth, from left to right. Open symbols indicate less reliable data (as defined in the respective da-ta reports). The dashed horizontal line marks the chloride concentration of the reference porewater at 8'500 mg/L. Data are from: Wersin et al. (2013), Mäder & Waber (2017) for Schlattingen-1 (SLA); Aschwanden et al. (2021) for TRU1-1; Mäder et al. (2021) for MAR1-1; Waber et al. (2003) for Benken (BENK); Mazurek et al. (2021) for BUL1-1; Aschwanden et al. (2022) for STA3-1; Zwahlen et al. (*in prep.*) for STA2-1; Gaucher et al. (*in prep.*) for BAC1-1.

Chloride concentrations from advective displacement and squeezing for the ZNO region are plotted in combination with chloride concentrations obtained from numerous aqueous extracts scaled to the chloride-accessible porosities ('free porosity') with scaling factors, f(Cl), as selected in the respective data reports (Fig. 4-8, references therein, data listed in Tab. 4-1 in Section 4.1.3). Note that the scaling of the aqueous extracts derived for data from Benken and Schlattingen-1 (5 km to NE from TRU1-1) is somewhat different compared to MAR1-1 and TRU1-1: a factor of 0.50 was used as chloride accessible porosity fraction in the former two boreholes, but 0.45 and 0.46 for the latter two boreholes, i.e. a difference of about 10%. This difference is further elaborated in Section 4.1.3 where the chloride-accessible porosity fraction is discussed in detail.

The chloride concentration profile for Benken (Fig. 4-8) is less well constrained by much fewer data points. It is evident that the two chloride concentrations obtained from Opalinus Clay by squeezing are located below the profile defined by the scaled aqueous extract data, despite the fact that the scaling was derived from the squeezing data ($f_{Cl} = 0.5$ for this figure). The reason for this is that the squeezing data obtained at a high pressure of 500 MPa were corrected by 25% to higher salinities to off-set the pressure-dependent decrease in chloride concentrations with step-wise increasing squeezing stresses as was established for samples from the Mont Terri rock laboratory (see Waber et al. 2003). Note that the Benken study was carried out at a time when these then new techniques were just emerging, mainly from development work carried out at the Mont Terri rock laboratory.

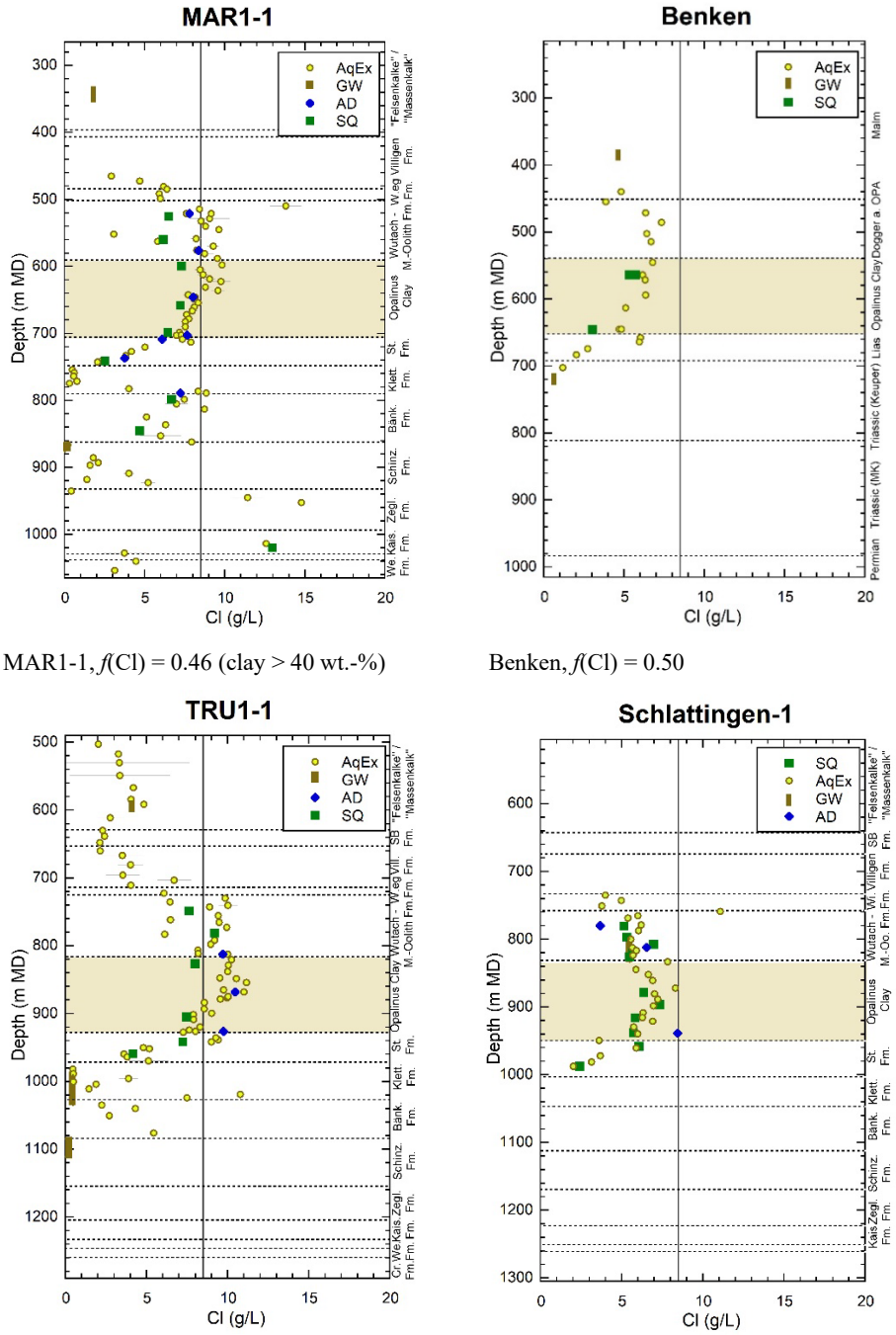

MAR1-1, f(Cl) = 0.46 (clay > 40 wt.-%)

Benken, f(Cl) = 0.50

TRU1-1, f(Cl) = 0.45 (clay > 40 wt.-%)

Schlattingen-1, f(Cl) = 0.50

Fig. 4-8: Cl concentration profiles with data from squeezing, advective displacement, aqueous extraction and groundwater samples from ZNO

Aqueous extraction data (leachates) re-calculated to Cl-accessible porosity, with f_{Cl} as indicated. A vertical line is drawn at 8'500 mg/L Cl concentration, the value adopted for the reference porewater for ZNO-NL. Data from Aschwanden et al. (2021, TRU1-1), Mäder et al. (2021, MAR1-1), Wersin et al. (2013, Benken) adopted from Mazurek et al. (2009) based on data by Gimmi & Waber (2004), Wersin et al. (2013, Schlattingen-1) with additional advective displacement data from Mäder & Waber (2017). SB Fm.: Schwarzbach Formation, St. Fm.: Staffelegg Fm.

The chloride concentration profile for the Schlattingen geothermal well (5 km to the ENE of TRU1-1) is well constrained (Fig. 4-8) and was performed with techniques very similar to those used for the TBO work. With the chloride scaling adopted for the aqueous extracts (f_{Cl} = 0.5 for this figure), the range for Opalinus Clay is 6'000 – 9'000◦mg/L. A datum from advective displacement for Opalinus Clay for the Schlattingen borehole was added to Fig. 4-8 (lower right, Mäder & Waber 2017) that was not yet available at the time of reporting by Wersin et al. (2013). This datum suggests that the scaled concentrations from aqueous extracts may be even larger than shown in the figure (see details on anion accessibility below). This is uncertain, however, because only one sample was processed with advective displacement from Opalinus Clay that has a rather low clay-content of 16 – 18◦wt.-%.

In summary, the region of the MAR1-1 – TRU1-1 (– Schlattingen-1) boreholes has quite similar chloride concentrations in the Opalinus Clay of 8'000 – 10'000◦mg/L (MAR1-1, TRU1-1), but it is decreasing towards the NW (Benken) where it is less well constrained at 5'000 – 7'000◦mg/L (or possibly 10 – 15% higher, depending on the adopted anion-accessible porosity fraction). As discussed below, the concentrations for Schlattingen-1 might also be somewhat higher than reported considering uncertainties in the anion-accessible porosity fraction (discussed below), quite similar to MAR1-1, but the supporting data are sparse and not conclusive.

Chloride concentrations from advective displacement and squeezing for the NL region are plotted in combination with chloride concentrations obtained from aqueous extracts scaled to the chloride-accessible porosities, with scaling factors, *f*(Cl), as selected in the respective data reports (Fig. 4-9, references therein, data listed in Tab. 4-1 in Section 4.1.3). The scaling factors applied to the aqueous extracts are: 0.45 or 0.47 for STA3-1, STA2-1 and BAC1-1, and 0.52 for BUL1-1. The *f*(Cl) for BAC1-1 adopted here is preliminary and may be slightly different in the final version reported by Gaucher et al. (*in prep.*). Also shown are the Cl concentrations from squeezing (at lowest pressure) and advective displacement (average of first two aliquots), and these either straddle the squeezing data (BUL1-1, STA3-1), or the AD data (BAC1-1), or are bracketed by these two direct sampling methods (STA2-1). This is further elaborated below where the chloride-accessible porosity fraction is discussed in detail.

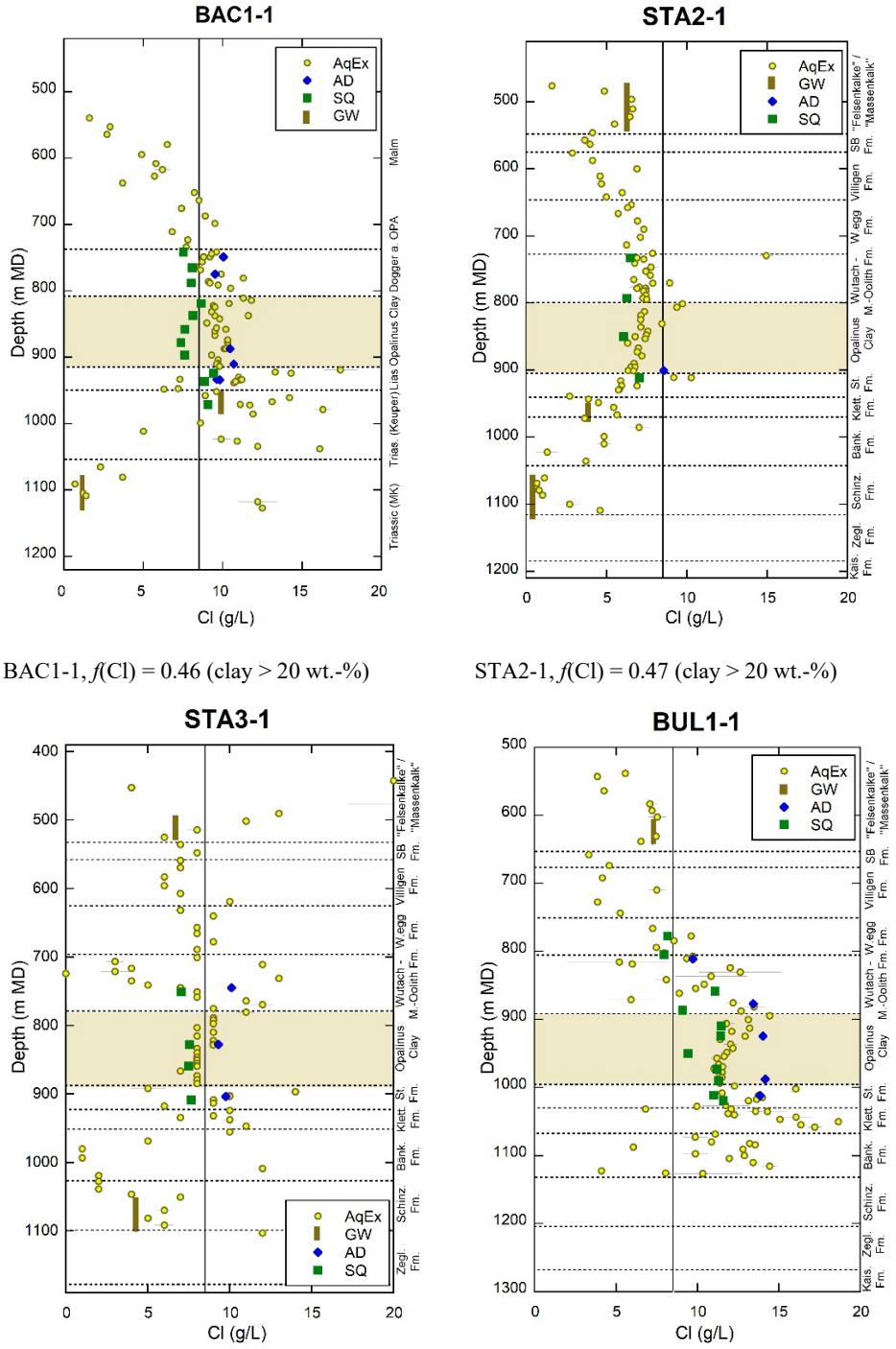

BAC1-1, f(Cl) = 0.46 (clay > 20 wt.-%)

STA2-1, f(Cl) = 0.47 (clay > 20 wt.-%)

STA3-1, f(Cl) = 0.45 (clay > 20 wt.-%)

BUL1-1, f(Cl) = 0.52 (clay > 20 wt.-%)

Fig. 4-9: Cl concentration profiles with data from squeezing, advective displacement, aqueous extraction, and groundwater samples from NL

Aqueous extraction data re-calculated to Cl-accessible porosity, f_{Cl}, indicated. The thin vertical line is drawn at 8'500 mg/L Cl concentration, the value adopted for the reference porewater for ZNO-NL. Data from Mazurek et al. (2020, BUL1-1), Aschwanden et al. (2022, STA3-1), Zwahlen et al. (*in prep.*, STA2-1), and Gaucher et al. (*in prep.*, BAC1-1). SB Fm.: Schwarzbach Formation, St. Fm.: Staffelegg Formation.

Some approximate chloride concentrations were derived (Meier & Mazurek 2011) for old samples from the Weiach borehole by aqueous leaching and an estimate of porosity / water content, either by measured densities or by a correlation of clay-content with water-content (water contents were not routinely measured in those days). The study evaluated also samples from Opalinus Clay (13 samples, from 560 – 660 m depth), and – when applying a chloride-accessible porosity fraction of 0.5 – yielded porewater chloride concentrations in the 'free porosity' of 3'300 – 5'100 mg/L, with error estimates of about ± 1'300 – 2'100 mg/L. The chlorinities are therefore on average less saline at Weiach (near the NW boundary of NL) compared to those 2.5 – 3 km to the SE observed at the STA2-1 and STA3-1 boreholes. This is a similar situation as in the ZNO region, with Benken having lower salinities towards the N and towards shallower present-day burial depths.

In summary, the NL region of the BUL1-1 – STA3-1 – STA2-1 – BAC1-1 boreholes has chloride concentrations in the Opalinus Clay towards the NE of 11'500 – 14'000 mg/L (BUL1-1), distinctly lower in the STA3-1 andSTA2-1 boreholes (7'500 – 9'500 mg/L, STA3-1; 6'200 – 7'500 mg/L, STA2-1), and more elevated again in the western part at BAC1-1 (7'500 – 10'000 mg/L). The lower bounds for the chloride concentrations are defined by the squeezing data, whereas the upper bounds by the advective displacement data (only 1 reliable AD data point for STA2-1). Chloride concentrations are decreasing towards the NW (Weiach), but this is not well constrained. As said in the introduction, apart from the more saline porewaters at BUL1-1, the 8'500 mg/L adopted for the chloride concentration for the reference porewater ZNO-NL is representing the chlorinities measured at STA3-1, STA2-1 and BAC1-1 to within ± 2'000 mg/L.

4.1.2.2 Sulphate concentrations in AD and SQ aliquots from ZNO-NL

Sulphate concentrations in ZNO boreholes obtained from the direct methods squeezing and advective displacement (Fig. 4-10, data listed in Tab. 4-1 in Section 4.1.3) are more variable than chloride concentrations, but show a clearly increasing trend with depth across the Opalinus Clay (and adjacent Formations). Concentrations range from 1'000 to 2'300 mg/L across boreholes TRU1-1, MAR1-1 and the geothermal well Schlattingen-1, with highest concentrations observed at MAR1-1. While there is good agreement for sulphate concentrations obtained by the two methods for MAR1-1, the squeezed aliquots from TRU1-1 are relatively less sulphate rich compared to the advectively displaced aliquots. Sulphate concentrations obtained from squeezing tests from the Benken borehole (Tab. 4-1, details in Waber et al. 2003) cannot be used because these early tests were not performed under exclusion of atmospheric oxygen, and this led to SO_4/Cl ratios that are twice as large as obtained from the recent squeezing and advective displacement experiments (likely due to pyrite oxidation).

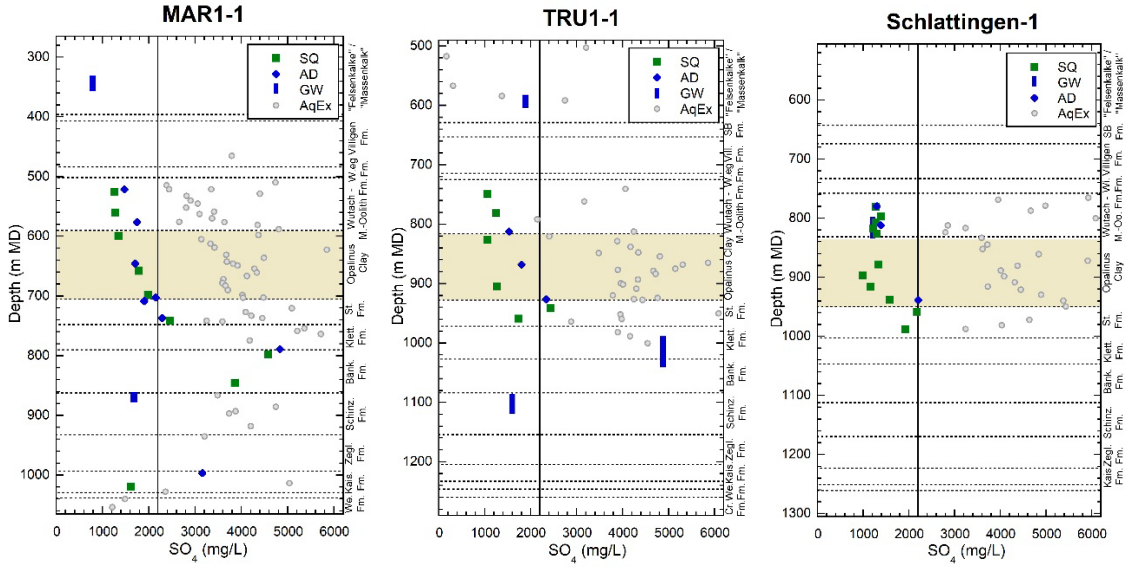

Fig. 4-10: Overview of the sulphate concentration profiles of the ZNO siting region

Data are from squeezing and advective displacement measurements, from boreholes MAR1-1 (Mäder et al. 2021) and TRU1-1 (Aschwanden et al. 2021). Data for Schlattingen-1 (SLA1) are included, located to the NE of ZNO. The profiles are aligned at the level of the Opalinus Clay. Data from aqueous extracts scaled to water content are shown in grey. A vertical line is drawn at the reference SO_4 concentration of 2'200 mg/L. SB Fm.: Schwarzbach Formation, St. Fm.: Staffelegg Formation.

Sulphate concentrations in boreholes from NL obtained from the direct methods squeezing and advective displacement (Fig. 4-11, data listed in Tab. 4-1 in Section 4.1.3) are about 2'200 – 2'700 mg/L in BUL1-1, and about 2'400 mg/L in STA3-1, the latter based on data only from squeezing (the datum obtained from advective displacement may be disturbed by artefacts). There appears to be a distinct gradient in SO_4 concentrations at STA2-1, decreasing from about 3'000 mg/L at the top to near 2'000 mg/L at the base of this formation. The sulphate concentrations obtained for BAC1-1 are near 2'700 mg/L based on two advective displacement experiments and covers a range from 1'940 – 2'330 mg/L in five squeezing samples. The squeezed aliquots of BUL1-1 show some scatter and are distinctly lower in SO_4 concentrations compared to the samples from advective displacement.

A concentration of 2'200 mg/L SO_4 was chosen for the common reference porewater ZNO-NL. This value is somewhat above the average of the concentrations from ZNO and below the average of the AD and SQ data from NL. The range covered by all AD and SQ experiments from both regions is 1'000 – 3'600 mg/L. The concentrations obtained from SQ samples tend to be somewhat lower than those from AD aliquots, in line with the general lower salinities obtained by the SQ methodology. The discrepancy between the AD and SQ data on one hand and the aqueous extract data on the other hand is discussed in Section 5.8.

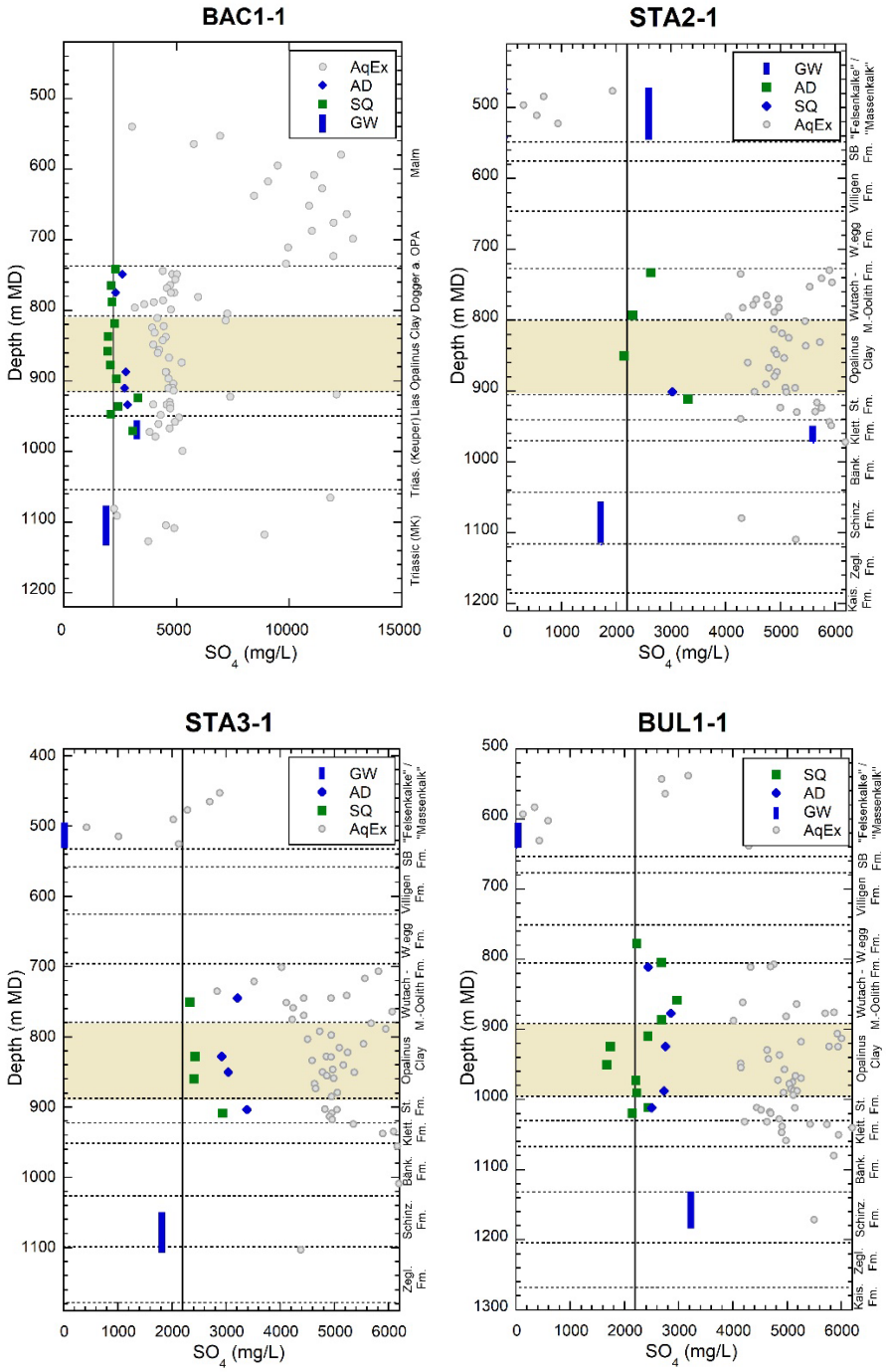

Fig. 4-11: Overview of the sulphate concentration profiles of the NL siting region

Data are from squeezing and advective displacement measurements, from boreholes BUL1-1 (Mazurek et al. 2021), STA3-1 (Aschwanden et al. 2021), STA2-1 (Zwahlen et al. *in prep.*) and BAC1-1 (Gaucher et al. *in prep.*). The profiles are aligned at the level of the Opalinus Clay. Data from aqueous extracts scaled to water content are shown in grey. A vertical line is drawn at the reference SO_4 concentration of 2'200 mg/L. SB Fm.: Schwarzbach Formation, St. Fm.: Staffelegg Formation.

4.1.3 Constraints on chloride-accessible porosity fraction for ZNO-NL

The chloride-accessible porosity fraction obtained from rock squeezing is derived by dividing the bulk porewater chloride concentration of a core sample by the chloride concentration of the aliquot squeezed at the lowest pressure. The bulk concentration is derived from the total inventory of chloride related to the initial water content, and the inventory is calculated from the sum of chloride in the squeezed aliquots (at all pressure steps) and the residual chloride derived from a post-mortem aqueous extract (details in Aschwanden et al. 2021 and Mäder et al. 2021). An additional alternate approach was performed for SQ samples for the STA3-1, STA2-1 and BAC1-1 boreholes, whereby conventional aqueous extracts were performed on adjacent sample pieces that were not subject to squeezing (e.g., Aschwanden et al. 2022, Zwahlen et al. *in prep.*). The chloride-accessible porosity fraction obtained from advective displacement is simply the ratio of the bulk porewater chloride concentration (derived by averaging aqueous extracts performed from sub-samples located just above and below the core segment used for advective displacement) and the chloride concentration in the earliest aliquots (average of the first two aliquots). There is an additional control on water content by performing post-mortem analyses of the core sample (details in Aschwanden et al. 2021 and Mäder et al. 2021).

Chloride concentrations for ZNO from TRU1-1 and MAR1-1 are shown in Fig. 4-7 and Fig. 4-8, and are listed in Tab. 4-1 below. While the two approaches share the same reference for the aliquots, namely the initial inventory of chloride in the bulk porewater, the way this reference is calculated is different. As a consequence of this common reference, the two methods should yield the same chloride-accessible porosity fractions if the chloride concentrations are the same in the squeezing aliquots and those from advective displacement. Tab. 4-1 is a summary of the chloride-accessible porosity fractions reported for TRU1-1 (Aschwanden et al. 2021), MAR1-1 (Mäder et al. 2021) and for the Benken borehole (Waber et al. 2003). It can be seen that there is almost perfect agreement for the reported chloride-accessible porosity fraction for Opalinus Clay from squeezing and advective displacement for TRU1-1 and MAR1-1, despite the above (Section 4.1.2.1) stated 10 – 25% difference in chloride concentration of the squeezed and advectively displaced aliquots (Fig. 4-7, Fig. 4-8, Tab. 4-1). Consequently, there is a data inconsistency of 10 – 25%, and either the chloride-accessible porosity fractions derived from squeezing should be 10 – 25% larger, or the frame of reference derived from the numerous aqueous extracts is incorrect – too large by 10 – 25%. The latter is rather unlikely, given the large number of aqueous extracts that had been performed by several laboratories, without indication that the chloride inventory is either significantly overestimated (e.g., by contamination from saline fluid inclusions, only observed when milling is used for sample preparation) or underestimated (a portion of porewater chloride not leached during aqueous extraction). It is therefore most likely that the data inconsistency is within the squeezing data sets, and that the calculated chloride-accessible porosity fractions reported for TRU1-1 and MAR1-1 cannot be used at face value as independent constraining data.

It is not straightforward to explain the difference in salinity (affecting all concentrations) of 10 – 25% between squeezed aliquots and advectively displaced aliquots, essentially an answer to the question of which type of aliquot is more closely related to the true 'free porewater' present in the tested core samples. Some discussion of this issue is included in the data reports (Aschwanden et al. 2021, Mäder et al. 2021), but for this report it is sufficient to note this difference and that there is an overall uncertainty (spread) in the order of 10 – 25% in constraining the chloride concentrations in the chloride-accessible porosity fraction, squeezing yielding a lower estimate and advective displacement a higher estimate for the chloride concentrations. It should be kept in mind that there is not a unique method that is able to extract a sample of what is termed 'free porewater' and therefore also not a method to uniquely define a chloride-accessible porosity fraction (yet an anion-accessible porosity fraction). 'Free porewater' and anion-accessible porosity fraction are

simplified operational concepts for a far more complicated situation where pore space is structured across spatial scales of many orders of magnitude, and anion-accessibility is a continuous distribution (as a function of distance from a charged surface, surface charge density, ionic strength, and the ionic charge of the ion in question) rather than confined to a discrete pore volume (see also Chapter 3 above, Wersin et al. 2020, and references therein).

Tab. 4-1: Chloride and sulphate concentrations and chloride accessible porosity fraction for Opalinus Clay from advective displacement and squeezing tests, ZNO and NL

See table on opposite page. Depth: mid-depth of sample segment; relates to sample ID as used in data reports. AD: advective displacement; SQ_{nnn}: squeezing, with pressure indicated (MPa); f_{Cl}: chloride-accessible porosity fraction, with values in brackets subject to data inconsistency (see text), a second datum given for SQ experiments is from an alternate assessment of the Cl inventory (see text); data in italics are less/not reliable as defined in the data reports; (pm) evaluation from post-mortem data of long-term advective displacement experiment, as documented in the data reports; (report) refers to the scaling factors used for aqueous extracts, References: (1) Wersin et al. (2013), (2) Wersin et al. (2020), Wersin et al. (2016), (3) Mäder & Waber (2017), (5) Aschwanden et al. (2021), (6) Mäder et al. (2021); (7) Waber et al. (2003), (b) with 25% correction for squeezing at 500 bar; (8) in Wersin et al. 2013; (9) Mazurek et al. (2021), (10) Aschwanden et al. (2022), (11) Zwahlen et al. (*in prep.*), (12) Gaucher et al (*in prep.*).

See opposite page.

Borehole/Depth [m]	Method [MPa]	Clay [wt.-%]	Qz-Fsp [wt.-%]	Carb [wt.-%]	Cl [mg/L]	SO_4 [mg/L]	SO_4/Cl [mol/mol]	f_{Cl}	Ref
SLA-878.45	SQ_{200}	45			6'351	1'324	0.077	0.54	1, 2
SLA-896.31	SQ_{200}	54			7'356	982	0.049	0.49	1, 2
SLA-915.87	SQ_{200}	56			5'821	1'163	0.074	0.57	1, 2
SLA-938.57	AD	83	14	3	8'442	2'050	0.090	0.38-0.47	3
SLA-937.89	SQ_{200}	71			5'726	1'573	0.101	0.51	1, 2
SLA (report)	AqEx							0.52	2
SLA (report)	AqEx							0.50	1
TRU1-1-826.93	SQ_{200}	55	31	10	7'997	1'063	0.049	[0.51]	5
TRU1-1-867.97	AD	41	35	25	10'455	1'801	0.064	0.42	5
TRU1-1-904.86	SQ_{200}	59	28	12	7'456	1'269	0.063	[0.46]	5
TRU1-1-926.14	AD				9'734	2'340	0.089	0.37	5
TRU1-1 (report)	AqEx							0.45	5
MAR1-1-599.33	SQ_{200}	52	31	16	7'291	1'341	0.068	[0.44]	6
MAR1-1-645.48	AD	52	34	12	8'029	1'702	0.078	0.46	6
MAR1-1-657.71	SQ_{300}	48	35	15	7'216	1'786	0.091	[0.46]	6
MAR1-1-698.47	SQ_{200}	66	22	12	6'440	1'981	0.114	[0.44]	6
MAR1-1-702.40	AD	67	20	11	7'652	2'151	0.104	0.43	6
MAR1-1 (report)	AqEx							0.46	6
Benk-563.85	SQ_{500}	52	29	18	7'360			0.42; 0.45	7 (b)
Benk-563.85	SQ_{500}	52	29	18	5'500	3'200	0.215	0.56; 0.6	7
Benk-645.65	SQ_{500}	68	15	16	*4'050*			*0.71; 0.60*	7 (b)
Benk-645.65	SQ_{500}	68	15	16	*3'030*	*2'290*	*0.279*	*0.94; 0.79*	7
Benk (report)	AqEx							0.48	7
Benk (report)	AqEx							0.50	8
BUL1-1-909.46	SQ_{300}	59	33	5	11'464	2'429	0.078	0.51	9
BUL1-1-924.18	AD	48	39	10	14'013	2'755	0.073	0.47 (pm)	9
BUL1-1-924.36	SQ_{300}	43	42	11	11'413	1'736	0.056	0.52	9
BUL1-1-950.43	SQ_{200}	61	28	6	*9'408*	*1'668*	*0.065*	*0.59*	9
BUL1-1-972.72	SQ_{300}	51	35	10	11'181	2'207	0.073	[0.43]	9
BUL1-1-987.55	AD	62	23	9	14'163	2'730	0.071	0.43; 0.42 (pm)	9
BUL1-1-990.66	SQ_{200}	63	25	7	11'315	2'225	0.073	[0.44]	9
BUL1-1 (report)	AqEx							0.52	9
STA3-1-827.93	AD	50	34	8	*9'313*	*2'921*	*0.116*	0.41	10
STA3-1-828.13	SQ_{200}	55	31	8	7'555	2'421	0.118	0.49; 0.54	10
STA3-1-849.98	AD	70	19	11	9'601	3'039	0.117	0.35	10
STA3-1-859.37	SQ_{200}	63	25	6	7'488	2'407	0.119	0.46; 0.48	10
STA3-1 (report)								0.45	10
STA2-1-850.29	SQ_{200}	60	28	6	6'057	2'139	0.130	[0.52]; 0.54	11
STA2-1-895.02	AD	63	25	7	*7'542*	*2'658*	*0.130*	disturbed	11
STA2-1-900.81	AD	70	20	8	8'552	3'026	0.131	0.36	11
STA2-1 (report)								0.47	11
BAC1-1-818.92	SQ	56	27	15	8'647	2'244	0.096	0.51	12
BAC1-1-837.16	SQ	56	30	13	8'123	1'966	0.089	0.56	12
BAC1-1-857.72	SQ	63	27	10	7'619	1'939	0.094	0.58	12
BAC1-1-877.64	SQ	67	24	7	7'362	2'072	0.104	0.57	12
BAC1-1-887.40	AD	61	26	11	10'468	2'759	0.097	0.44	12
BAC1-1-896.50	SQ	68	20	11	7'599	2'329	0.113	0.46	12
BAC1-1-910.21	AD	64	24	10	10'690	2'694	0.093	0.41	12
BAC1-1 (report)	AqEx							0.45 (prelim)	12

The above discussed method-specific differences are similar for boreholes BUL1-1 and STA3-1 in the NL region where chlorinities also differ by 20 – 25% in the Opalinus Clay (Fig. 4-9, Tab. 4-1) between squeezing and advective displacement aliquots. For BUL1-1, also the derived chloride-accessible porosity fractions differ for two of the squeezing samples from those of a nearby advective displacement sample – although by only about 15% (Tab. 4-1). Two other squeezing samples, deeper in the Opalinus Clay, also show a 20 – 25% difference in chloride concentrations (compared to advective displacement) but yield Cl-accessible porosity fractions that are the same as a nearby advective displacement sample (Tab. 4-1, Tab. 5-1). Also, this is a manifestation of an inconsistency within the squeezing data for evaluating f(Cl), referenced to the smooth scaled profiles from aqueous extracts. The chlorinities also differ by 20 – 25% for STA3-1 between the two methods (Fig. 4-9) but in this case also the chloride-accessible porosities differ by about 20% (near 0.5 for squeezing, near 0.4 for advective displacement, Tab. 4-1), and this data set is therefore fully consistent within analytical uncertainties. The situation cannot be clearly assessed for STA2-1 because there is only one reliably datum available from advective displacement in the Opalinus Clay that yields a low f(Cl) of 0.36 compared to averages, but it is also an unusually clay-rich sample (70°wt.-%). For BAC1-1, the chloride concentrations in the AD aliquots are distinctly higher compared to the SQ aliquots by ca. 30%, and the corresponding f(Cl) for the SQ data are correspondingly larger (Tab. 4-1, Gaucher et al. *in prep.*), with one apparent outlier within the SQ data set that yielded a low f(Cl).

There appears to be a small dependence of f(Cl) as a function of chlorinity seen in the data from advective displacement for the NL region (Tab. 4-1): BUL1-1 with highest salinities (14'000°mg/L Cl in AD aliquots) has an f(Cl) of 0.43 – 0.47, whereas at STA3-1 this is 0.35 – 0.41 (9'500°mg/L Cl), and 0.36 (only one datum) at STA2-1 where salinities are slightly lower (8'500 mg/L Cl) than at STA3-1. A similar difference in f(Cl) between BUL1-1 and STA3-1 is also seen in the SQ data but shifted to larger values. Such a difference is what one might expect from theory as detailed in Chapter 3. For BAC1-1, data from advective displacement yield a f(Cl) of 0.41 – 0.44 at salinities of 10'500°mg/L, slightly larger than at STA3-1. This trend is perhaps difficult to corroborate as a hard fact in light of the small number of samples and data ranges, it nevertheless indicates a small dependence of f(Cl) on salinity, that is similar in magnitude as observed by Wigger & Van Loon (2017). These authors derived an averaged increase of 0.03 in f(Cl) for every increase of 0.1 moles of NaCl (3'540°mg/L) between 0.1 and 1 molal NaCl, albeit with a method and evaluation that is quite different from advective displacement or squeezing (see also discussion for JO, Section 4.2.3).

4.2 JO region (Jura Ost)

The siting region Jura Ost (JO) is located in the Deformed Tabular Jura between the autochthonous Tabular Jura in the NW and the Folded Jura in the south (Fig. 4-12). The Deformed Tabular Jura is delineated by the E-W running Jura Main Thrust about 5 km south of BOZ2-1 and the Mandach Thrust (WSW-ENE) about 3°km NNW of BOZ2-1. Tectonically, the Deformed Tabular Jura is compressively overprinted by the Alpine forefront. This is for example manifested by a thrust of the Mesozoic sediments to the north with an estimated transport distance of about 200°m (Egli et al. 2017), which is assumed to have occurred along the Triassic salt layers of the Zeglingen Formation (Muschelkalk; Nagra 2014).

According to seismic interpretations, no relevant faults have been identified in the Mesozoic layers at the borehole locations. However, field and seismic data indicate the occurrence of NNE-SSW striking subvertical strike-slip faults (Madritsch & Hammer 2012). The regional dip of the Mesozoic layers is sub-horizontal towards the SE.

The Bözberg-1-1 (BOZ1-1) exploratory borehole is the fourth borehole drilled within the framework of the TBO project (2020), and Bözberg-2-1 (BOZ2-1) is the fifth borehole drilled (2020/2021). Riniken is an older borehole drilled in 1983/1984 with only limited data produced that is relevant for porewater geochemistry.

The two new boreholes within the JO perimeter reveal a similar lithostratigraphy for the Mesozoic strata and the clay-rich confining units («Brauner Dogger[1]» to Lias) in particular. The borehole depths are 1'037°m for BOZ1-1, 829°m for BOZ2-1, and 1'800°m for the older borehole Riniken. Permian strata (Rotliegend) are present in the Riniken borehole (816 – 1'800°m depth, end of borehole) at the eastern margin of JO, and in TBO borehole BOZ1-1 in the south (below about 990°m) but was not reached in borehole BOZ2-1 that ended in the Zeglingen Fmormation. The Permian strata are part of a WSW-ENE trending large Permo-Carboniferous trough deepening towards the South, encountered in earlier exploratory boreholes Riniken and Weiach (NL), the TBO boreholes MAR1-1 and TRU1-1 of the ZNO region, in the Schlattingen-1 geothermal well further to the ENE, as well as in all four TBO boreholes of the NL region (BUL1-1, STA3-1, STA2-1, BAC1-1). The distribution of anhydrite-rich rocks in the Muschelkalk (Zeglingen Formation) and Gipskeuper is also similar in the boreholes, with a main difference being the occurrence of rock salt (Zeglingen Formation, «Salzlager»): not reached in the BOZ2-1 borehole, only 1.3°m thick in BOZ1-1, and 2.4°m thick at Riniken. The Staffelegg Formation (Lias) underlying the Opalinus Clay is of uniform thickness of 38°m at all borehole locations of JO. The Opalinus Clay is intersected at a uniform thickness of 120 – 122°m, and the Formation's depth is shallowest at Riniken in the east (331 – 451°m), deeper in BOZ2-1 in the northern part of JO (452 – 574°m), and deepest at BOZ1-1 (530 – 651°m) in the south. The Dogger above Opalinus Clay is in the region of the facies change from the clay-rich Klingnau Formation towards the east to the Hauptrogenstein carbonate platform towards the west. Consistent with this facies change, groundwater from the Hauptrogenstein aquifer could only be samples in borehole BOZ2-1 in the northwest of the area. The Malm strata are ca 300°m thick at BOZ1-1 and BOZ2-2, but only 184 m thick at Riniken, and comprise units from the Wildegg Formation to the Villigen Formation. The region is overlain by 25°m of Quaternary strata (Riniken), but none or almost none at BOZ1-1 and BOZ2-1. Molasse rocks are only present at BOZ1-1 (96°m).

Complete geochemical data is contained in the topical Dossier reports for the TBO boreholes, Wersin et al. (2022a) for BOZ1-1, Gimmi et al. (2022) for BOZ2-1, and Matter et al. (1987) for the older borehole Riniken.

[1] Here we use the term «Brauner Dogger» for the Dogger units above Opalinus Clay. In earlier work, the term «Brauner Dogger» was restricted to clay rich units east of the lower Aare valley (ZNO, NL).

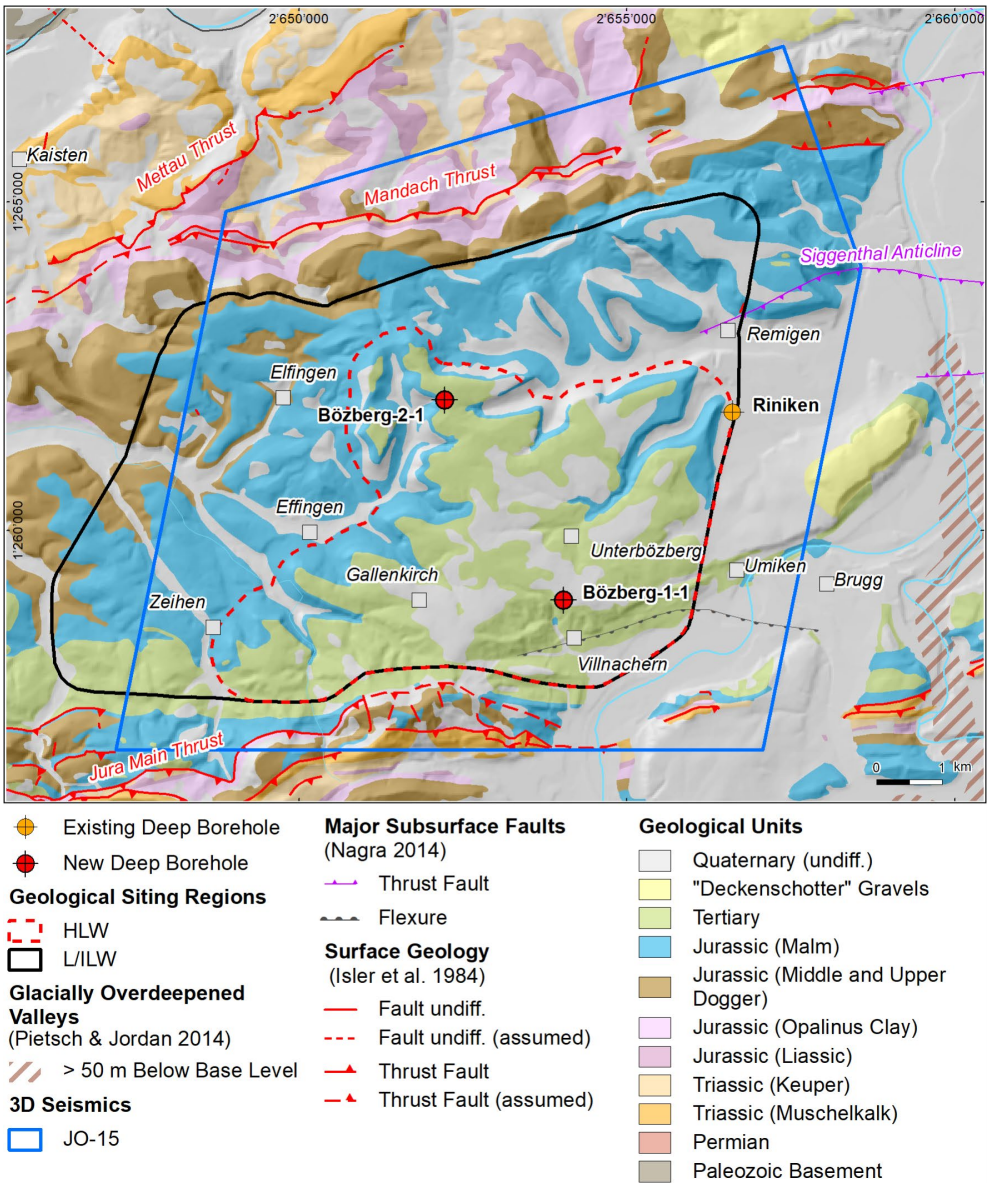

Fig. 4-12: Overview map of the investigation area in the Jura Ost (JO) siting region

Location of boreholes BOZ1-1, BOZ2-1 are marked, and an older borehole Riniken.

4.2.1 Chloride and water stable isotopes in depth profiles for JO

The porewaters in the JO region – at least the central part constrained by the two new deep boreholes – have evolved to display smooth depth profiles for the clay-rich confining units, as constrained by water stable isotope profiles (Fig. 4-13) and the salinity profiles (here shown as chloride, Fig. 4-14). The chloride concentrations are recalculated to the measured water content and thus represent bulk concentrations rather than those present in the free porosity (see subsequent sections for constraints on the latter quantity). The shapes of the bulk porewater profiles are comparable to those defined by the chloride concentrations in the chloride-accessible porosity because the chloride-exclusion effect is not very dependent on clay-content in the clayey confining units (see scaled profiles in Section 4.2.2), with some exceptions.

Both profiles share evidence for the effects of a Keuper aquifer below the confining units, but an overlying aquifer in the Hauptrogenstein was only evident in the BOZ2-1 profile where it was also sampled. The Keuper aquifer at BOZ1-1 could not be sampled but its effect is clearly visible in the $\delta^{2}H$ and $\delta^{18}O$ profiles (Fig. 4-13), and the chloride concentration profile (Fig. 4-14). The shapes of the water stable isotope ratio profiles (Fig. 4-13) are quite different: rather shapeless for BOZ1-1 (with a small Keuper signature), but a much more curved shape culminating in the Opalinus Clay for BOZ2-2. The chlorinity profiles (Fig. 4-14) share more communalities, with some differences in the «Brauner Dogger» but showing only slightly decreasing concentrations with depth across the Opalinus Clay. The absolute chloride concentrations differ significantly (higher in BOZ1-1). Both profiles display a marked gradient across the Staffelegg Formation to very low chloride concentrations (also seen in the groundwater sampled at BOZ2-1).

The mineralogy of these units across the region is also comparable, both in terms of clay mineral content and also the types of clay minerals present. The same is true for the carbonate mineralogy, quartz, feldspars, pyrite, and the absence of sulphates detectable by XRD methods. There is intrinsically more heterogeneity in the overlying Passwang Formation and Hauptrogenstein compared to the Opalinus Clay and the Staffelegg Formation. This – and some variation in chloride-accessible porosity fraction – may be a reason why the data becomes 'noisy' in parts of the overlaying units, and in the uppermost Staffelegg Formation.

Based on these similarities, and the absence of large differences, it is concluded that the JO region contains also similar porewaters within the clay-rich confining units, varying within the observed ranges, and extrapolating spatially over at least short distances (limited by regional faults) according to observed gradients between boreholes. Detailed concentration data are presented and discussed below.

Sulphate concentrations as constrained by the direct sampling methods squeezing and advective displacement are presented in Section 4.2.2. Details of aqueous extracts are reported in the Dossier reports by Wersin et al. (2022a) for BOZ1-1 and Gimmi et al. (2022) for BOZ2-1.

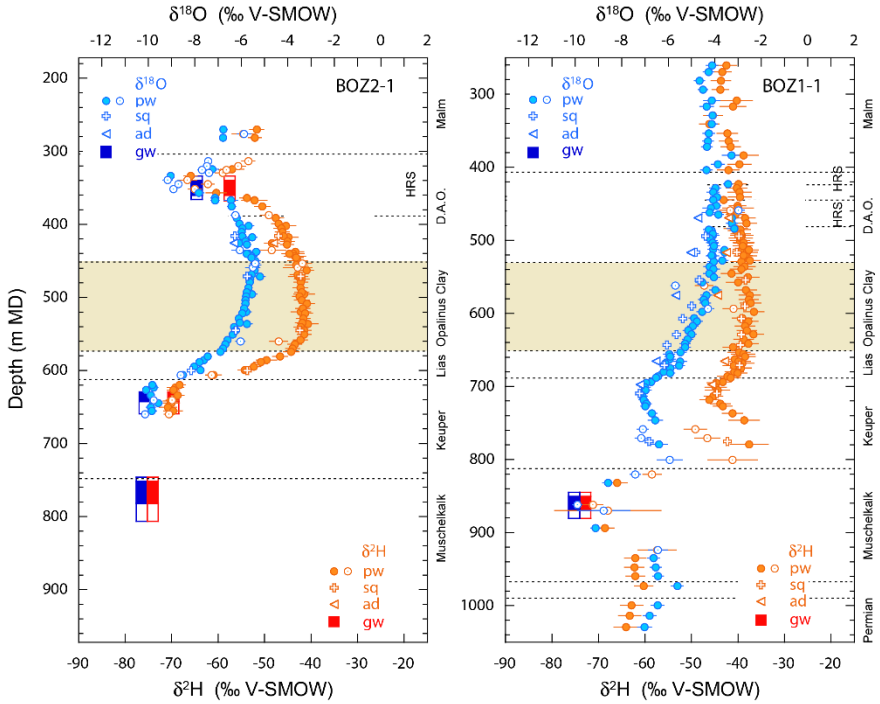

Fig. 4-13: Overview of the pore- and groundwater stable isotope profiles of the JO region

Modified figure based on Gimmi et al. (2022) and Wersin et al. (2022a). Blue: $\delta^{18}O$, orange: $\delta^{2}H$. Porewater data from isotope diffusive exchange (pw, open symbols are less reliable), squeezing (sq) and advective displacement (ad), as well as groundwater data (gw, open rectangles extend over packer interval, symbols show probable inflow zone). Error bars for porewater data represent propagated analytical errors. D.A.O.: Dogger above Opalinus Clay; HRS: Hauptrogenstein.

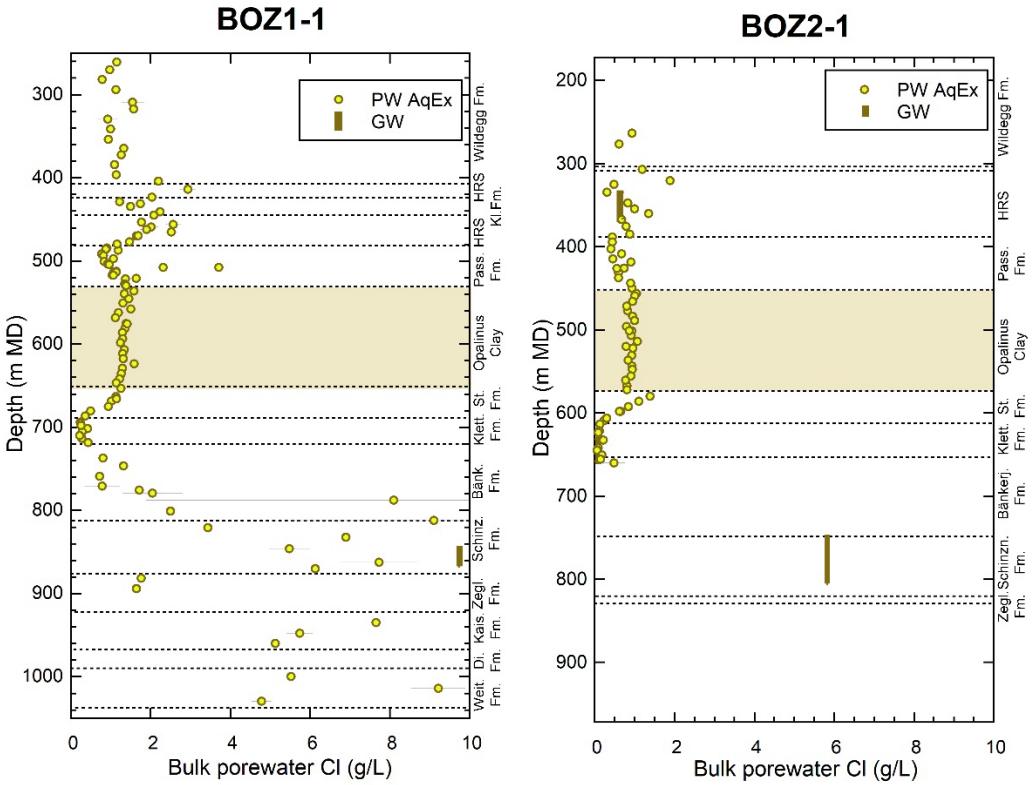

Fig. 4-14: Overview of the chloride concentration profiles (aqueous extracts) of the JO region

Data are scaled to bulk water content, from boreholes at BOZ1-1 (Wersin et al. 2022a) and BOZ2-1 (Gimmi et al. 2022) The profiles are aligned at the level of the Opalinus Clay. Values for aquifers (GW) are provided where known (sampled). HRS: Hauptrogenstein, St. Fm.: Staffelegg Formation.

4.2.2 Chloride and sulphate concentrations in AD and SQ aliquots for JO

As detailed in Section 4.1.2, chloride concentrations are best constrained by measurements from the so-called direct methods, advective displacement (AD) and squeezing (SQ) (Waber et al. 2020 for methods). Data for Opalinus Clay are available for several samples from the two TBO boreholes located in the JO region. To calculate concentrations for conservative components like Cl in the 'free porosity' from aqueous extracts requires knowledge of the Cl-accessible porosity fraction, and this factor can be derived from the direct methods. A chloride-accessible porosity can also be evaluated from through-diffusion experiments that were performed for 33 samples from BOZ1-1.

It is evident in the squeezing and advective displacement data from BOZ1-1 (Fig. 4-15, Fig. 4-16) that there is a systematic and significant difference in chloride concentrations between advective displacement early aliquots and squeezing aliquots (obtained at lowest pressures), with the latter being 20 – 25% lower in chloride concentration. This is very similar to the data obtained from ZNO (TRU1-1, MAR1-1; Section 4.1.2). There is only one sample examined by advective displacement from the Opalinus Clay, but it also shows a distinctly higher chlorinity than all five squeezing samples from OPA. This is also true for data from adjacent strata but there it is less evident due to a larger heterogeneity, also in the chloride-accessible porosity fraction (e.g., discussion in Mäder et al. 2021), and the presence of large concentration gradients in the Staffelegg

Formation. This difference in chlorinities between the two methods cannot be reliably assessed for BOZ2-1 (Fig. 4-16) because only three samples in total were processed for advective displacement, and two of these experiments (one from Opalinus Clay) suffered from an artefact that produced very high initial nitrate concentrations in the outflow (details in Gimmi et al. 2022). The advective displacement sample from the OPA in fact has a slightly lower chloride concentration than the two samples processed for squeezing. A systematic difference in chloride concentrations (seen in BOZ1-1, and all boreholes from ZNO and NL) is in principle not surprising given the contrasting mechanisms by which porewater is mobilised from a core sample: by a large hydraulic gradient in case of advective displacement, and by mechanical compaction implying shear movement and deformation of pore space in case of rock squeezing. Given this systematic difference, the two methods are therefore not probing the same pore sub-volume, and/or are differently affected by experimental artefacts, although in case of chloride, artefacts are thought to be insignificant. The data derived from the two methods do share communalities and in tandem provide important anchor points for the chloride profiles and on other porewater components, like sulphate.

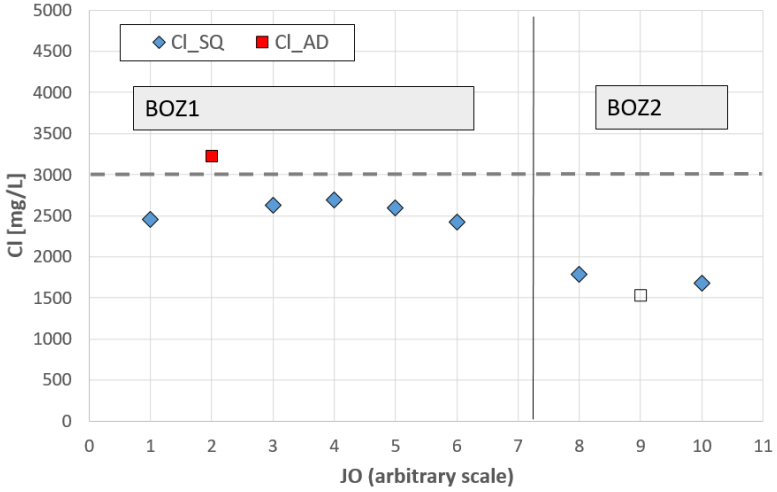

Fig. 4-15: Cl concentrations with data from squeezing and advective displacement for JO

For each borehole, data are arranged in sequence according to borehole depth, from left to right. Open symbols indicate less reliable data (as defined in the respective data reports).

Chloride concentrations from advective displacement and squeezing for the JO region are plotted in combination with chloride concentrations obtained from numerous aqueous extracts scaled to the chloride-accessible porosities with scaling factors as selected in the respective data reports (Fig. 4-16, references therein). Note that through-diffusion data suggest distinctly smaller chloride-accessible porosity fractions that would lead to higher concentrations when scaling aqueous extracts accordingly (see Section 4.2.3 below).

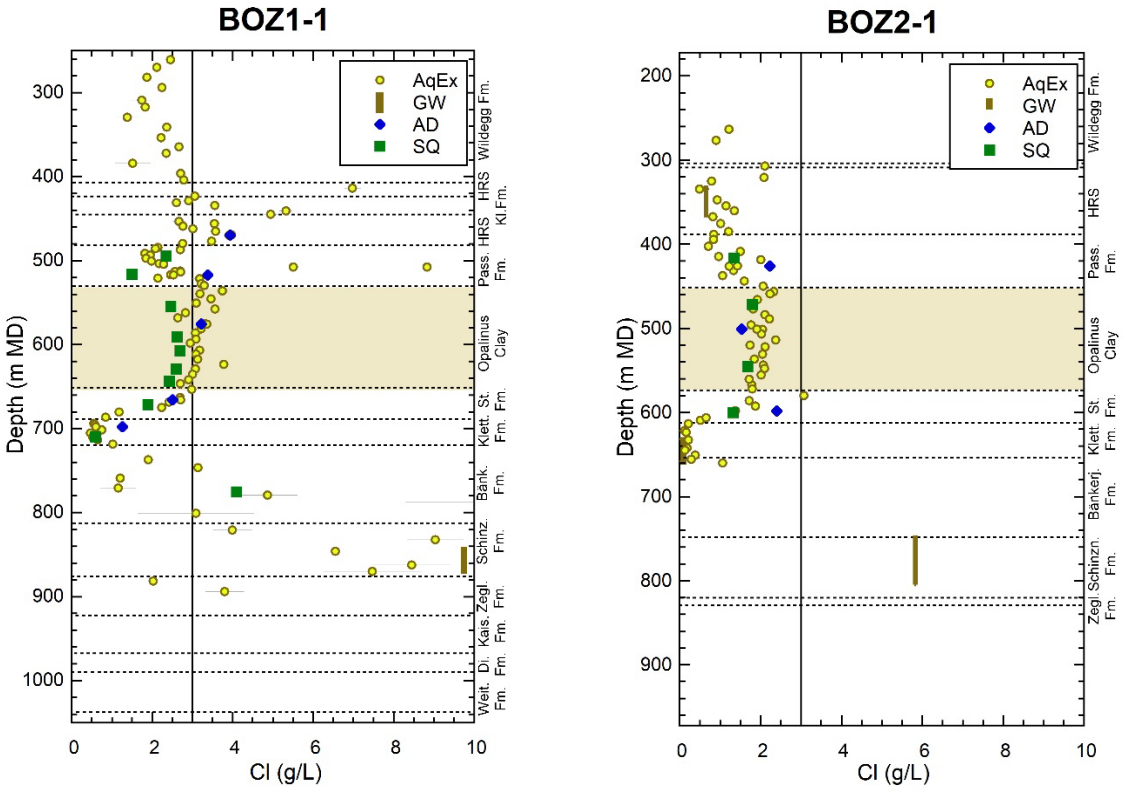

BOZ1-1, f(Cl)=0.42 (clay > 25 wt.-%)

BOZ2-1, f(Cl)=0.42 (clay > 25 wt.-%)

Fig. 4-16: Cl concentration profiles with data from squeezing, advective displacement, aqueous extraction, and groundwater samples for JO

Aqueous extraction data re-calculated to Cl-accessible porosity, f_{Cl}, as indicated. A vertical line is drawn at 3'000 mg/L Cl concentration, the value adopted for the reference porewater for JO. Data from Wersin et al. (2022a) for BOZ1-1, and Gimmi et al. (2022) for BOZ2-1. The depth scale is aligned at the level of the Opalinus Clay.

Some approximate data was derived (Meier & Mazurek 2011) for old samples from the Riniken borehole by aqueous leaching and an estimate of porosity / water content either by measured densities or by a correlation of clay-content with water-content (water contents were not routinely measured in those days). The study evaluated also samples from Opalinus Clay (12 samples, from 335 – 447 m depth), and – when applying a chloride-accessible porosity fraction of 0.5 – yielded porewater chloride concentrations of 2'000 – 4'000 mg/L for 10 samples, with error estimates of about ± 700 – 1'700 mg/L. The chlorinities are therefore on average similar at Riniken (near the eastern boundary of JO) compared to those at BOZ1-1 located 4 km to the SSW, near the southern margin of JO.

In summary, the JO region with BOZ1-1 and BOZ2-1 boreholes, and the older borehole Riniken, has chloride concentrations in the Opalinus Clay of 2'500 – 3'500 mg/L in the southern part (BOZ1-1) and eastern part (Riniken), and somewhat lower concentrations of 1'600 – 2'200 mg/L in the northern part (BOZ2-1). The lower bounds for the chloride concentrations are defined by the squeezing data, whereas the upper bounds by the advective displacement data (no reliable AD data for BOZ2-1). The 3'000 mg/L adopted for the chloride concentration for the reference porewater is representing the chlorinities measured at BOZ1-1, BOZ2-1 and likely also Riniken to within ± 1'500 mg/L.

Sulphate concentrations in JO boreholes obtained from the direct methods squeezing and advective displacement (Fig. 4-17) are more variable than chloride concentrations and are broadly constant across the Opalinus Clay. Concentrations range from 2'200 to 2'700◦mg/L at BOZ1-1 and 1'800 – 2'500◦mg/L at BOZ2-1. A value of 2'600◦mg/L was selected for the reference pore-water for JO, and this value represents the upper range of measurements for samples from squeezing and advective displacement. Note that sulphate concentrations measured in aqueous extracts are larger than the above values, when scaled to water content (bulk porosity, Fig. 4-17 right side), and correspondingly much larger when scaling to an anion/accessible porosity (see discussion in Section 5.8).

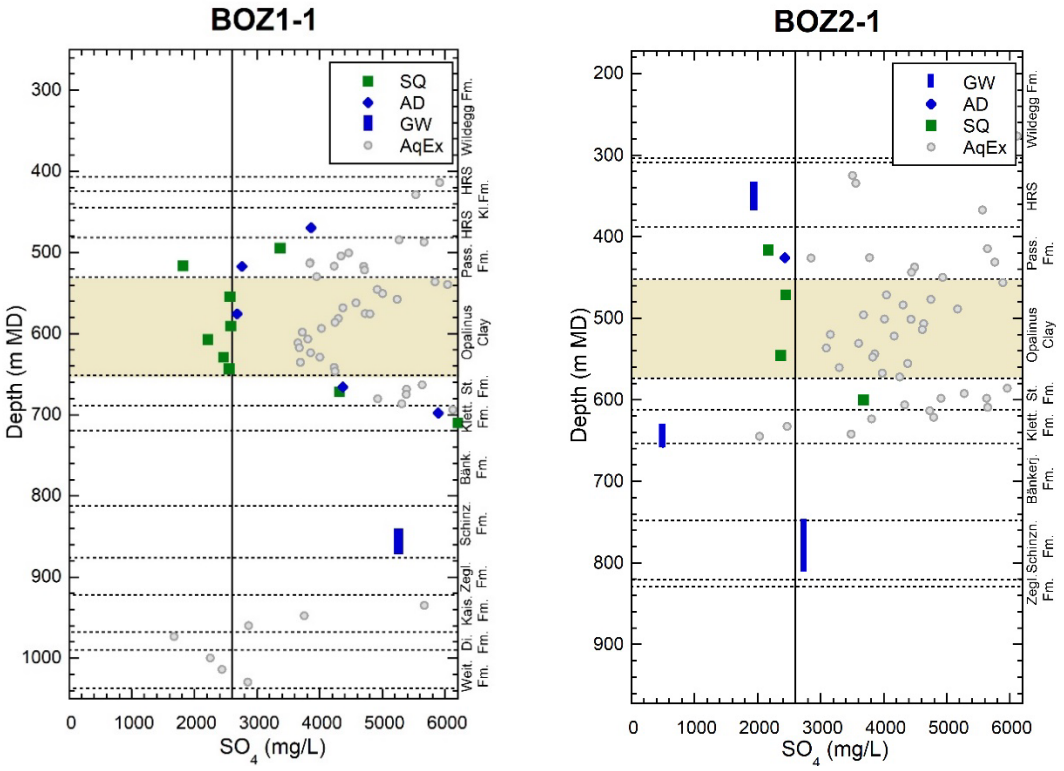

Fig. 4-17: Overview of the sulphate profiles (squeezing and advective displacement) of the JO siting region

Data from boreholes BOZ1-1 (Wersin et al. 2022a) and BOZ2-1 (Gimmi et al. 2022). The profiles are aligned at the level of the Opalinus Clay. Data from aqueous extracts scaled to water content are shown in grey. A vertical line is drawn at the reference SO_4 concentration of 2'600 mg/L.

4.2.3 Constraints on chloride-accessible porosity fraction for JO

The chloride-accessible porosity fraction obtained from rock squeezing is derived by dividing the bulk porewater chloride concentration of a core sample by the chloride concentration of the aliquot squeezed at the lowest pressure. The bulk concentration is derived from the total inventory of chloride related to the initial water content, and the inventory is calculated from the sum of chloride in the squeezed aliquots (at all pressure steps) and the residual chloride derived from a post-mortem aqueous extract (details in Wersin et al. 2022a and Gimmi et al. 2022). An additional

alternate approach was performed for SQ samples for the BOZ2-1 borehole, whereby conventional aqueous extracts were performed on adjacent sample pieces that were not subject to squeezing (Wersin et al. 2022a). The chloride-accessible porosity fraction obtained from advective displacement is simply the ratio of the bulk porewater chloride concentration (derived by averaging aqueous extracts performed from sub-samples located just above and below the core segment used for advective displacement) and the chloride concentration in the earliest aliquots (average of the first two aliquots). There is an additional control on water content by performing post-mortem analyses of the core sample (details in Wersin et al. 2022a and Gimmi et al. 2022).

Chloride concentrations for JO from BOZ1-1 and BOZ2-1 are shown in Fig. 4-15 and Fig. 4-18, and listed for Opalinus Clay in Tab. 4-2. While the two approaches share the same reference for the aliquots, namely the initial inventory of chloride in the bulk porewater, the way this reference is calculated is different. As a consequence of this common reference, the two methods should yield the same chloride-accessible porosity fractions if the chloride concentrations are the same in the squeezing aliquots and those from advective displacement.

Tab. 4-2: Chloride and sulphate concentrations and chloride accessible porosity fraction for Opalinus Clay from advective displacement and squeezing tests, JO

Depth: mid-depth of sample segment; relates to sample ID as used in data reports. AD: advective displacement; SQ_{nnn}: squeezing, with pressure indicated (MPa); f_{Cl}: chloride-accessible porosity fraction; data in italics are less/not reliable as defined in the data reports; references: (1) Wersin et al. (2022a); (2) Gimmi et al. (2022); second value given for SQ: f_{Cl} evaluated by conventional aqueous extract (second value listed); numbers in italics: likely disturbed Cl and SO_4 due to high nitrate, (a) f_{Cl} derived from end of long-term experiment (Gimmi et al. 2022).

Borehole/Depth [m]	**Method [MPa]**	**Clay [wt.-%]**	**Qz-Fsp [wt.-%]**	**Carb [wt.-%]**	**Cl [mg/L]**	**SO_4 [mg/L]**	**SO_4/Cl [mol/mol]**	**f_{Cl}**	**Ref**
BOZ1-1 554.36	SQ_{200}	58	28	8	2'458	2'565	0.39	0.47	1
BOZ1-1 575.26	AD	45	39	12	3'224	2'681	0.31	0.42	1
BOZ1-1 590.32	SQ_{200}	60	31	5	2'623	2'576	0.36	0.47	1
BOZ1-1 607.13	SQ_{200}	64	27	6	2'690	2'212	0.30	0.41	1
BOZ1-1 629.09	SQ_{200}	65	23	5	2'591	2'459	0.35	0.46	1
BOZ1-1 643.35	SQ_{200}	65	23	6	2'427	2'552	0.39	0.42	1
BOZ2-1 471.15	SQ_{200}	62	28	8	1'790	2'444	0.50	0.47; 0.39	2
BOZ2-1 500.93	AD	52	33	10	*1'533*	*1'602*	*0.39*	0.45	2 (a)
BOZ2-1 545.15	SQ_{200}	50	41	7	1'678	2'366	0.52	0.46; 0.49	2

Tab. 4-2 is a summary of the chloride-accessible porosity fractions as reported for BOZ1-1 (Wersin et al. 2022a) and BOZ2-1 (Gimmi et al. 2022). The averaged Cl-accessible porosity fraction adopted by Wersin et al. (2022a) for BOZ1-1 is 0.42, a value that coincides with that derived for the single advective displacement sample and is about 10% smaller than the average value obtained for squeezing samples from Opalinus Clay (0.45). The difference between the chloride concentration measured in the advective displacement sample and the average from squeezing is 25%, much larger than that in the derived chloride-accessible porosity fractions. It is for this reason that the scaled aqueous extracts plot on the data point of the advective displace-

ment sample, but significantly above the ensemble of the squeezing samples (Fig. 4-16). As discussed in Section 4.1.3 (ZNO-NL) this is a manifestation of a data inconsistency within the squeezing data, most likely related to an underestimation of the chloride inventory of the samples.

For samples from BOZ-2, the chloride inventory for squeezing samples was additionally and independently evaluated by conventional aqueous extracts on un-squeezed material, and therefore two values for *f*(Cl) can be derived (Tab. 4-2). There is no reliable chloride concentration available from advective displacement due to some artefact related to mobilisation of nitrate (details in Gimmi et al. 2022), but a chloride-accessible porosity fraction could be derived from evaluating the latest stage of one long-term experiment. The *f*(Cl) adopted by Gimmi et al. (2022) was 0.42 and the scaled aqueous extracts (Fig. 4-16) plot at the location of the constraining concentrations from squeezing and advective displacement. There is no data inconsistency for *f*(Cl) for the BOZ-2 data set from squeezing (see also Fig. 4-18).

A large difference is seen for BOZ1-1 when comparing chloride-accessible porosity fractions obtained by advective displacement or squeezing with values derived from through-diffusion experiments performed at PSI (Fig. 4-18, Van Loon & Glaus *in prep*., data also shown in Wersin et al. 2022a). The *f*(Cl) derived from diffusion tests range from 0.25 – 0.30 for 9 samples for Opalinus Clay. This large difference is presently not understood. The squeezing and advective displacement tests yield *f*(Cl) for JO that are rather similar to those obtained for ZNO and NL, and only slightly smaller on average. The corollary of such small chloride-accessible porosity fractions would be significantly higher calculated chloride porewater concentrations for JO when scaling the concentrations from aqueous extracts accordingly, and when adopting the same simplified concept of total chloride exclusion in the porosity affected by the charged clay mineral surfaces (e.g., the balance of the 'free porosity' to total porosity, representing the chloride-inaccessible porosity). According to theory (and observed in smectite-dominated bentonite) the thickness of diffuse layers should increase with decreasing ionic strength (less shielding of the surface charge). There is only one study (Wigger & Van Loon 2017) examining through-diffusion of HTO and ^{36}Cl as a function of NaCl ionic strength on the same sample of Opalinus Clay (Schlattingen-1 borehole). They observe an increase in the chloride-accessible porosity fraction from 0.35 ± 0.06 at 0.1 M (3'540 mg/L) to 0.61 ± 0.09) at 1 M NaCl. Assuming this gradient to be linear, an increase of 0.03 in Cl-accessible porosity fraction may be expected for every 0.1 M increase in ionic strength. This seems to be a much smaller gradient than may explain the apparent discrepancy observed between the diffusion data and that from advective displacement and squeezing. In conclusion, the strongly reduced Cl-accessible porosity fractions obtained from diffusion data compared to SQ and AD are difficult to reconcile but cannot be ruled out at the present stage.

Note that the concentration of 3'000 mg/L for chloride adopted for the reference porewater was chosen to represent the upper range measured for the direct methods (Fig. 4-16) and this accounts at least partially for a possibility that *f*(Cl) values may indeed be smaller than derived from the direct methods, in comparison to those obtained from the through-diffusion experiments.

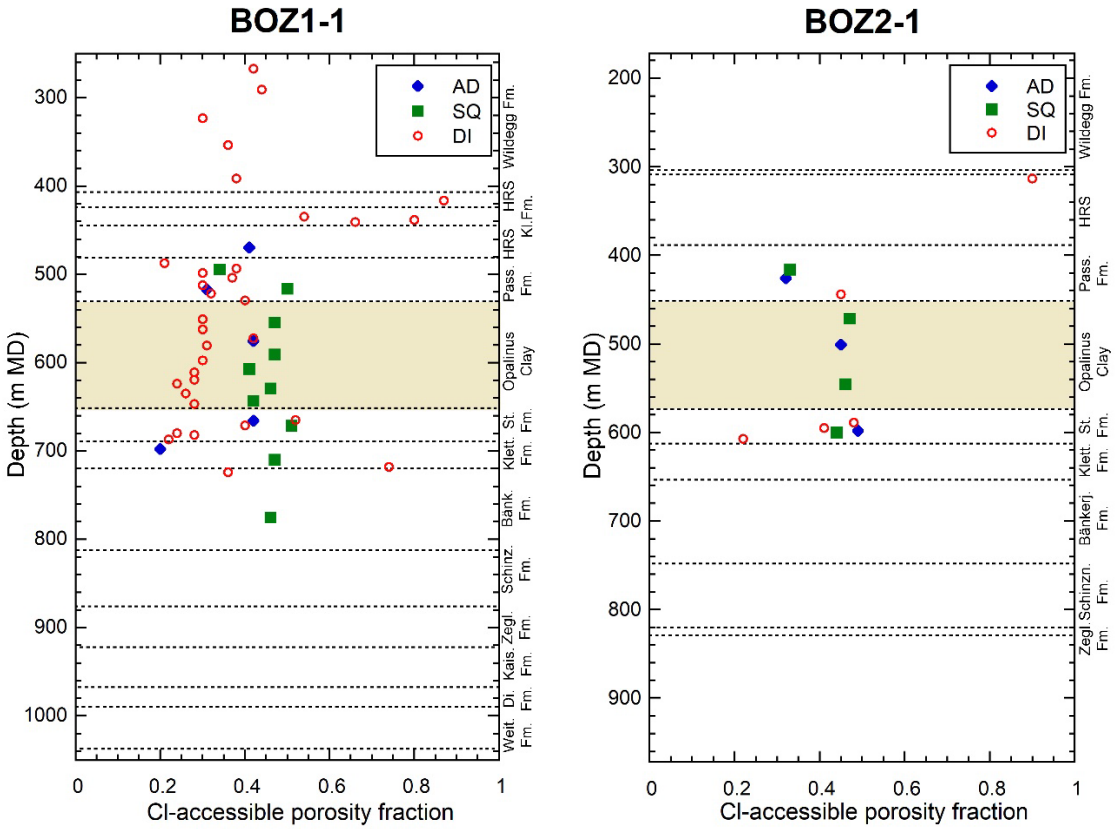

Fig. 4-18: Chloride-accessible porosity fractions for BOZ1-1 and BOZ2-1 for JO

Data from through-diffusion tests performed at the Paul Scherrer Institut are included (Van Loon & Glaus in prep.). Data for advective displacement (AD) and squeezing (SQ) from Wersin et al. (2022a) for BOZ1-1, and Gimmi et al. (2022) for BOZ2-1. HRS: Hauptrogenstein, St. Fm.: Staffelegg Formation.

4.3 Composition of groundwaters in bounding aquifers for ZNO, NL and JO regions

The concentrations of chloride measured in the bounding aquifers of the Malm and the Keuper aquifers (where sampling was possible) are indicated in the figures of the depth profiles (Fig. 4-8 for ZNO; Fig. 4-9 for NL). Likewise, the chloride concentrations for the Hauptrogenstein and Keuper aquifers, where present / sampled, are plotted in Fig. 4-16 for the two boreholes near Bözberg (JO). Note that these groundwater compositions are derived from pumped samples mixed with drilling fluid to various degrees (usually a time-series is taken), and some had been corrected to an uncontaminated state by procedures detailed in dedicated reports. Data shown here were adopted from the Dossier-VIII reports and – at least for chloride – are corrected and represent final values for all but possibly the latest boreholes were some of this correction work may still be in progress (corrections are rather small).

The groundwater compositions per se have no influence on how the reference porewater is defined. The reference porewaters for Opalinus Clay relates to the smooth formation-scale profiles established at all borehole locations (Fig. 4-8, Fig. 4-9, Fig. 4-16) and approximately capture the present-day composition of these porewaters within the Opalinus Clay. Clearly, these formation-scale profiles have evolved over geologic time, affected among other factors by the

bounding aquifers above and below the clay-rich confining units in between them. There are dedicated reports about the details of the sampled groundwater compositions for each borehole with key data represented in the Dossier-VIII reports cited in this work, and a regional summary of all earlier deep groundwaters (established from many additional locations and sources of information) is provided in Waber & Traber (2022).

4.4 Composition of the clay exchanger for ZNO, NL and JO regions

The composition of the clay-exchanger for a core sample is determined by cation-selective aqueous extraction techniques whereby both, the cation exchange capacity but also the cation occupancy are determined. A large number of samples was analysed for each borehole (except for BAC1-1) at the Paul Scherrer Institut (Baeyens & Fernandes 2022), including 5 – 9 samples of Opalinus Clay for each borehole, and using Cs^+ and Ni-en as the indexing cation. A smaller and variable number of samples were processed at the University of Bern using Ni-en as the indexing cation. The data from the University of Bern along with a short summary of the data from PSI are reported in the respective Dossier-VIII reports (ZNO: Aschwanden et al. 2021, Mäder et al. 2021; NL: Mazurek et al. 2021, Aschwanden et al. 2022, Zwahlen et al. *in prep.*, Gaucher et al. *in prep.*; JO: Wersin et al. 2022a, Gimmi et al. 2022).

There are some differences in the data obtained that are related to the different methodologies: the Cs-method allowed determining also exchangeable ammonium (NH_4^+) and also TIC in the selective extracts, that is a measure of calcite dissolution that may have occurred during extraction. The correction schemes for cation contributions from porewater and mineral dissolution applied by the two laboratories are therefore somewhat different. The University of Bern corrected either just Na to match measured Cl+SO_4, or Na for Cl and Ca for SO_4. Data from PSI (Baeyens & Fernandes 2022) were corrected for Na to match Cl+SO_4 or treated SO_4 differently if dissolution of a sulphate phase was indicated. Data from PSI were additionally corrected for measured TIC to correct Ca accordingly. Note that in case of PSI data, extractions were carried out at a much lower solid/liquid ratio compared to Uni Bern data, resulting in a higher amount of carbonate mineral dissolution. The two data sets generally show a good overall consistency, with the exception of exchangeable potassium that is significantly larger in the Cs-extracts (PSI) compared to the Ni-en extracted data set (Uni Bern). More details and discussions are provided in the references given above.

Fig. 4-19 shows all cation selectivity measurements obtained for Opalinus Clay from the PSI laboratory (dashed lines) and from the University of Bern (solid lines). Data are shown as equivalent fractions, and the following correction schemes are applied: Na for Cl and Ca for SO_4 (porewater contribution), and for PSI data, also Ca is corrected for TIC (contribution from calcite dissolution). Well visible is the above mentioned systematically larger potassium occupancy in the PSI data set, and a systematic difference in the Ca occupancy, but more pronounced for the data from the NL and ZNO regions (lower Ca occupancies in the PSI data set). The significantly larger potassium occupancy in the PSI data set has a scaling effect and lowers the other cation fractions in proportion, relative to the Uni Bern data set. This is seen in the Na occupancy but also explains a part of the difference in the Ca occupancy. Other than that, all data sets across the three regions are rather similar in terms of the composition of the clay exchanger. Accordingly, one may also expect that the porewaters share communalities with respect to major component cation ratios (and Sr as a minor component). Some more details are provided and discussed in Section 5.3 where specifically Ca/Mg ratios are discussed.

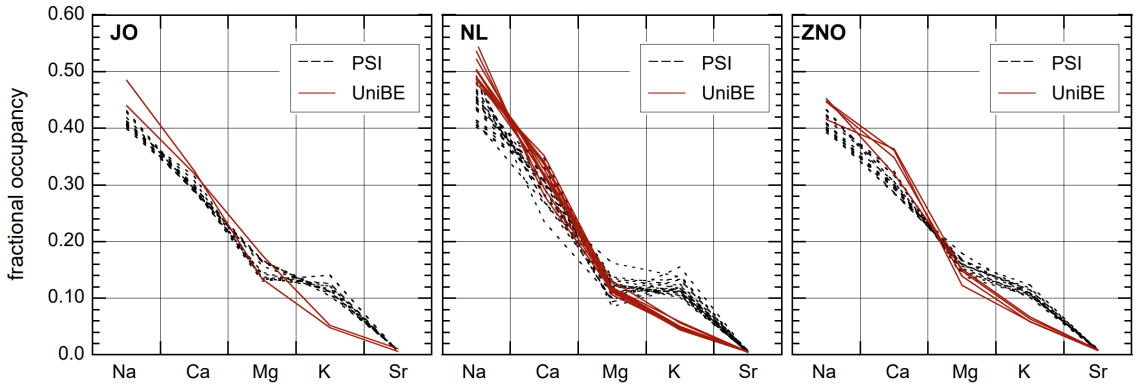

Fig. 4-19: Composition (equivalent fractions) of the clay exchanger for ZNO, NL and JO

Data as reported in Dossier-VIII reports, including data from PSI (dashed lines, reported also separately in Baeyens & Fernandes 2022). Na is corrected for Cl, and Ca for SO_4 (for PSI data additionally Ca for TIC).

4.5 Partial pressure of CO_2 in ZNO, NL and JO regions

Both, pH and the partial pressure of CO_2 (and also alkalinity / total inorganic carbon) in a clay-rock, react sensitively to disturbances, including those related to drilling, sampling, pressure-temperature changes, preservation, storage and sample preparation for laboratory tests (e.g., pore-water squeezing, advective displacement, out-gassing experiments of CO_2). The close coupling of pH-P_{CO2} via carbonate equilibria (and also a coupling via Ca to the clay exchanger and Ca-SO_4 system, of lesser importance) makes this pair of correlated parameters difficult to constrain by measurement or modelling interpretation. The coupling is such that an increase in one order of magnitude of P_{CO2} corresponds to a decrease of 0.5°pH units, e.g. when using the model elaborated below. This situation had led to a practice of bracketing P_{CO2} – and thus also pH – between limits established by multiple lines of evidence (interpreted measurements) and/or by models including aluminosilicates (a subset of end-member clay minerals) that fix pH-P_{CO2} by solubility constraints according to the Gibbs phase rule (see Chapter 5 for details).

Mäder (2009) adopted a value of $10^{-2.2}$°bar for P_{CO2} for a generic reference porewater for Opalinus Clay and «Brauner Dogger», the same value as proposed by Pearson et al. (2003) and Waber et al. (2003) for Opalinus Clay at Mont Terri and Benken, respectively. This value is associated with uncertainty and reflects an expert decision based on geochemical reasoning. Uncertainties were large at that time, in part also due to methods that were not yet fine-tuned to these delicate clayrock systems (e.g., protection from atmosphere, required sample mass for analysis, minimised dead volumes, measurement techniques). As detailed in Pearson et al. (2011), Wersin et al. (2020) and Wersin et al. (2022b) significantly more good-quality data became available from the Mont Terri rock laboratory and the deep borehole at Schlattingen-1. This included three out-gassing experiments with Opalinus Clay samples from Schlattingen-1 that yielded equilibrated partial pressures of CO_2 from $10^{-2.2}$ to $10^{-2.3}$°bar. Wersin et al. (2020) propose a range from $10^{-2.0}$ to $10^{-3.0}$°bar for Mont Terri based on aliquots from long-term borehole sampling and outgassing experiments. Wersin et al. (2022b) compiled a range of $10^{-1.7}$ to $10^{-2.9}$°bar (most data cluster between $10^{-2.0}$ and $10^{-2.5}$°bar) from the most reliable borehole water samples and P_{CO2} measurements across Opalinus Clay at Mont Terri. Benken is not well constrained by direct measurements.

The interpretation of squeezing aliquots and those from advective displacement may also yield constraints on P_{CO2}, and there is a substantial amount of data from all TBO boreholes except for RHE1-1. These aliquots are invariably strongly supersaturated with respect to calcite, and

squeezing samples also have strongly elevated pH values. A simplest possible interpretation is that this calcite supersaturation is a result of outgassing of CO_2 during either the experiment and/or during storage or measurement of the aliquots. Under this assumption, calcite saturation may be restored by modelling, whereby CO_2 is added until calcite saturation is reached. This will increase P_{CO2}, lower the pH, but is keeping the carbonate alkalinity constant. The procedure is detailed, for example, in Wersin et al. (2022a) for borehole BOZ1-1. This level of detail in data interpretations has not yet been completed for all boreholes, but preliminary results indicate that squeezing aliquots, when corrected as outlined above, yield partial pressures of CO_2 of $10^{-1.5}$ to $10^{-2.7}$°bar, with a corresponding pH range from 6.6 – 7.6. Aliquots from advective displacement tend to cluster at somewhat higher P_{CO2} values and at a slightly lower pH range, when treated the same way.

Note, that CO_2 outgassing during the experiments and sample storage is likely not the only process affecting the composition of these aliquots. Specifically, pressure-induced calcite dissolution during squeezing may modify aliquot compositions (pH, P_{CO2}, alkalinity, Ca), as suggested by Wersin et al. (2013, 2020) and Mazurek et al. (2015). Likewise, also processes such as mineral dissolution/precipitation and microbially induced artefacts may operate during advective displacement experiments.

Strictly speaking, the measurements cited above do not directly relate to the partial pressure of CO_2 in the undisturbed state, but to either borehole conditions, or the state of a core sample that is being tested. The clayrock-porewater system is effectively buffered to a considerable extent (carbonate equilibria, cation ion exchange capacity) and it is therefore believed that the measurements also relate to an undisturbed state, but there remains some uncertainty because the exact processes that operate during disturbances are not accurately known. The potential effect of temperature is specifically addressed in Chapter 5.

In conclusion, the adopted value for P_{CO2} of the reference porewater of $10^{-2.2}$°bar represents best available information, and the high-P_{CO2} and low-P_{CO2} variants with $10^{-1.8}$°bar and $10^{-2.8}$°bar, respectively, bracket most measurements and account for remaining uncertainties. The corresponding pH range is 6.87 – 7.37 for ZNO-NL, and 7.13 – 7.65 for JO (Chapter 5). Note that this pH range is the outcome of modelling, with the input being the adopted range in P_{CO2} and the combined mineral saturations constraints, an approximate exchanger population, and pre-scribed concentrations of chloride and sulphate.

5 Model for reference porewaters for the ZNO-NL and JO regions

A consistent modelling approach was chosen for ZNO-NL and the JO region based on equilibrium thermodynamics. As elaborated further below, a reference case was modelled for each region, and key uncertainties were addressed by porewater variants with bounding values of key parameters, also generated with the same model.

5.1 Choice of thermodynamic database

Ideally, all modelling interpretations of porewater and groundwater data, solubility and sorption calculations for radionuclide species, as well as reactive transport calculations (near-field, far-filed) should be based on the same thermodynamic database (TDB), including all relevant minerals, gases, aqueous species, surface complexes and their dependence on temperature and pressure of interest. In addition, a reliable activity model for aqueous species valid up to the pertinent concentrations (ionic strength) should be used. Such a situation has not yet been achieved owing to in part contrasting requirements and a tendency for specialisation within the respective disciplines. Specifically, the interpretation of deep groundwaters may require a larger temperature and pressure range, as well as higher concentrations, e.g. in aquifers containing Ca-sulphate minerals or halite. This is not the case for reference porewaters in the clay-rich confining units, or for radionuclide solubility and speciation calculations in these porewaters, particularly in case these are being performed at a reference temperature of 25 °C and pressure of 1 bar.

A newly released, enlarged and updated PSI/Nagra thermodynamic database (PSI Chemical Thermodynamic Database 2020, Version 1-3; Hummel & Thoenen 2023), has been significantly expanded in terms of radionuclide species, some mineral phases such as layer silicates, and temperature dependences have been implemented for a subset of the chemical composition space. This review is largely (but not exclusively) based on recommended values continuously released in the framework of the NEA TDB project. In order to extrapolate conditional constants to zero ionic strength, the SIT (specific ion-interaction theory) model has been adopted for electrolyte ion interaction (activity coefficients), replacing earlier versions that used extended Debye-Hückel-type activity models such as the Davies equation or the WATEQ Debye-Hückel equation (also named Truesdell-Jones Debye-Hückel equation). Apart from a change of the activity model, also many minerals of the former core-data set have been modified (log-K values), such as for calcite, dolomite, gypsum, anhydrite, celestite, among others. The core data set includes main components of a porewater, with some key-minerals and species that are thought to be well constrained, and that normally do not differ significantly in different databases (e.g., WATEQ4F / PHREEQC, THERMOCHIMIE, older PSI-Nagra versions etc.). The present situation is that this revised database does not contain the functionality for interpretation of deep groundwaters, and its use for porewater calculations is somewhat hampered by some significant differences (from an application point of view) compared to earlier versions of the core data set. The use of this database was requested by Nagra in order to assure a consistent approach with the modelling of radionuclide speciation and solubility.

A decision was therefore made to perform the reference porewater calculations also with two earlier versions of the PSI-Nagra database, one being used for groundwater interpretation, and one that is currently used for speciation and saturation calculations of the findings of the current TBO deep boreholes (all borehole-specific geochemical data reports, Dossier VIII). The former database represents one of the early versions of the PSI-Nagra developments that did contain temperature dependencies for the relevant groundwater components and minerals. Both of these earlier versions give very similar results, because the thermodynamic properties are nearly identical for the core data, with a main difference being the use of different ion activity models

(WATEQ Debye-Hückel vs. Davies). The database used for speciation calculations for the TBO geochemical data was also used in earlier versions of radionuclide solubility and speciation calculations performed in the past, and for designing synthetic porewater compositions for TBO laboratory experiments that required such a test solution (e.g., through-diffusion experiments). There is also a 4th set of calculations for the reference porewaters performed using the WATEQ4F database that is nearly identical to the PHREEQC database but with more chemical components. This database is also very similar to the earlier versions of the PSI-Nagra database. While the earlier PSI-Nagra TDB versions and the WATEQ4F TDB give nearly identical reference pore-water compositions, the new PSI-Nagra thermodynamic database 2020 (v1-3) does result in some notable differences, but that are not large in absolute terms for major and minor components (see discussion of results). These differences are a consequence of revised log-K values for many mineral phases of the core data set, but also due to the adoption of the SIT ion activity model. The THERMOCHIMIE and THERMODDEM databases were used for calculations at elevated temperatures in this report (Chapter 5).

The different thermodynamic databases used for this report are:

- NAPSI_290502.DAT (Nagra / PSI Chemical Thermodynamic Data Base Version 01/01) (Hummel et al. 2002)
- PSINA_110615_DAV_s.dat (The PSI/Nagra Chemical Thermodynamic Database Version 12/07) (Thoenen et al. 2014)
- PSINagra2020v1-3.dat (PSI Chemical Thermodynamic Database 2020, Version 1-3) (Hummel & Thoenen 2023)
- WATEQ4F thermodynamic database from the PHREEQC software distribution (Parkhurst & Appelo 1999)
- THERMOCHIMIE (Version 11a, Rodriguez et al. 2022), THERMODDEM (Blanc et al. 2012)

All TDBs are provided in a format compatible with the PHREEQC geochemical modelling soft-ware (Parkhurst & Appelo 1999, 2013, Version 3.4.6), and are thus based on log-K values (minerals, gases, aqueous species), and on an electrolyte ion activity model (for obtaining activity coefficients), but do not contain data for surface reactions (surface complexation, ion-exchange). Temperature dependencies of log-K values – if present – are implemented as a temperature grid in log-K, as explicit polynomial equations, or as an enthalpy of reaction (Van't Hoff relationship), depending on the type of the TDB and availability of data. The ion activity models are:

- WATEQ Debye-Hückel equation for NAPSI_290502.DAT, WATEQ, THERMOCHIMIE and THERMODDEM
- Davies equation for PSINA_110615_DAV_s.dat
- SIT parameters for PSINagra2020v1-3.dat

The NAPSI_290502.DAT database uses the WATEQ Debye-Hückel parameters if they are provided and is adopting the Davies equation if no other parameters are given. Dissolved gases and neutral electrolyte species are assigned unity activity coefficients for versions using the DAVIES equation or the SIT model, but are assigned an activity coefficient >1 in case of the WATEQ Debye-Hückel model, where a type of Sechenov relationship is implemented (salting-out effect, increasing activity coefficient with increasing ionic strength, simply the $b_i \cdot I$-term in the equation below, when z is set to 0).

$$log\gamma_i = -\mathrm{A}z^2\left(\frac{\sqrt{\mathrm{I}}}{1+Ba_i\sqrt{I}}\right) + b_i I \quad \text{WATEQ Debye-Hückel or Truesdell-Jones D-H}$$

In the equation above, A and B are solvent constants (but temperature-dependent), a_i and b_i are ion-specific parameters (ion-size parameter and an empirical parameter), I is the effective ionic strength, and z_i is the charge of the ion.

$$log\gamma_i = -Az^2\left(\frac{\sqrt{I}}{1+\sqrt{I}} - 0.3I\right) \quad \text{Davies}$$

The Davies equation is a simplification, omitting the ion-size parameter (setting $B{\cdot}a_i = 1$), and substituting $[b_i/(Az^2)]$ with 0.3. The Davies equation is clearly less flexible, and this is a limiting factor, particularly for divalent ions such as Mg^{2+}, Ca^{2+} and SO_4^{2-}, where differences between activity coefficients are already notable at moderate ionic strength below that of seawater. Literature (e.g., Langmuir 1997) generally attests the Davies equation a range of applicability to 0.5 – 0.7◦molal ionic strength, and about 1 – 2◦molal for the WATEQ Debye-Hückel equation (especially in NaCl-dominant electrolytes).

In the SIT model, the ion activity coefficients are based on a Debye-Hückel term with an extension constructed from binary interaction parameters for all complexes that involve the ion of interest. It is somewhat similar to the Pitzer model used for concentrated electrolytes, but it is based on a full speciation model rather than on components (and few additional species where needed). The interaction parameters are fitted to experimental data or derived from estimation schemes.

$$log\gamma_i = -\frac{0.51\sqrt{I}}{1+1.5\sqrt{I}} + \sum_k \epsilon_{ik} m_k \quad \text{SIT model}$$

In the equation above, ϵ_{ik} are the SIT binary interaction parameters for all complexes including the ion of interest, and with a molal concentration m_k. The equation collapses to a simplified extended Debye-Hückel formulation if no binary interaction parameters are provided. One advantage of the SIT model is that it potentially may be valid to higher concentrations compared to other models, but it does require experimental data or correlations to derive the empirical interaction parameters. Because of a lack of an ion-size parameter, it is less accurate at lower ionic strength compared to the Davies or WATEQ Debye-Hückel equations.

The effect of the different ion activity models on the activity coefficients for divalent species appears to be systematic at the compositions and ionic strength of the reference porewater for ZNO-NL and JO: smallest activity coefficients for the SIT model, intermediate for the WATEQ Debye-Hückel model, and largest for the Davies model. This was tested in an exploratory mode for Mg^{2+}, Ca^{2+}, CO_3^{2-} and SO_4^{2-}, and the spread was largest for sulphate, and less for the cations and carbonate. The corollary of these systematic differences is that ion activity products relevant for mineral solubility, such as $[Ca^{2+}][SO_4^{2-}]$ (gypsum, anhydrite), $[Sr^{2+}][SO_4^{2-}]$ (celestite), $[Ca^{2+}][CO_3^{2-}]$ (calcite), and $[Ca^{2+}][Mg^{2+}][CO_3^{2-}]^2$ (dolomite) multiply this effect and become notably smaller with data from the revised PSI-Nagra TDB, implying that concentrations are increased to satisfy the respective mineral saturations. For groundwaters, this implies that compositions that were previously (older TDB with WATEQ Debye-Hückel model) concluded to be at saturation with gypsum or anhydrite, for example, are now slightly undersaturated with the revised TDB.

Different databases were used in order to evaluate the impact on the resulting porewater concentrations. Differences and their effects are thus fully documented and are available to the user of such reference porewater compositions.

5.2 Selectivity coefficients for ion-exchange equilibria

The selectivity coefficients for modelling ion-exchange were adopted either form literature (recent porewater modelling) or from a generic data set included in the PHREEQC default thermodynamic database, based on work by Appelo & Postma (2005). Modellers use several alternate formalisms for treating ion exchange. A reason for this is that there is a lack of a theory

for ion activity coefficients for ion-exchange complexes. This leads to the use of so-called conventions for formulating the ion-exchange equilibria, and these may even be used in combination with the ion-activity coefficients calculated for the corresponding electrolyte species (e.g., WATEQ Debye-Hückel equation). PHREEQC is a flexible geochemical modelling tool that allows the implementation of different conventions and additional activity coefficients. Normally, some kind of consensus evolves with the continued application of these models to experimental data for a particular rock type, such as Opalinus Cly. There is uncertainty in these apparent ion-exchange equilibrium constants because the underlying experiments (determination of cation population on the exchanger by aqueous extracts with a complexing agent) are relatively involved and require some corrections (e.g., Waber et al. 2020, Wersin et al. 2013).

There is also a choice of conventions available that deal with the issue of relating the activities of cations on the exchanger to their mole fraction on the exchanger (the quantity that can be measured). Here, we adopt a commonly used convention that uses the equivalent fractions as activities and the exchange half-reactions are formulated according to the Gaines-Thomas convention. There is no agreement as to the values of the log-*K* values (distribution coefficients) for these exchange reactions, and there is a flurry of choices and conventions adopted in literature.

There has been an early effort done by Pearson et al. (2003) by comparing measurements of log-*K* values for K, Mg, Ca, Sr and in part NH_4 relative to Na, obtained by different laboratories (Tab. 5-1), obtained at chloride concentrations > 200 mmol/L. Also listed are the generic values by Appelo & Postma (2005) (provided with PHREEQC Database).

Tab. 5-1: Summary of ion-exchange constants reported by Pearson et al. (2003)

Samples form Opalinus Clay from the Mont Terri rock laboratory, based on laboratory analyses by CIEMAT, PSI, Uni Bern and BRGM, and using the PHREEQC Database and the Gaines-Thomas convention.

	Uni Bern > 0.2 mol Cl^-		**CIEMAT**		**PSI**	**BRGM 1-site model**	**PHREEQC Database Parkhurst & Appelo (1999)**
	Mean	SD	Mean	SD			
log $K_{H\text{-}Na}$						1.5	
log $K_{K\text{-}Na}$	0.75	0.05	0.84	0.01	0.70	0.63	0.7
log $K_{NH4\text{-}Na}$						0.62	0.6
log $K_{Ca\text{-}Na}$	0.70	0.02	0.79	0.04	0.67	0.80	0.8
log $K_{Mg\text{-}Na}$	0.57	0.05	0.60	0.07	0.59	0.62	0.6
log $K_{Sr\text{-}Na}$	0.47	0.09	0.71	0.02			0.91

The main findings of this study were:

- Good agreement for log$K_{Mg\text{-}Na}$: 0.57 – 0.62 (0.60 in PHREEQC TDB)
- Bimodal distribution for log$K_{Ca\text{-}Na}$: 0.67, 0.70 (PSI, Uni Bern) and 0.79, 0.80 (CIEMAT, BRGM) (0.80 in PHREEQC TDB)
- Clearly, log$K_{Ca\text{-}Na}$ > log$K_{Mg\text{-}Na}$; the lab-internal difference is 0.08 – 0.19 (0.2 in PHREEQC TDB)
- log$K_{K\text{-}Na}$: 0.63–0.84 (0.70 in PHREEQC TDB)

- log*K* for K-Na and NH_4-Na are the same – but only measured by BRGM (0.63, 0.62; and 0.7) (0.6 in PHREEQC TDB)
- $\log K_{Sr\text{-}Na}$: 0.47 (Uni Bern) and 0.71 (CIEMAT) (0.91 in PHREEQC, largest discrepancy of all components)
- BRGM data is quite similar to PHREEQC (no Sr measured), largest difference for K-Na (0.63 vs. 0.7)

CIEMAT used acetate solutions (NH_4 and Na) and this is thought to dissolve more calcite than the other methods (also done aerobically, not the others), and this may explain the high Ca selectivity obtained. BRGM used Co-hexamine but also obtained a high Ca-selectivity, and this may also be attributed to the method (e.g., Wersin et al. 2013). Uni Bern and PSI used Ni-en for extractions.

Pearson et al. (2003) also state that the log-*K* value (measured or generic) for Na-K exchange led to distinctly too high potassium concentrations compared to borehole seepage waters when calculating an equilibrium K/Na ratio from a measured exchanger composition. This was later addressed in more detail by Tournassat et al. (2007) with a more complex ion-exchange model with a dependence of the exchange coefficient on potassium concentration. For most purposes, adjusting the generic value for this log-*K* value to something that better matches the samples from long-term sampling is a simple solution, and this was done also for this work (see also Pearson et al. 2011, Wersin et al. 2020). Apart from this, these early studies are in general support of the generic selectivity coefficients, particularly also for a distinct difference between the coefficients for Ca and Mg, although Pearson et al. (2011) adopted equal values of 0.7 for log-K of the Ca-Na, Mg-Na and Sr-Na exchange for their modelling.

5.3 The calcite – dolomite equilibrium and its diagnostic capabilities

An important geochemical control by carbonates may be prevalent in rock formations that contain both, calcite and dolomite. Such a combined solubility constraint fixes the activity ratio of Mg^{2+}/Ca^{2+} according to the following combined equilibrium:

$$\frac{a_{Ca^{2+}}}{a_{Mg^{2+}}}\frac{a^{Do}_{CaMg(CO_3)_2}}{\left(a^{Cc}_{CaCO_3}\right)^2} = \frac{\gamma_{Ca^{2+}}m_{Ca^{2+}}}{\gamma_{Mg^{2+}}m_{Mg^{2+}}}\frac{a^{Do}_{CaMg(CO_3)_2}}{\left(a^{Cc}_{CaCO_3}\right)^2} = 10^{(2logK_{Cc}-logK_{Do})}$$

In the equation above, the equilibrium constants, *K*, for calcite and dolomite are written as dissociation equilibria, and the activity terms for the solids indicate the activity of the $CaCO_3$ or $CaMg(CO_3)_2$ components in the calcite and dolomite solid-solutions, respectively. If assuming pure phases and equal activity coefficients for Ca^{2+} and Mg^{2+}, the resultant molality ratio assumes a constant value:

$$\frac{m_{Ca^{2+}}}{m_{Mg^{2+}}} = 10^{(2logK_{Cc}-logK_{Do})} = 10^{0.13} = 1.35$$

This ratio may vary somewhat towards higher ionic strength where the activity coefficient for Ca^{2+} is becoming somewhat smaller than that for Mg^{2+}, and the compositions of the carbonates may have an additional effect, although diagenetic calcites and dolomites are reasonably pure as not to significantly shift this ratio.

An early discussion of this simultaneous equilibrium constraint goes back to Stumm & Morgan (1996, 3rd ed.) where the authors quote data from the Florida aquifer where groundwater samples display a range of Ca and Mg concentrations, but the Ca/Mg ratios cluster near 1.28, a value close to that calculated by assuming calcite – dolomite equilibrium and using the then available log-*K* value for dolomite from Nordstrom et al. (1990) of −17.09 (using basis species CO_3^{2-}, Tab. 5-2). This observation was used as a corroboration of this log-*K* value that otherwise appeared much

more uncertain based on quite a spread of available literature data on dolomite solubility. This log-*K* value for dolomite (ordered dolomite) is still present in almost all TDBs, along with a log-*K* for calcite that fixes the difference ($2 \cdot \log K_{Cc} - \log K_{Do}$) to 0.13. The log-*K* values for calcite and dolomite were slightly revised in the PSINagra2020v1-3 database, yielding a difference of 0.212 for this delta-value (Tab. 5-2). The Ca/Mg ratio fixed at 1.35 with previously used TDBs now becomes 1.63 with the revised version, a measurable difference concerning a cation ratio including major components. In view of an uncertainty of ±0.37 log units associated with the log-*K* for ordered dolomite (Hummel & Thoenen 2023) this shift from the former to the revised value is well within thermodynamic uncertainties. There are also small differences compared to PHREEQC / WATEQ4F in the dolomite log-*K* proposed in the THERMODDEM and THERMOCHIMIE databases (Tab. 5-2). Notably, there is a phase named Dolomite(ordered) in the THERMODDEM database that is very different from all other values for ordered dolomite, and that would lead to a Ca/Mg activity ratio at calcite – dolomite equilibrium of 8.7. This latter log-*K* value is very similar to ordered dolomite provided in the LLNL Thermodynamic Database. Clearly, these latter log-*K* values for ordered dolomite should not be used as they are grossly inconsistent with observations and revised log-*K* values, as most recently detailed by Hummel & Thoenen (2023).

There is some debate as to whether log-*K* values for ordered or disordered dolomite should be used, although thermodynamically, the stable phase at low temperature is ordered dolomite (see discussion in Hummel & Thoenen 2023). In view of the findings of Stumm & Morgan (1996) in the Florida aquifer, commonly a choice in favour of ordered dolomite is made. Adopting disordered dolomite would increase the Ca/Mg activity ratio well above 2. The phase disordered dolomite was removed from the latest release of the PSI-Nagra TDB, a main argument being the uncertain thermodynamic data for this phase.

There is hardly any data on the structural state of dolomite in Opalinus Clay or similar lithologies. The type of dolomite selected is not always the ordered form as done in the earliest work by Pearson et al. (2003), and also for the preliminary reference porewater for Opalinus Clay for all four siting regions (at that time) by Mäder (2009). For example, Gaucher et al. (2009) used disordered dolomite. Ordered and disordered dolomite were used in Wersin et al. (2013). Pearson et al. (2011) used ordered dolomite, and so did Wersin et al. (2020).

Tab. 5-2: Calcite and dolomite properties in different TDBs, and Cc – Do equilibrium.

(1) Basis species CO_3^{2-}, (2) Basis species H^+, HCO_3^-,(3) Mineral name: Dolomite(ordered), (4) Mineral name: Dolomite. The energy unit underpinning log-*K* is kJ/mol.

Item TDB	log-K Do-ord	log-K Cc	log-K 2CC-Do	Activity Ca/Mg	Activity Mg/Ca	Comment
WATEQ4F, PHREEQC	-17.09	-8.48	0.13	1.35	0.741	1
PSINA_110615_DAV_s	3.568	1.849	0.13	1.35	0.741	2
NAPSI_290502	3.568	1.849	0.13	1.35	0.741	2
PSINagra2020v1-3	3.54605	1.879	0.21195	1.63	0.614	2
THERMODDEMv1_10	2.754	1.847	0.94	8.71	0.115	2, 3
THERMODDEMv1_10	3.533	1.847	0.161	1.45	0.690	2, 4
ThermoChimie_v11a	-17.13	-8.48	0.17	1.48	0.676	1

Independent of any other constraints, one may therefore expect that porewater aliquots should have an approximate Ca/Mg ratio of 1.35 or 1.63 (new PSI-Nagra TDB) at 25°°C. This may also be applied to the total concentrations because the activity coefficient ratio of γ_{Ca}/γ_{Mg} is close to 1.0, and the extent of aqueous complexation is similar for Ca and Mg. Such a ratio may deviate, of course, from this theoretical value, if the thermodynamic properties of the dolomite in the rock are not identical to that in the TDB, or if solid-solution effects are significant. In these cases, some systematics should be evident at a value of Ca/Mg that differs somewhat from 1.35. The delta-log*K* values (Tab. 5-2) are distinctly temperature dependent (e.g., using the new PSI-Nagra TDB), shifting the Ca/Mg activity ratio towards 1 at 13°°C corresponding to in situ temperatures at Mont Terri, and towards 2 at 50°°C, the maximum temperatures reached in TBO boreholes where Opalinus Clay is at greatest depth.

Data from advective displacement, squeezing, and porewater samples from borehole intervals (repeatedly sampled, or closed for years, or circulated long-term) show some systematics (Tab. 5-3). Squeezing and advective displacement aliquots from ZNO-NL and Schlattingen-1 invariably show Ca/Mg ratios > 2, but those for Mont Terri are significantly lower (< 1 for few early data, and 1.4 for a sample from Mazurek 2017). Seepage waters from select boreholes as presented by Wersin et al. (2020) have Ca/Mg ratios near 1 (0.86 – 1.16). So, clearly, there is quite a range obtained from different methods, and the data appear to be not consistent with a uniform calcite – dolomite equilibrium interpreted at 25°°C. Data become more consistent when considering the temperature dependence of the mutual calcite – dolomite equilibrium for the borehole waters (13°°C), as discussed by Pearson et al. (2003, 2011). Conversely, it may well be that the TBO samples inherited a higher-temperature signature that also lowers the apparent discrepancy of the measured Ca/Mg activity ratios in squeezing and advective displacement aliquots, compared to modelling done at 25°°C. The Ca/Mg ratios are distinctly lower in the JO region compared to ZNO-NL, and this may correlate with a shallower position of the Opalinus Clay in BOZ1-1 and BOZ2-1 (450 – 650°m). More detailed porewater modelling is in progress and may further clarify these issues.

Note that for several of the listed samples from Mont Terri, the saturation indices for calcite and dolomite are reasonably close the zero, and this was generally quoted as being indicative or compatible with mutual calcite – dolomite equilibrium. Clearly, the Ca/Mg ratio would be a much more discriminating criterion for this carbonate equilibrium condition, but it is rarely used in this way except for discussions by Pearson et al. (2003, 2011).

One possibility for the rather high Ca/Mg ratios – even when considering temperature dependencies – of advective displacement and squeezing aliquots is that some experimental process is driving this ratio away from its in-situ value, such as dissolution of some calcite. This may be plausible for stress/strain induced enhanced dissolution processes during squeezing, but calcite dissolution may also be operating during advective displacement by induced processes, but this has not yet been examined in detail.

Tab. 5-3: Data for Ca/Mg ratio in Opalinus Clay: advective displacement, squeezing, and borehole intervals

[1]: AD from Mäder and Waber (2017); SQ from Wersin et al. (2013), squeezed at 200 MPa; [2]: borehole interval waters: BPC-C1, PWS-A, BWS-A3, BCI-4, BBN; [3]: data by Vinsot et al. (2008) as reported in Wersin et al. (2022b), PC-C Experiment; [4]: data by Vinsot et al. (2014), as reported in Wersin et al. (2022b), HT Experiment; [5]: data by Bleyen et al. (2017), as reported in Wersin et al. (2022b), BN Experiment; [6]: Squeezing waters: HT-1m, WSA-1, DB-A_221 (as given by Wersin et al. 2022b); [7]: data by Mazurek et al. (2017), as reported in Wersin et al. (2022b), DBA borehole; only data with Cl concentrations > 5'000 mg/L; [8]: data by Fernandez et al. (2014), as reported in Wersin et al. (2022b), HT and DR Experiments. TBO references: Mäder et al. 2021 (MAR1-1), Aschwanden et al. 2021 (TRU1-1), Mazurek et al. 2021 (BUL1-1), Aschwanden et al. 2022 (STA3-1), Zwahlen et al. *in prep.* (STA2-1), Gaucher et al. *in prep.* (BAC1-1), Wersin et al. 2022 (BOZ1-1), Gimmi et al. (BOZ2-1).

Data	**AD: Ca/Mg or range (no of samples)**	**SQ: Ca/Mg or range (no of samples)**	**Comment**
Schlattingen-1	2.65	2.63-2.97 (4)	AD, SQ aliquots [1]
MAR1-1	1.94-2.05 (2)	1.99-2.46 (3)	AD, SQ aliquots TBO
TRU1-1	2.08-2.31 (2)	2.20-2.41 (2)	AD, SQ aliquots TBO
BUL1-1	2.30-2.40 (2)	2.42-3.35 (5)	AD, SQ aliquots TBO
STA3-1	2.59 (1)	2.42-2.50 (2)	AD, SQ aliquots TBO
STA2-1	2.59 (1)	2.70 (1)	AD, SQ aliquots TBO
BAC1-1	2.36-2.43 (2)	1.93-3.33 (5)	AD aliquots TBO
Average ZNO-NL	2.35	2.52	average of averages
BOZ1-1	2.12 (1)	2.12-2.47 (5)	AD, SQ aliquots TBO
BOZ2-1		1.68-1.68 (2)	SQ aliquots TBO
Average JO	2.12	1.98	average of averages
Mont Terri – borehole	0.86; 0.95; 1.15; 0.94; 1.16		Wersin et al. 2020 [2]
Mont Terri – borehole	0.86 (0.021 std) (9)		3-year time series [3]
Mont Terri – borehole	0.83-0.88 (2)		1-year time series [4]
Mont Terri – borehole	1.16-1.21 (3)		repeat measurements [5]
Mont Terri		0.76; 0.93; 1.40	Wersin et al. (2020) [6]
Mont Terri		1.26-1.47 (6)	Section across OPA [7]
Mont Terri		0.76; 1.09	Wersin et al. (2022) [8]

The Ca/Mg activity ratio in the porewater may also be directly linked to the measured exchanger cation occupancy, and thus also the mutual calcite – dolomite equilibrium condition:

$$\frac{a_{Ca^{2+}}}{a_{Mg^{2+}}} = \frac{m_{Ca^{2+}}}{m_{Mg^{2+}}}\frac{\gamma_{Ca^{2+}}}{\gamma_{Mg^{2+}}} = \frac{1}{10^{(logK_{Ca\backslash X2} - logK_{Mg\backslash X2})}}\frac{CaX2}{MgX2}$$

Where the subscript Ca\X2 denotes the half reaction $Ca^{2+}+2X^{-} = CaX2$ (and Mg\X2 in analogy), m and γ denote molality and the activity coefficient, and CaX2 and MgX2 are the equivalent fractions of these cations on the exchanger. Activity coefficients for Ca and Mg are very similar

at moderate concentrations, and the degree of complexation of Ca and Mg is also quite comparable such that this Ca/Mg activity ratio in the porewater is approximately also that of the total Ca/Mg molal concentrations. Adopting the ion exchange coefficients (apparent equilibrium constants) used in this work (Appelo & Postma 2005), the difference of log-*K* values of the half-reactions Ca\X2 − Mg\X2 is 0.2 log units, and the equation simplifies to:

$$\frac{m_{Catot}}{m_{Mgtot}} \approx 0.63 \frac{CaX2}{MgX2}$$

If the Ca/Mg ratio in the porewater would have the ratio of 1.35 according to the thermodynamic data at mutual calcite – dolomite equilibrium (25°°C), the ratio of the equivalent fractions, CaX2/MgX2, would have to be 2.14 (1.35/0.63). The exchanger compositions from the samples measured for ZNO-NL (Tab. 5-4) indeed are approximately compatible with the above analysis. Note that the range in exchanger composition also depends on the borehole location, with highest values of NaX near 0.50 in BUL1-1, and lowest values of 0.40 in MAR1-1. The corresponding range for CaX2 is 0.20 – 0.35, and 0.10 – 0.19 for MgX2.

Tab. 5-4: Exchanger composition of Opalinus Clay for samples from ZNO, NL and JO

Data	**Ave ZNO_NL (Std)**	**Ave ZNO_NL (Std)**	**Ave JO (Std)**	**Ave JO (Std)**	**Comment**
Correction [1]	Na (Cl, SO_4)	Na (Cl), Ca (SO_4)	Na (Cl, SO_4)	Na (Cl), Ca (SO_4)	Uni BE & PSI data
NaX	0.40 (0.04)	0.44 (0.04)	0.41	0.44	Uni BE & PSI data
KX	0.05 (0.01)	0.05 (0.01)	0.08	0.08	Only Uni BE data
CaX2	0.34 (0.03)	0.30 (0.04)	0.34	0.31	Uni BE & PSI data
MgX2	0.13 (0.02)	0.13 (0.02)	0.15	0.15	Uni BE & PSI data
SrX2	0.0064 (0.0024)	0.0064 (0.0024)	0.008	0.008	Uni BE & PSI data
NH_4	0.03 (0.02)	0.03 (0.02)	0.020	0.020	Only PSI data
CaX2/MgX2	2.51	2.24	2.24	2.05	

Pearson et al. (2011) propose revised exchange coefficients, namely having equal log-*K* values for Ca and Mg exchange reactions (relative to Na). This would have the effect that the ratio of the CaX2/MgX2 equivalent fractions would be equal to the Ca/Mg activity ratio in the porewater, or also approximately equal to the molal concentration ratio. This would lead to Ca/Mg ratios > 2 that would not be compatible with the mutual calcite – dolomite equilibrium assumption, but it would be compatible with the measured ratios in the advective displacement and squeezing aliquots. This inconsistency among constraints is the main reason that we adopted the more generic exchange coefficients of Appelo & Postma (2005), only adjusted for potassium as elaborated further below. This is in fact the same data also used by Pearson et al. (2003) except for potassium.

It is quite obvious that the TBO data set cannot satisfy simultaneously the exchanger data (with the adopted selectivity coefficients), the advectively displaced or squeezed aliquots and the mutual calcite – dolomite equilibrium assumption. This is in fact a main issue for a modelling interpretation – apart from possibly uncertain sulphate concentrations – and the thermodynamic model essentially brings the data into thermodynamic agreement by adjustments to this ratio in both, the porewater but also the ion exchanger. A decision was made to use and impose the calcite – dolomite equilibrium assumption, and let the model deviate somewhat from the measured Ca/Mg activity ratios in the aliquots from squeezing and advective displacement, and also the CaX2/MgX2 ratio from the averages measured on the exchanger. Note that these differences and adjustments are not large in absolute terms and do not significantly affect the subsequent calculations for safety analysis.

5.4 Existing models for porewater composition

Thermodynamic models for the porewater composition of Opalinus Clay were first developed for the Mont Terri locality (Pearson et al. 2003, Bradbury & Baeyens 1997, 1998) and then adapted to the Benken locality (Nagra 2002) for Nagra's Safety Case for Opalinus Clay. Earlier developments and a complete review of all existing model variants up to 2008 are detailed in Wersin et al. (2009). A detailed review pertinent to Opalinus Clay was provided by Mäder (2009) in the context of defining preliminary reference porewaters for siting regions during the early stages of the Sachplan procedure (SGT), based on data from the Benken borehole, apart from Mont Terri. More recent accounts of porewater models and modelling approaches are provided by Pearson et al. (2011) and Wersin et al. (2020).

All models use a combination of directly measured concentrations, mineral saturation constraints, constraints from the exchangeable cation population and possibly some assumed fixed parameters. The models have evolved from using several constraints based on expert judgement (e.g., a fixed partial pressure of CO_2, a fixed SO_4/Cl ratio) to models that are fully constrained by mineral saturation equilibria and ion exchange equilibria (reviewed in Wersin et al. 2009, Gaucher et al. 2009, Mäder 2009, Pearson et al. 2011, Wersin et al. 2020). Models that include layer-silicate minerals may be used to fully constrain pH and alkalinity/P_{CO2} without any assumption about the partial pressure of CO_2, for example. See Chapter 5 for details.

5.5 Model for reference porewaters for ZNO-NL and JO

We have adopted a modelling approach that is very similar to previous reference porewater models proposed by Nagra (2002) for Benken and by Mäder (2009) for the four siting regions considered during the early stage of the site selection process. A key feature is that these models constrain directly the partial pressure of CO_2 by an expert judgment, based on multiple lines of argument, and the uncertainty associated with this choice is addressed with some model variants that bracket the partial pressure of CO_2 with a lower and upper limit. The value adopted is in fact the same as used by Mäder (2009) for an earlier version of a reference porewater from SGT Stage 2. This value has bee proposed by Perason et al. (2003) and remained essentially unchanged through further porewater modelling work and data reviews (e.g., Gaucher et al. 2009, Pearson et al. 2011, Wersin et al. 2013, 2020). There are some alternatives invoking additional mineral equilibrium constraints with hydrous silicates that lead to a fully constrained porewater composition (in the sense of the phase rule), including pH and P_{CO2}. The expert decision is deferred to the choice of silicates to be at equilibrium and uncertainties relate to thermodynamic properties of chemically complex silicates for which exact compositional data and calorimetric or solubility data are largely lacking (in case of Opalinus Clay), and therefore need to be substituted by end-member compositions from literature.

The modelling approach is identical for the reference porewater for ZNO-NL and JO. It differs only by the input parameters that constrain the chloride and sulphate concentrations, and the composition of the ion exchanger. Otherwise, the mineral equilibrium phases are the same, and also the imposed partial pressure of CO_2. Likewise, the redox state is also constrained by the same mineral equilibria but relate to different pre-scribed sulphate concentrations.

A value of $10^{-2.2}$ bar is adopted as best estimate for the partial pressure of CO_2 based on earlier work and arguments by Pearson et al. (2003) and Mäder (2009). Such a value is also consistent with more recent data digests by Pearson et al. (2011) and Wersin et al. (2020). The uncertainty range is also reasonably well constrained, covering approximately a log-unit, from −1.8 to −2.8 selected for both reference porewater models. See Section 4.5 for more details.

Key uncertainties are also addressed in the same way for both reference porewaters (ZNO-NL and JO), namely by providing porewater variants that are modelled in analogous fashion but perturbed by the main compositional uncertainties: (1) a low-P_{CO2} variant, (2) a high-P_{CO2} variant, and (3) a high-sulphate variant. Other uncertainties are either coupled to the above variants (e.g., alkalinity, pH), or minor or are not a sensitive issue for computing radionuclide sorption, speciation and solubility. The redox condition is constrained by the pyrite – siderite equilibrium, and it is thus dependent on P_{CO2} and pH, and the variants (1) and (2) also bracket the redox potential.

In short, the following describes the ingredients of the thermodynamic model for the base case of a reference porewater – our best estimate of the averaged porewater composition for the Opalinus Clay in a region, interpreted at 25 °C and 1 bar pressure.

1. Chloride concentration, sulphate concentration are fixed as detailed below.
2. A simplified Na-Ca-Mg composition is used, based on the above sum of the anions, and fulfilling approximately the calcite – dolomite equilibrium ratio of Ca/Mg, and an approximate ratio of Na/Ca that is also near that suggested by the ion-exchange equilibria. A rough initial estimate is sufficient.
3. The exchanger composition (equivalent fractions) is defined based on measured data. The exchange capacity chosen is not large such that the multiple mineral equilibria have some leverage on the composition of the porewater, but sufficiently large that the exchanger composition is approximately respected. This capacity does not correspond to the measured capacity because it is an operational parameter solely for initiating the model.
4. A list of mineral saturation constraints is defined that makes 'geochemical sense' (see below), extended with some arbitrary choices (mostly end-members of solid-solutions) where data are lacking.
    - 4.1. Calcite – dolomite equilibrium is imposed
    - 4.2. P_{CO2} is imposed ($10^{-2.2}$ bar); this, along with a) fixes pH and alkalinity
    - 4.3. Siderite equilibrium fixes Fe(II) at given pH and alkalinity
    - 4.4. Pyrite equilibrium at given sulphate and Fe(II) fixes sulphide and the redox potential, and thus also Fe(III)
    - 4.5. Quartz is used to fix Si concentration
    - 4.6. Kaolinite is used to fix Al at given Si and pH
    - 4.7. Celestite is used to fix Sr at a given sulphate concentration
    - 4.8. Fluorite is used to fix F at a given Ca concentration
    - 4.9. Barite is used to fix Ba at a given sulphate concentration
    - 4.10. Rhodochrosite is used to fix Mn(II) at given pH and alkalinity

Of the above mineral saturation constraints, those involving quartz, fluorite, celestite and barite determine compositions that are relatively independent of pH, all others are distinctly pH-dependent, including the redox potential. The multiple mineral saturation constraints are achieved by allowing the modelling software to add or subtract small amounts of the mineral phases. It is therefore an open-system calculation, but with a fixed chloride composition and an almost fixed sulphate composition (minor amounts of celestite and barite dissolution/precipitation are involved).

While there is geochemical justification to select calcite, dolomite, quartz and pyrite as approximately pure phases, siderite is a proxy for Fe-carbonate that shows quite a variable composition. Also, ankerite (Fe-dolomite) is present (as solid-solution), and other iron phases are present (silicates, oxides, hydroxides) and the control on the iron system is therefore not exactly known.

5.6 Reference porewater for ZNO-NL

The most straightforward constraint is that for chloride concentrations provided by aliquots from advective displacement and porewater squeezing. Apart from some conceptual uncertainties regarding the chloride-accessible porosity fraction, the measured concentrations are taken at face value to represent the 'free porewater' not affected by positively charged clay surfaces. Fig. 4-8 is a summary of the data available for Opalinus Clay for boreholes of ZNO and NL. The concentrations are systematically higher for samples from advective displacement compared to those from porewater squeezing. This is perhaps not surprising given the very different processes that are operating during the two contrasting methods. We have adopted an average value of 8'500◦mg/L. This value is a bit below the average value from advective displacement and a bit above that for porewater squeezing. Only the BUL1-1 borehole yields chloride concentrations that are distinctly above this value: either by about 2'500◦mg/L for squeezing data, or by 5'500◦mg/L when compared to advective displacement aliquots.

Constraining sulphate concentrations is a more involved topic. Advective displacement samples and squeezing samples show some broad agreement with a tendency for somewhat higher concentrations in the advective displacement samples due to the generally larger ionic strengths. Upscaling of aqueous extract concentrations leads to much larger sulphate concentrations. The exact reason for this discrepancy is presently unclear, an issue observed with all borehole data from Opalinus Clay (see discussion in Section 5.8). This has led to select a sulphate concentration of approximately 23◦mmol/L (2'200◦mg/L) that is at the upper limit of the measured sulphate concentrations in samples from advective displacement.

A high-sulphate variant was created containing twice as much sulphate to account for this uncertainty towards possible larger sulphate concentrations indicated by the aqueous extracts. This variant will have Ca concentrations that are only about half of those of the base case, and also the Mg concentrations will be much lower due to the imposed calcite – dolomite equilibrium that fixes the Ca/Mg activity ratio.

Other variants to cover uncertainty are as discussed in Section 5.5 concerning the low-P_{CO2} and high-P_{CO2} variants that also cover uncertainty ranges in alkalinity and pH.

The following is the PHREEQC input file for the ZNO-NL reference porewater, base case, using the latest PSI-Nagra 2020 TDB.

```
DATABASE C:\phreeqc\database\PSINagra2020v1-3.dat
TITLE  Ref pore water for Opalinus Clay ZNO and NL: generic exchange properties, no gammas, SIT
EXCHANGE_MASTER_SPECIES
        X       X-
EXCHANGE_SPECIES
        X- = X-
        log_k   0.0
        Na+ + X- = NaX
        log_k   0.0
        K+ + X- = KX
        log_k   1.20    # revised value from Paul Wersin NTB
        Ca+2 + 2X- = CaX2
        log_k   0.80    # Appelo & Postma 1993
        Mg+2 + 2X- = MgX2
        log_k   0.60    # Appelo & Postma 1993
        Sr+2 + 2X- = SrX2
        log_k   0.91    # Appelo & Postma 1993
        Fe+2 + 2X- = FeX2  # phreeqc TDB / Appelo & Postma
        log_k   0.44
        Ba+2 + 2X- = BaX2 # phreeqc TDB / Appelo & Postma
        log_k   0.91
        Mn+2 + 2X- = MnX2
        log_k   0.52
SOLUTION 1 OPA # from AD samples MAR1-1 / TRU1-1 / Benken, OPA ; SO4 at upper end of AD range;
        pe      4.0 # initial value only
        redox  pe
        temp 25.0
        units   mol/kgw
        pH      7.0   # not sensitive
        Cl      0.240 # 8508 mg/l: average TRU-MAR-Benken  (6500-10000 mg/l)
        S       0.023 # higher-end of AD data
        Na      0.222  charge # charge balance initial: Cl+2*SO4-2Ca-2Mg
        Ca      0.018 # prime with some Ca and Mg, with Ca/Mg = 1.35 (approx); near Na/Ca constrained by
        exchanger
        Mg      0.014 # with Ca/Mg = 1.35 (approx)
EXCHANGE 1 measured exchanger # from CEC/Xi of MAR1-3-AD AqEx OPA (645.48 m)  UniBE Data
        NaX     0.045  #0.45  #
        KX      0.007  #0.07  #
        MgX2    0.015  #0.15  #
        CaX2    0.032  #0.32  #
        SrX2    0.0005  #0.009  # prime near saturation with celestite; measured value was 0.0009
        exchange_gammas false
EQUILIBRIUM_PHASES 1
        CO2(g)          -2.2 1.0 # range -1.8 to -2.8
        Calcite         0.0  1.0
        Dolomite        0.0  1.0 # wateq4f and phreeqc and NAPSI2020 TDB for ordered Dol
        Quartz          0.0  1.0
        Celestite       0.0  1.0 # used as upper limit; pervasiveness of celestite unclear/debated
        Siderite        0.0  1.0 # proxy for Fe-carbonate (ankerite and siderite solid solutions;
        heterogeneous compositions)
        Pyrite          0.0  1.0 # ubiquitous; high-surface area, reactive on disturbances
        Fluorite        0.0  1.0 # include fluoride to fix F (at fixed Ca)
        Kaolinite       0.0  1.0 # Al best fixed by kaolinite (fixed, as Si and also pH are more or less set)
        Barite          0.0  1.0 # fix Ba at given SO4
        Rhodochrosite   0.0  1.0 # fix Mn at given pH/alkalinity
END
```

The PHREEQC programme with the above input initialises the initial simplified solution composition. This is followed by applying all listed mineral saturation constraints. The saturation condition is reached by adding or subtracting small amounts of the mineral phases to or form the solution composition until all constraints are satisfied. The specified exchanger composition with its capacity is also included in the calculation. This exchanger composition will shift somewhat according to the mass transfers caused by the mineral saturation process. Finally, a complete description of the solution and the exchanger is provided, including physico-chemical parameters like ionic strength, activity of water, alkalinity, redox potential, saturation indices for all solid phases contained in the TDB for this chemical sub-system, and some more properties. Tab. 5-5 is a summary output providing the chemical composition (mostly total concentrations, some species concentrations) and relevant physico-chemical parameters. This is provided for all porewater variants (low-P_{CO2}, high-P_{CO2}, high-SO_4), and the reference porewater (base case) is provided using four different TDBs as discussed in Section 6.1. A full speciation output with all mineral saturation states is provided in App. A.

Tab. 5-5: Reference porewater composition for ZNO-NL, including variants. Yellow background: Reference porewater and variants with official TD

PSINagra2020v1-3: PSI Chemical Thermodynamic Database 2020, Version 1-3, LAST MOD. 05-NOV-2021 (SIT ion activity model); NAPSI: PSI/Nagra Thermochemical Database Version 12/07, LAST MOD. 11-JUN-2015; PSINA_110615_DAV_s.dat (Davies ion activity model); NAPSI0101: Nagra/PSI Chemical Thermodynamic Database Version 01/01 (Nagra/PSI TDB 01/01); WATEQ4F: WATEQ3F TDB from PHREEQC software distribution.

Variant	Unit	Ref	Ref	Ref	Ref	low(P_{CO2})	low(P_{CO2})	high(P_{CO2})	high(P_{CO2})	high(SO_4)	high(SO_4)
TDB		NAPSI	WATEQ 4F	NaPSI 0101	**PSINagra 2020v1-3**	**NAPSI**	**PSINagra 2020v1-3**	**NAPSI**	**PSINagra 2020v1-3**	**NAPSI**	**PSINagra 2020v1-3**
CHARGE_ BALANCE	mol	-2.1E-11	1.2E-13	1.7E-14	-5.4E-12	-5.0E-11	-6.1E-12	1.3E-14	-4.4E-12	2.4E-14	1.1E-11
PERCENT_ ERROR	diff/sum	-3.9E-09	2.2E-11	3.2E-12	-9.8E-10	-9.3E-09	-1.1E-09	2.3E-12	-8.1E-10	3.9E-12	1.8E-09
MU	mol	0.317	0.320	0.320	0.324	0.316	0.323	0.318	0.326	0.353	0.365
a(H_2O)		0.992	0.991	0.991	0.992	0.992	0.992	0.991	0.992	0.990	0.991
ALK	meq/kgH_2O	1.78	1.78	1.80	0.99	0.91	0.99	2.79	0.99	3.64	0.99
pH		7.06	7.05	7.05	7.07	7.36	7.37	6.86	6.87	6.98	6.99
pe		-2.61	-2.61	-2.61	-2.76	-2.96	-3.10	-2.38	-2.53	-2.50	-2.64
logP_{CO2}	log(bar)	-2.20	-2.20	-2.20	-2.20	-2.80	-2.80	-1.80	-1.80	-1.80	-1.80
Calcite	SI	0.00	0.00	0.00	0.00	0.00	0.00	0.00	0.00	0.00	0.00
Dolomite(ord)	SI	0.00	0.00	0.00	0.00	0.00	0.00	0.00	0.00	0.00	0.00
Quartz	SI	0.00	0.00	0.00	0.00	0.00	0.00	0.00	0.00	0.00	0.00
Celestite	SI	0.00	0.00	0.00	0.00	0.00	0.00	0.00	0.00	0.00	0.00
Siderite	SI	0.00	0.00	0.00	0.00	0.00	0.00	0.00	0.00	0.00	0.00
Pyrite	SI	0.00	0.00	0.00	0.00	0.00	0.00	0.00	0.00	0.00	0.00
Fluorite	SI	0.00	0.00	0.00	0.00	0.00	0.00	0.00	0.00	0.00	0.00
Kaolinite	SI	0.00	0.00	0.00	0.00	0.00	0.00	0.00	0.00	0.00	0.00
Barite	SI	0.00	0.00	0.00	0.00	0.00	0.00	0.00	0.00	0.00	0.00
Rhodochrosite	SI	0.00	0.00	0.00	0.00	0.00	0.00	0.00	0.00	0.00	0.00
Strontianite	SI	-1.14	-1.13	-1.12	-1.02	-1.14	-1.02	-1.15	-1.03	-1.23	-1.08
Gypsum	SI	-0.12	-0.14	-0.14	-0.16	-0.13	-0.17	-0.12	-0.16	-0.04	-0.11
Anhydrite	SI	-0.34	-0.36	-0.36	-0.53	-0.34	-0.53	-0.34	-0.52	-0.26	-0.47
Magnesite	SI	-0.32	-0.58	-0.32	-1.00	-0.32	-1.00	-0.32	-1.00	-0.32	-1.00
Na	mmol/kgH_2O	201	202	202	202	201	202	201	203	276	278
K	mmol/kgH_2O	1.14	1.22	1.22	1.16	1.14	1.15	1.14	1.16	1.22	1.23
Ca	mmol/kgH_2O	24.07	24.54	24.95	26.48	23.86	26.24	24.32	26.77	16.18	17.78
Mg	mmol/kgH_2O	18.38	17.34	17.06	15.60	18.22	15.46	18.56	15.77	12.63	10.37
Sr	mmol/kgH_2O	0.28	0.30	0.29	0.38	0.28	0.38	0.28	0.38	0.15	0.22
Fe(II)	mmol/kgH_2O	0.10	0.10	0.10	0.10	0.10	0.10	0.11	0.10	0.07	0.07
Fe(III)	mmol/kgH_2O	4.0E-09	4.0E-09	4.0E-09	1.2E-06	1.1E-08	1.1E-06	2.2E-09	1.2E-06	1.9E-09	1.3E-06
Si	mmol/kgH_2O	0.18	0.10	0.16	0.17	0.18	0.17	0.18	0.17	0.18	0.17
Al	mmol/kgH_2O	8.1E-06	2.0E-05	1.3E-05	2.0E-05	1.3E-05	2.0E-05	9.2E-06	2.7E-05	9.7E-06	2.8E-05
Mn	mmol/kgH_2O	0.068	0.069	0.058	0.098	0.067	0.097	0.070	0.099	0.045	0.065
Ba	mmol/kgH_2O	1.6E-04	1.8E-04	1.8E-04	1.6E-04	1.6E-04	1.6E-04	1.6E-04	1.6E-04	1.0E-04	9.5E-05
Cl	mmol/kgH_2O	240	240	240	240	240	240	240	240	240	240
S(VI)	mmol/kgH_2O	23.16	23.20	23.20	23.38	23.16	23.38	23.16	23.38	45.83	45.98
S(-II)	mmol/kgH_2O	9.5E-09	9.9E-09	9.8E-09	2.5E-07	8.5E-09	4.3E-07	1.1E-08	2.0E-07	1.2E-08	2.1E-07
C(IV)	mmol/kgH_2O	1.98	1.97	1.98	2.11	0.95	1.01	3.32	3.52	4.16	4.46
HCO_3	mmol/kgH_2O	1.47	1.48	1.49	1.60	0.74	0.80	2.33	2.52	3.13	3.41
F	mmol/kgH_2O	0.13	0.13	0.13	0.16	0.13	0.16	0.13	0.16	0.15	0.19
SO_4/Cl	mol/mol	0.10	0.10	0.10	0.10	0.10	0.10	0.10	0.10	0.19	0.19
Ca/Mg	mol/mol	1.31	1.42	1.46	1.70	1.31	1.70	1.31	1.70	1.28	1.71
Na/Ca	mol/mol	8.36	8.25	8.10	7.64	8.43	7.71	8.28	7.57	17.07	15.63
Na_X	eq_fraction	0.447	0.440	0.441	0.440	0.448	0.441	0.446	0.439	0.636	0.622
K_X	eq_fraction	0.040	0.039	0.039	0.040	0.040	0.040	0.040	0.040	0.044	0.044
Ca_X2	eq_fraction	0.345	0.351	0.350	0.369	0.345	0.369	0.346	0.370	0.216	0.237
Mg_X2	eq_fraction	0.162	0.164	0.164	0.143	0.161	0.143	0.162	0.143	0.101	0.092
Sr_X2	eq_fraction	0.0052	0.0055	0.0055	0.0068	0.0052	0.0068	0.0052	0.0068	0.0027	0.0039
Fe_X2	eq_fraction	5.9E-04	6.0E-04	5.9E-04	5.7E-04	5.9E-04	5.7E-04	5.9E-04	5.7E-04	3.7E-04	3.7E-04
Mn_X2	eq_fraction	4.1E-04	4.1E-04	4.1E-04	7.7E-04	4.0E-04	7.7E-04	4.1E-04	7.7E-04	2.5E-04	4.9E-04
Ba_X2	eq_fraction	2.4E-06	2.5E-06	2.5E-06	2.8E-06	2.4E-06	2.8E-06	2.4E-06	2.8E-06	1.2E-06	1.6E-06
Sum_exchanger	eq_fraction	1.000	1.000	1.000	1.000	1.000	1.000	1.000	1.000	1.000	1.000

5.7 Reference porewaters for JO

The most straightforward constraint is that for chloride concentrations provided by aliquots from advective displacement and porewater squeezing. Apart from some conceptual uncertainties regarding the chloride-accessible porosity fraction, the measured concentrations are taken at face value to represent the 'free porewater' not affected by positively charged clay surfaces. Fig. 4-16 is a summary of the data available for Opalinus Clay for boreholes of JO.

The concentrations are systematically higher for samples from advective displacement compared to those from porewater squeezing. This is perhaps not surprising given the very different processes that are operating during the two contrasting methods. We have adopted an average value of 3'000◦mg/L. This value is somewhat below a value obtained for BOZ1 from advective displacement, and somewhat above the average obtained from squeezing tests. The chloride concentrations are lower at BOZ2, about 1'600 – 1'800◦mg/L, based on squeezing data. The reference porewater therefore represents the higher salinities representative of the southern part of JO, where the Opalinus Clay formation is also located at greater depth, e.g. below 500◦m at BOZ1.

Constraining sulphate concentrations is a more involved topic. Advective displacement samples and squeezing samples show some broad agreement with a tendency for somewhat higher concentrations in the advective displacement samples due to the generally larger ionic strengths (higher chloride concentrations). Upscaling of aqueous extract concentrations leads to much larger sulphate concentrations. The exact reason for this discrepancy is presently unclear. This has led to select a sulphate concentration of approximately 27 mmol/L (2'600◦mg/L) that is at the upper limit of the measured sulphate concentrations in samples from advective displacement and squeezing for BOZ1. A difference between the two reference porewaters is the much higher SO_4/Cl ration in JO (0.3 – 0.5◦mol/mol, with highest values at BOZ2) compared to ZNO-NL (0.05 – 0.13◦mol/mol), although the absolute sulphate concentration is not much larger for JO.

A high-sulphate variant was created containing twice as much sulphate to account for this uncertainty towards possible larger sulphate concentrations indicated by the aqueous extracts. This variant will have Ca concentrations that are only about half of those of the base case, and also the Mg concentrations will be much lower due to the imposed calcite – dolomite equilibrium that fixes the Ca/Mg activity ratio.

Other variants to cover uncertainty are as discussed in Section 5.8 concerning the low-P_{CO2} and high-P_{CO2} variants that also cover uncertainty ranges in alkalinity and pH.

The following is the PHREEQC input file for the JO reference porewater, base case, using the latest PSI-Nagra 2020 TDB.

The PHREEQC programme with the above input initialises the initial simplified solution composition. This is followed by applying all listed mineral saturation constraints. The saturation condition is reached by adding or subtracting small amounts of the mineral phases to or form the solution composition until all constraints are satisfied. The specified exchanger composition with its capacity is also included in the calculation. This exchanger composition will shift somewhat according to the mass transfers caused by the mineral saturation process. Finally, a complete description of the solution and the exchanger is provided, including physico-chemical parameters like ionic strength, activity of water, alkalinity, redox potential, saturation indices for all solid phases contained in the TDB for this chemical sub-system, and some more properties. Tab. 5-6 is a summary output providing the chemical composition (mostly total concentrations, some species concentrations) and relevant physico-chemical parameters. This is provided for all porewater variants (low-P_{CO2}, high-P_{CO2}, high-SO_4), and the reference porewater (base case) is provided using four different TDBs as discussed in Section 5.1. A full speciation output with all mineral saturation states is provided in App. B.

```
DATABASE C:\phreeqc\database\PSINagra2020v1-3.dat
TITLE  Ref pore water for Opalinus Clay JO: PSI_2020 TDB, generic exchange properties, no gammas, SIT
activities
EXCHANGE_MASTER_SPECIES
        X       X-
EXCHANGE_SPECIES
        X- = X-
        log_k   0.0
        Na+ + X- = NaX
        log_k   0.0
        K+ + X- = KX
        log_k   1.20    # revised value from Paul Wersin NTB
        Ca+2 + 2X- = CaX2
        log_k   0.80    # Appelo & Postma 1993
        Mg+2 + 2X- = MgX2
        log_k   0.60    # Appelo & Postma 1993
        Sr+2 + 2X- = SrX2
        log_k   0.91    # Appelo & Postma 1993
        Fe+2 + 2X- = FeX2  # phreeqc TDB / Appelo & Postma
        log_k   0.44
        Ba+2 + 2X- = BaX2 # phreeqc TDB / Appelo & Postma
        log_k   0.91
        Mn+2 + 2X- = MnX2
        log_k   0.52
SOLUTION 1 OPA # from AD and SQ samples BOZ1-1 and BOZ2-1; slanted towards AD BOZ1-1 with higher salinity
        pe      4.0 # initial value only
        redox  pe
        temp 25.0
        units   mol/kgw
        pH      7.0   # not sensitive
        Cl      0.085 # 3000 mg/L: AD BOZ1-1  (3220 mg/l)
        S       0.027 # 2600 mg/L; AD from BOZ1-1 (2680 mg/L)
        Na      0.131 charge # charge balance initial: Cl+2*SO4-2Ca-2Mg  (139 meq anions and cations)
        Ca      0.002 # prime with some Ca
        Mg      0.002 # prime with some Mg
EXCHANGE 1 measured exchanger # from CEC/Xi of BOZ1 and BOZ2 OPA data (UniBE and PSI) (note: nearly
identical with ZNO-NL)
        NaX     0.046  #0.46
        KX      0.007  #0.05  increased, to avoid very low K in APW
        MgX2    0.015  #0.15
        CaX2    0.032  #0.32
        SrX2    0.0008 #0.008  very near celestite saturation
EQUILIBRIUM_PHASES 1
        CO2(g)          -2.2 1.0 # range -1.8 to -2.8
        Calcite         0.0  1.0
        Dolomite        0.0  1.0 # wateq4f, phreeqc and NaPSI-2020 TDB for ordered Dol
        Quartz          0.0  1.0
        Celestite       0.0  1.0 # used as upper limit; pervasiveness of celestite unclear/debated
        Siderite        0.0  1.0 # proxy for Fe-carbonate (ankerite and siderite solid solutions;
        heterogeneous compositions)
        Pyrite          0.0  1.0 # ubiquitous; high-surface area, reactive on disturbances
        Fluorite        0.0  1.0 # include fluorite to fix F (at fixed Ca)
        Kaolinite       0.0  1.0 # Al best fixed by kaolinite (fixed, with Si and pH set)
        Barite          0.0  1.0 # fix Ba at given SO4
        Rhodochrosite   0.0  1.0 # fix Mn at given pH/alkalinity
END
```

Tab. 5-6: Reference porewater composition for JO, including variants. Yellow background: Reference porewater and variants with official TDB

PSINagra2020v1-3: PSI Chemical Thermodynamic Database 2020, Version 1-3, LAST MOD. 05-NOV-2021 (SIT ion activity model); NAPSI: PSI/Nagra Thermochemical Database Version 12/07, LAST MOD. 11-JUN-2015; PSINA_110615_DAV_s.dat (Davies ion activity model); NAPSI0101: Nagra/PSI Chemical Thermodynamic Database Version 01/01 (Nagra/PSI TDB 01/01); WATEQ4F: WATEQ3F TDB from PHREEQC software distribution.

Variant	Unit	Ref	Ref	Ref	Ref	low(P_{CO2})	low(P_{CO2})	high(P_{CO2})	high(P_{CO2})	high(SO_4)	high(SO_4)
TDB		NAPSI	WATEQ 4F	NaPSI 0101	**PSINagra 2020v1-3**	**NAPSI**	**PSINagra 2020v1-3**	**NAPSI**	**PSINagra 2020v1-3**	**NAPSI**	**PSINagra 2020v1-3**
CHARGE_ BALANCE	mol	3.1E-10	-1.0E-13	1.1E-10	8.4E-13	3.4E-15	8.4E-13	-2.5E-12	8.4E-13	1.1E-09	9.2E-12
PERCENT_ ERROR	diff/sum	1.2E-07	-4.0E-11	4.1E-08	3.2E-10	1.3E-12	3.2E-10	-9.4E-10	3.1E-10	3.1E-07	2.6E-09
MU	mol	0.159	0.159	0.158	0.162	0.157	0.160	0.160	0.163	0.219	0.227
a(H_2O)		0.996	0.996	0.996	0.996	0.996	0.996	0.996	0.996	0.995	0.995
ALK	meq/kgH_2O	1.00	1.00	1.00	1.00	1.00	1.00	1.00	1.00	0.99	1.00
pH		7.30	7.29	7.29	7.34	7.60	7.65	7.09	7.13	7.08	7.12
pe		-2.89	-2.88	-2.88	-3.06	-3.23	-3.41	-2.65	-2.82	-2.60	-2.78
logP_{CO2}	log(bar)	-2.20	-2.20	-2.20	-2.20	-2.80	-2.80	-1.80	-1.80	-1.80	-1.80
Calcite	SI	0.00	0.00	0.00	0.00	0.00	0.00	0.00	0.00	0.00	0.00
Dolomite(ord)	SI	0.00	0.00	0.00	0.00	0.00	0.00	0.00	0.00	0.00	0.00
Quartz	SI	0.00	0.00	0.00	0.00	0.00	0.00	0.00	0.00	0.00	0.00
Celestite	SI	0.00	0.00	0.00	0.00	0.00	0.00	0.00	0.00	0.00	0.00
Siderite	SI	0.00	0.00	0.00	0.00	0.00	0.00	0.00	0.00	0.00	0.00
Pyrite	SI	0.00	0.00	0.00	0.00	0.00	0.00	0.00	0.00	0.00	0.00
Fluorite	SI	0.00	0.00	0.00	0.00	0.00	0.00	0.00	0.00	0.00	0.00
Kaolinite	SI	0.00	0.00	0.00	0.00	0.00	0.00	0.00	0.00	0.00	0.00
Barite	SI	0.00	0.00	0.00	0.00	0.00	0.00	0.00	0.00	0.00	0.00
Rhodochrosite	SI	0.00	0.00	0.00	0.00	0.00	0.00	0.00	0.00	0.00	0.00
Strontianite	SI	-0.92	-0.92	-0.92	-0.77	-0.91	-0.76	-0.93	-0.78	-1.20	-1.03
Gypsum	SI	-0.35	-0.34	-0.34	-0.42	-0.36	-0.43	-0.34	-0.40	-0.06	-0.15
Anhydrite	SI	-0.57	-0.56	-0.56	-0.78	-0.58	-0.79	-0.56	-0.77	-0.28	-0.52
Magnesite	SI	-0.32	-0.58	-0.32	-1.00	-0.32	-1.00	-0.32	-1.00	-0.32	-1.00
Na	mmol/kgH_2O	112	112	112	118	111	118	112	119	154	163
K	mmol/kgH_2O	0.69	0.72	0.72	0.80	0.68	0.79	0.69	0.81	0.80	0.94
Ca	mmol/kgH_2O	8.21	8.14	8.22	7.40	7.97	7.13	8.48	7.71	11.51	10.45
Mg	mmol/kgH_2O	6.40	6.11	6.08	4.36	6.22	4.20	6.61	4.54	9.13	6.09
Sr	mmol/kgH_2O	0.16	0.16	0.15	0.19	0.16	0.19	0.16	0.19	0.12	0.15
Fe(II)	mmol/kgH_2O	0.03	0.03	0.03	0.03	0.03	0.03	0.04	0.03	0.05	0.05
Fe(III)	mmol/kgH_2O	3.0E-09	2.9E-09	3.0E-09	1.1E-06	9.1E-09	9.7E-07	1.5E-09	1.1E-06	1.7E-09	1.2E-06
Si	mmol/kgH_2O	0.18	0.10	0.17	0.18	0.18	0.18	0.18	0.18	0.18	0.18
Al	mmol/kgH_2O	1.2E-05	3.0E-05	1.9E-05	2.4E-05	2.1E-05	2.9E-05	1.0E-05	2.9E-05	1.0E-05	2.9E-05
Mn	mmol/kgH_2O	0.021	0.020	0.018	0.028	0.020	0.027	0.022	0.030	0.028	0.039
Ba	mmol/kgH_2O	1.1E-04	1.1E-04	1.1E-04	7.8E-05	1.1E-04	7.8E-05	1.1E-04	7.9E-05	8.5E-05	6.0E-05
Cl	mmol/kgH_2O	85	85	85	85	85	85	85	85	85	85
S(VI)	mmol/kgH_2O	27.01	27.00	27.00	27.38	27.02	27.39	27.01	27.36	53.61	53.83
S(-II)	mmol/kgH_2O	1.5E-08	1.5E-08	1.5E-08	3.2E-07	1.4E-08	5.2E-07	1.6E-08	2.6E-07	1.4E-08	2.4E-07
C(IV)	mmol/kgH_2O	2.91	2.84	2.85	3.24	1.43	1.60	4.75	5.24	4.75	5.31
HCO_3	mmol/kgH_2O	2.49	2.43	2.43	2.79	1.26	1.42	3.89	4.35	3.84	4.37
F	mmol/kgH_2O	0.17	0.18	0.17	0.22	0.18	0.22	0.17	0.22	0.17	0.22
SO_4/Cl	mol/mol	0.32	0.32	0.32	0.32	0.32	0.32	0.32	0.32	0.63	0.63
Ca/Mg	mol/mol	1.28	1.33	1.35	1.70	1.28	1.70	1.28	1.70	1.26	1.72
Na/Ca	mol/mol	13.60	13.79	13.63	15.98	13.95	16.50	13.21	15.42	13.40	15.62
Na_X	eq_fraction	0.440	0.436	0.437	0.396	0.443	0.399	0.437	0.391	0.517	0.456
K_X	eq_fraction	0.042	0.042	0.042	0.042	0.043	0.042	0.042	0.042	0.042	0.041
Ca_X2	eq_fraction	0.346	0.349	0.348	0.396	0.344	0.393	0.348	0.399	0.297	0.358
Mg_X2	eq_fraction	0.162	0.163	0.163	0.152	0.161	0.151	0.163	0.153	0.139	0.137
Sr_X2	eq_fraction	0.0088	0.0087	0.0087	0.0133	0.0089	0.0135	0.0086	0.0130	0.0039	0.0065
Fe_X2	eq_fraction	5.9E-04	5.9E-04	5.9E-04	6.1E-04	5.8E-04	6.1E-04	5.9E-04	6.1E-04	5.0E-04	5.5E-04
Mn_X2	eq_fraction	4.1E-04	4.1E-04	4.1E-04	7.9E-04	4.0E-04	7.8E-04	4.1E-04	7.9E-04	3.5E-04	7.1E-04
Ba_X2	eq_fraction	4.0E-06	4.0E-06	4.0E-06	5.6E-06	4.1E-06	5.7E-06	4.0E-06	5.5E-06	1.8E-06	2.7E-06
Sum_exchanger	eq_fraction	1.000	1.000	1.000	1.000	1.000	1.000	1.000	1.000	1.000	1.000

5.8 Comparison of reference porewater composition to the constraining data and discussion

Fig. 5-1 is a Schoeller diagram of the constraining concentrations for aliquots from squeezing and advective displacement, along with the composition of the two reference porewaters, ZNO-NL and JO. There is an overall good 'average match' to the spread in data. The main components Cl and Na were not matched to the highest salinities observed in Bülach-1-1 for the NL region, as explained in Chapter 2 and Section 4.1.2. There is a slight mismatch of the reference porewaters in Ca and Mg in all regions due to the fixed Ca/Mg activity ratio resulting from assuming calcite – dolomite equilibrium (see Section 5.3 for details). TIC is somewhat larger in the reference porewaters compared to measurements, but a direct comparison is not valid, because the squeezing and adjectively displaced aliquots are all strongly supersaturated with respect to calcite indicating a disturbance to the carbonate system (this may be addressed by modelling performing a back-correction to a calcite-saturated state). This is also why the measured pH values of the squeezing and adjectively displaced aliquots cannot be compared directly. Measured pH values of aliquots from advective displacement are quite close to those of the reference porewaters, but the squeezing aliquots show a strongly elevated and disturbed pH. The pH of the reference porewaters is the result of assuming a fixed partial pressure of CO_2 and the imposed carbonate equilibria and related speciation and ion-exchange equilibria.

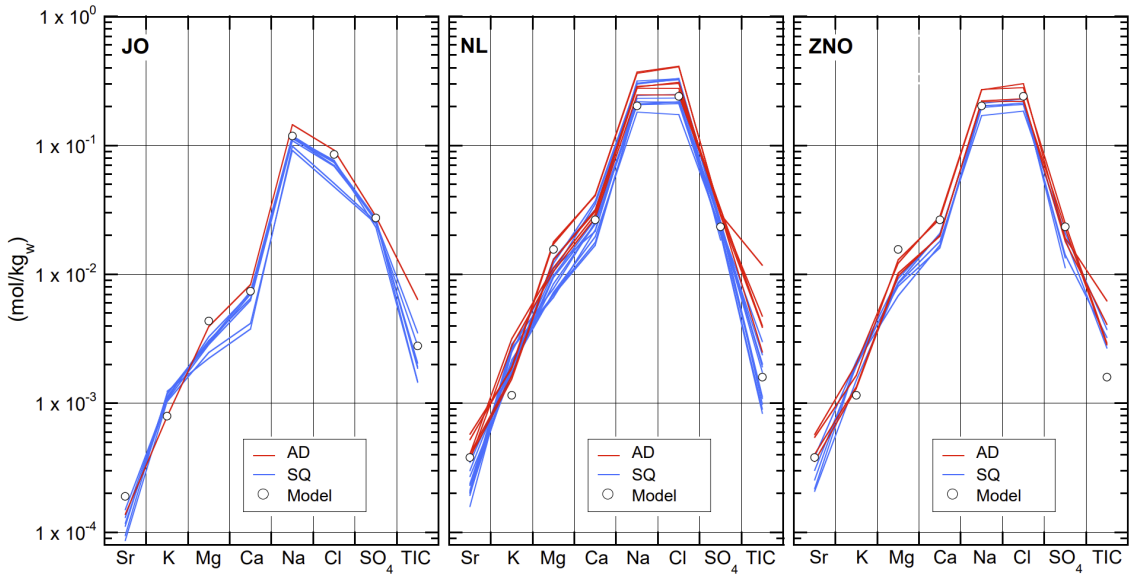

Fig. 5-1: Schoeller diagrams of the squeezing and advective displacement aliquots and the reference porewater composition (Model) for ZNO, NL and JO

Circles represent the composition of the reference porewater (same for NL and ZNO). Lines in red are advective displacement aliquots, and squeezing aliquots are shown in blue. The logarithmic scale diminishes differences of the more concentrated ions.

The calculated composition of the clay exchanger (Tab. 5-4, Tab. 5-5, Tab. 5-6) of the reference porewaters differs somewhat from a best-fit to the measured composition, mainly because the fixed Ca/Mg activity ratio imposed by calcite – dolomite equilibrium in the porewater fixes the CaX_2/MgX_2 activity ratio on the clay exchanger, according to the chosen selectivity constants (Section 5.2). This has the effect that mainly the Mg occupancy in the reference porewaters is smaller than measured for ZNO and NL, but not for JO, where mainly the calculated CaX2 is

smaller than the measured values. The K-occupancy calculated is smaller than the averages of the measured values in all regions. This is mainly an effect of the larger values measured with the Cs-method carried out at PSI that tend to dominate the averages. The values obtained by the Ni-en method at Uni Bern are more in line with the calculated values. Sr turns out invariably to be supersaturated with respect to celestite when using the exchanger composition as constraint and the selectivity coefficients of Appelo and Postma (2005) adopted here. The exchanger population for Sr used for initiating the reference porewaters was therefore reduced compared to average measurements, to avoid such an effect. An alternative option would have been to adjust the selectivity constant that is presently the one showing the largest spread in data derived by different laboratories (Section 5.2, Tab. 5-1). Apart from this, the calculated exchanger composition is a fairly good match to the measured data that do have a considerable spread for some components (Tab. 5-7). The ratio of Na to the sum of the divalent components (CaX2+MgX2) is well captured for ZNO and NL but is somewhat smaller in the calculated ratio compared to the measurements. This ratio should in fact be decreasing with decreasing ionic strength (as present in the JO region) as calculated for the reference porewaters reflecting the increased preference for divalent cations to occupy the exchanger. Interestingly, this is only slightly evident in the measured data (there is a considerable standard deviation). It can also be observed that the data spread in the measured occupancies is largest in the NL region as evidenced by distinctly larger standard deviations. This may in part be due to the larger differences in salinities in this region compared to ZNO and JO.

Tab. 5-7: Composition of clay exchanger (equivalent fractions) in ZNO, NL, JO, and that calculated with the reference porewater compositions

Minor amounts of Fe, Mn and Ba are omitted (see Tab. 5-5 and Tab. 5-6); [1)] Correction for porewater contribution: Na: corrected for $Cl+SO_4$; Na, Ca: Na corrected for Cl, Ca corrected for SO_4. Data for BAC1-1 are not included (Gaucher et al. *in prep*.).

	ZNO	ZNO	NL	NL	Ref-PW ZNO-NL	JO	JO	Ref-PW JO
Correction	Na	Na, Ca	Na	Na, Ca		Na	Na, Ca	[1)]
NaX	0.39 (0.02)	0.42 (0.02)	0.41 (0.04)	0.45 (0.04)	0.44	0.41	0.44	0.40
KX	0.10 (0.02)	0.10 (0.02)	0.10 (0.04)	0.10 (0.04)	0.040	0.08	0.08	0.042
CaX2	0.34 (0.02)	0.31 (0.02)	0.34 (0.04)	0.30 (0.05)	0.369	0.34	0.31	0.40
MgX2	0.15 (0.01)	0.51 (0.01)	0.12 (0.02)	0.12 (0.02)	0.143	0.15	0.15	0.15
SrX2	0.009 (0.001)	0.009 (0.001)	0.005 (0.001)	0.005 (0.001)	0.007	0.008	0.008	0.013
NH_4^+	0.020 (0.001)	0.018 (0.001)	0.032 (0.021)	0.032 (0.021)	0.00	0.020	0.020	0.00
CaX2/MgX2	2.35 (0.35)	2.05 (0.34)	2.79 (0.47)	2.47 (0.51)	2.6	2.24 (0.34)	2.05 (0.30)	2.6
NaX/ (CaX2+MgX2)	0.78 (0.04)	0.90 (0.04)	0.90 (0.11)	1.08 (0.14)	0.86	0.83 (0.07)	0.95 (0.08)	0.72

The calculated Fe(II) and Fe(III) concentrations on the basis of an assumed siderite equilibrium and the linked redox potential (Eh or pε) assuming pyrite equilibrium cannot be rigorously assessed by independent means. Attempts to measure the redox potential (in situ field experiments, laboratory experiments) have invariably not delivered the negative values required to maintain pyrite a stable phase. Pyrite is ubiquitously present as a phase with a high specific surface area (framboidal pyrite of diagenetic origin, that readily is prone to oxidation during intrusive measures), and experiments are thought to be affected by oxygen diffusion and/or interactions with equipment surfaces. The sampling and measurement of Fe-species is notoriously difficult and suffers from artefacts related to drilling, instrumentation, sampling and analysis. It is also not clear which mineral phase or phases do control the Fe concentrations and/or sulphide concentrations. This approach is a relative robust assumption, and it places the redox condition on the sulphate-rich side (relative to sulphide) of the pyrite stability field. Because the Fe-carbonate observed in Opalinus clay is not pure (both, calcite-siderite and dolomite-ankerite solid solutions are commonly present) the 'true' Fe concentrations and therefore also the 'true' redox potential may be somewhat displaced from the model condition. Different Fe-bearing phases have also been proposed as controlling minerals (see e.g. Pearson et al. 2011) but there is at present no clear evidence that this may be more appropriate. The pyrite – Fe-carbonate equilibrium should be viewed as a robust proxy to constrain the redox state. Note that this is a static equilibrium view of the system. When disturbing processes are considered, the redox system reacts sensitively, and also microbial processes will be influencing fluid-mineral interactions as soon as geochemical gradients can provide nutrients and electron donors/acceptors.

A key-assumption for the carbonate system and pH of the reference porewaters is the assumed fixed value of a partial pressure of CO_2 of $10^{-2.2}$ bar, mainly based on previous work (e.g., Pearson et al. 2003, Mäder 2009, Pearson et al. 2011, Wersin et al. 2013, 2020, details in Section 4.5). The new data, aliquots from squeezing and advective displacement, from the TBO campaign have not yet been interpreted in-depth to provide values of P_{CO2} from the strongly supersaturated states with respect to calcite (see Wersin et al. 2022a, Gimmi et al. 2022 for some preliminary interpretations of squeezing aliquots from Bözberg boreholes). The carbonate system is not an independent system, but it is linked via Ca and Mg also to the exchanger population and also to sulphate and strontium via celestite as a potentially solubility limiting phase. At this stage, this appears to be a reasonable approach for a static view. Some alternatives are discussed in Chapter 5, and reviewed in Pearson et al. (2011) and Wersin et al. (2020). The estimated uncertainty of a range of 1 log-unit in P_{CO2} is accounted for by the two variants, with a high-P_{CO2}/low-pH/high-C(IV) and a low-P_{CO2}/high-pH/low-C(IV). This approach has proven useful at a previous stage of the site selection process (Mäder 2009) and is also easily implemented in subsequent calculations for the safety case.

An issue concerning sulphate is a large discrepancy between larger concentrations obtained from hundreds of aqueous extracts scaled to porewater content and significantly lower concentrations measured in aliquots from squeezing and advective displacement, and also lower concentrations measured in porewater sampling boreholes at Mont Terri. The aqueous extracts suggest twice the sulphate concentrations even when conservatively scaled to the 'free porosity' and accounting for ion complexation. Despite concert efforts, this discrepancy could not yet be resolved, because the available 'pools' of sulphur that may contribute sulphate during aqueous extraction are relatively very small (associated with carbonates, small amounts of celestite or Ba-Sr solid solutions, very limited oxidation of pyrite) (Jenni et al. 2019, Mazurek & Aschwanden 2020, Aschwanden & Wersin 2020, Wersin et al. 2013, 2020, and references therein). The concentration profiles of Cl/SO_4 ratios obtained across many boreholes in Opalinus Clay (see TBO profiles, and well resolved profiles from Mont Terri) also appear to preclude significant sulphate mineral dissolution, because such a process should lead to scatter and apparent outliers in Cl/SO_4 due to an uneven distribution of mineral concentrations. Alternatively, it may be possible that the squeezing process and the advective displacement procedure led to a saturation-limited state (aliquots are

invariably very close or slightly above celestite saturation) and precipitation of a sulphate phase and thus an underestimation of sulphate concentrations. But also, such a process is limited by mass-balance constraints, e.g. a limited availability of a counter-cation for extensive mineral precipitation (e.g., Sr in case of celestite). To account for potentially significant higher sulphate concentrations in the reference porewaters, a high-sulphate variant was modelled having approximately twice the sulphate concentrations. This variant has a higher ionic strength due to the extra sulphate included, and associated charge-balancing cations. The corollary of this is that the Ca and Mg concentrations are reduced relative to Na, in order to stay below saturation with respect to sulphates gypsum and celestite, while the Ca/Mg activity ratio is also fixed by the assumed calcite – dolomite equilibrium. The resultant variant also leads to a different cation occupancy on the clay exchanger compared to the measured populations, and when adopting the same selectivity coefficients.

The differences between the reference porewater compositions, including variants, are very small when using different thermodynamic databases (Tab. 5-5 ZNO-NL, Tab. 5-6 for JO). Minor differences between the newly revised PSI-Nagra TDB and the older versions (and WATEQ4F) are: a slightly higher HCO_3^- concentration (because pH is higher by 0.04 – 0.05 units), a distinctly lower Mg concentration relative to Ca (higher Ca/Mg ratio, as discussed in Section 5.3), slightly higher Sr concentrations (mainly due to a revised log-*K* for celestite), and slightly higher Al and Mn (revised log-*K* for rhodochrosite) concentrations. These differences are well within the overall uncertainties associated with the spread of the constraining data and the uncertainties associated with choosing the mineral phases for imposing solubility constraints. A large relative difference is seen in Fe(III) and S(-II) concentrations: Fe(III) concentrations are more than two orders of magnitude larger (new PSI-Nagra TDB) than with the others, and S(-II) concentrations obtained with the new TDB are also much larger compared to results with the other TDBs. This is due to the adoption of a new Fe(III)-carbonate aqueous species, $Fe(OH)CO_3$, added to the new TDB that is not present in the others. Charged Fe(III) species remain at concentrations at least three orders of magnitude below total Fe(III), and at concentrations similar than calculated with the other TDBs. This higher solubility of pyrite is also an effect of a revised log-*K* value adopted in the latest PSI-Nagra TDB (−21.32 vs. −18.5 in earlier versions) (see Hummel & Thoenen 2023 for details).

Note that all calculations were performed at a temperature of 25 °C and 1 bar pressure. The constraining data, such as advective displacement, squeezing and aqueous extraction have also been performed at room temperature. The composition of the reference porewaters are therefore biased towards the constraining data elaborated at ambient temperature and pressure. This approach had been chosen because the subsequent calculations performed with these reference porewaters will also be calculated at these conditions. The processes that affect samples – and thus also porewater composition – during drilling, core recovery, sample conditioning, transport, cold storage and preparation are complex, and the link from the laboratory results to the in situ porewater composition is not trivial, and not a subject of this report. A main issue, the expected effects due to changes in temperature, are discussed in the next section.

6 Effect of temperature on the porewater composition

6.1 Introduction

Considerations on porewater composition discussed so far have not addressed the effect of temperature. The proposed model for reference porewater (Chapter 5) is based on laboratory experiments carried out at room temperature and thermodynamic data at standard conditions (25°°C, 1°bar). In-situ temperatures of the OPA porewater, however, will be up to about 50 °C depending on the location and depth of the HLW repository. Initially, due to decay heat of the waste, temperatures in the host rock will be even higher close to the emplacement tunnels.

In general, changes of porewater compositions relative to 25°°C are not expected to be large because of the weak dependence of most log-*K* constants for mineral solubility with temperature. It should be noted, however, that the solubility of gases generally shows a stronger dependence on temperature than that of minerals, and the solubility of gases increases even more strongly with pressure and therefore also along geothermal gradients. In this context the decrease of the solubility of CO_2 with increasing temperature leading to an increase of P_{CO2} at higher temperatures is relevant as also indicated from experimental data on porewaters from the Callovo-Oxfordian Formation (Vinsot et al. 2015, Beaucaire et al. 2012, Gailhanou et al. 2017).

In this chapter, we will estimate the effect of temperature on reference OPA porewater composition by considering the thermodynamic model elaborated in Chapter 5 and the (generally well-established) temperature parameters associated to the log-*K* constants as implemented in the selected thermodynamic databases (see Section 6.3). There is one issue that needs to be addressed specifically in the model when considering higher temperatures, namely the constraints on P_{CO2} (and pH which is closely related to this parameter). In the 'standard' model for reference porewaters, P_{CO2} is used as input parameter with a value of −2.2 log(bar) based on expert judgement. The latter is based primarily on findings gained at Mont Terri (a low temperature environment) and CO_2 measurements on core samples at ambient temperatures (Lassin et al. 2003, Gaucher et al. 2010, Wersin et al. 2016). At higher temperature, a change in P_{CO2} (and pH) is expected and this parameter can no longer be treated as input parameter (see for example discussion in Wersin et al. 2020). To overcome this issue, selected aluminosilicate (clay mineral) equilibria are added to the model as discussed in the next sections. It is worth noting that the consideration of Al silicate equilibria for modelling porewaters of clayrocks is not new and has for example been applied to the Callovo-Oxfordian Formation (Gaucher et al. 2009) and the Opalinus Clay (Pearson et al. 2011).

6.2 Role of aluminosilicates

The positive dependence of P_{CO2} on temperature has been shown for porewaters and groundwaters from a number of geological formations since decades. For example, Coudrain-Ribstein & Gouze (1993) and Coudrain-Ribstein et al. (1998) showed clear trends for aquifers in sedimentary formations. These could be explained by the authors by equilibrium with carbonate and aluminosilicate mineral assemblages. This has been confirmed by more recent modelling studies (Ceriotti et al. 2017, Lu et al. 2020).

The effect of temperature on the porewater chemistry of the COx formation has been investigated by two research teams (CEA, BRGM) as part of Andra's research programme (Beaucaire et al. 2012, Gailhanou et al. 2017). In summary, these results reveal similar trends. Notably, a clear dependence of P_{CO2} and pH with temperature was observed in the experimental data. Otherwise, changes were rather small. Thus, major components (Na, Ca, Mg, K, Cl, SO_4) exhibited only minor changes at higher temperatures. The behaviour of solutes could be adequately modelled by both teams considering mineral and cation exchange equilibria. Both modelling approaches were

based on a similar thermodynamic framework but differed regarding underlying thermodynamic data and assumed mineral assemblage. Thus, Beaucaire et al. (2012) considered equilibria with endmember clay minerals (clinochlore, kaolinite) in their model whereas Gailhanou et al. (2017) considered 'natural' clay minerals with a fixed composition (ripidolite, illite). One outcome of both modellings was that cation exchange equilibria seemed rather insensitive to temperature.

Controls of P_{CO2} and pH by clay mineral equilibria in OPA have been discussed at various stages of the Mont Terri Project. Different levels of uncertainty were identified in the first synthesis report of Pearson et al. (2003), including uncertain pH, P_{CO2} conditions in borehole waters as well as poor-quality thermodynamic data and sluggish kinetics of clay minerals. Improved borehole water data (e.g., from PC-C experiment, Vinsot et al. 2008) indicated near-to-constant P_{CO2} levels across the OPA formation in spite of a clear compositional gradient (Wersin et al. 2009, 2022b). This lends support to control by an internal mineral phase assemblage including carbonate and clay minerals. Considering model developments of the COx porewaters (Gaucher et al. 2006, 2009), Pearson et al. (2011) carried out a modelling exercise to simulate the PC-C porewater including a sensitivity analysis with a selected set of clay mineral pairs. The overall finding was that the different model variants all matched the major elements fairly well, thus displaying only minor differences in major cations and anions. The differences in pH and P_{CO2} were somewhat larger. It should be noted that the precise composition of the clay minerals (illite, illite/smectite, kaolinite, chlorite) is not known for the Opalinus Clay which adds to the uncertainty of model results.

6.3 Setup of equilibrium model

The core of the porewater model including clay mineral equilibria is identical to that set up for the reference porewater composition. Thus, equilibrium with the mineral phases calcite, dolomite, celestite, quartz, siderite, pyrite, rhodochrosite and fluorite is also assumed. Moreover, the model considers a fixed exchanger composition based on experimental data[2]. In addition, a pair of clay minerals is included to constrain the Al and pH – P_{CO2} and to satisfy the Gibbs phase rule as discussed in previous porewater modelling studies (Gaucher et al. 2009, Pearson et al. 2011, Wersin et al. 2020).

Three different pairs of clay minerals were selected as model variants to address the uncertainty regarding the exact nature of clay phases controlling the porewater chemistry. This includes iron-free illite and chlorite minerals with endmember mineral compositions and kaolinite:

1. Kaolinite/Mg-chlorite (clinochlore)
2. Kaolinite/Mg-illite
3. Mg-chlorite/Mg-illite

The reason of selecting iron-free minerals is to avoid influencing redox constraints imposed by the SO_4 – pyrite – siderite equilibrium assumed in the "standard" model.

Cation selectivity coefficients were assumed to be independent of temperature within the considered temperature range (25 – 80 °C), which is based on experimental studies (Beaucaire et al. 2012, Gailhanou et al. 2017).

The primary thermodynamic database was the new PSI 2020 v1-3 database which includes temperature-dependent log-*K* data for all relevant chemical reactions. In addition, the newest version of well-established THERMOCHIMIE database (Version 11a, Rodriguez et al. 2022),

[2] Note that fixing the exchanger composition and assuming dolomite equilibrium leads to an overconstraint on Mg. In the equilibrium calculations, equilibrium with dolomite overrides that of exchange, leading to a slight change in the Mg concentration on the exchanger.

developed within the French and British radioactive waste disposal programmes, was applied to compare results obtained from the PSI database. Since Mg-chlorite (clinochlore) is not contained in the PSI database, this phase was taken from THERMOCHIMIE. Finally, selected calculations were also conducted with THERMODDEM, a database developed and maintained by BRGM (Blanc et al. 2012).

Model runs were carried out for the ZNO-NL porewater with PHREEQC (Version 3.7.3) within a temperature range of 25 – 80°C. Gypsum and anhydrite which have retrograde solubilities were allowed to precipitate if saturation was reached.

6.4 Results and discussion

In a first step the model with the three variants described above was run at 25°C to compare with the 'standard' model described in Section 5. The results are shown in Tab. 6-1 (unshaded columns). In general, they yield very similar results for all model variants compared to the reference model, also with respect to pH/P_{CO2} conditions. This a priori could not be expected because of the inherent uncertainty related to clay mineral equilibria, their reaction kinetics and the clay mineral composition in OPA (see discussion above). This uncertainty is further explored by considering further thermodynamic databases besides the PSI TDB (see below).

In a second step, calculations were run at 50°C for the three model variants (Tab. 6-1 shaded areas). The results indicate only minor changes relative to 25°C regarding the main components. Si and Al are increased due to the higher solubility of silicates. The largest change is indicated for the carbonate system manifested by lower pH and higher P_{CO2}. The same trend was reported in the experimental studies for COx (Beaucaire et al. 2012, Gailhanou et al. 2017) and previous more general studies on sedimentary basins (Coudrain-Ribstein & Gouze 1993, Coudrain-Ribstein et al. 1998). Note that all waters remain undersaturated with regard to gypsum and anhydrite at these temperatures.

Tab. 6-1: Results from equilibrium model for NL-ZNO OPA porewater with PSI 2020 TDB considering three different clay mineral equilibria

Values are indicated for 25 °C and 50 °C.

Concentrations in mmol/kgw. Blue font: components showing significant changes with temperature.

	Ref. Model	Illite(Mg)/Clinochlore		Illite(Mg)/Kaolinite		Kaolinite/Clinochlore	
Temp. (°C)	25	25	50	25	50	25	50
pH (-)	7.07	7.05	6.51	6.94	6.54	7.03	6.49
pe (-)	-2.76	-2.73	-2.66	-2.61	-2.69	-2.71	-2.64
Cl	240.0	240.01	240.02	239.99	239.99	240.01	240.01
SO_4	23.38	23.38	23.38	23.39	23.39	23.38	23.38
Na	202.0	202.40	202.25	202.16	201.75	202.39	202.20
Ca	26.48	26.49	29.90	26.84	30.18	26.53	29.97
Mg	15.6	15.61	12.73	15.82	12.86	15.63	12.77
K	1.16	1.19	1.23	0.81	0.67	1.16	1.16
Sr	0.38	0.38	0.39	0.38	0.39	0.38	0.39
Fe	0.10	0.10	0.10	0.10	0.10	0.10	0.10
Si	0.17	0.17	0.34	0.17	0.34	0.17	0.34
Al	2.0E-5	1.5E-05	9.5E-05	2.4E-05	1.1E-04	2.1E-05	1.2E-04
$CO_{3,t}$	2.11	2.21	4.07	2.89	3.71	2.35	4.25
log P_{CO2} (bar)	-2.2	-2.16	-1.27	-1.95	-1.34	-2.11	-1.24
SI (gypsum)	-0.16	-0.16	-0.16	-0.16	-0.16	-0.16	-0.16
SI (anhydrite)	-0.53	-0.53	-0.26	-0.52	-0.25	-0.53	-0.26

Tab. 6-2 shows the same calculations with the THERMOCHIMIE database. Looking first at the results at 25°°C, differences with results obtained using the PSI database are rather minor. Slight differences in Ca and Mg are evident. In fact, THERMOCHIME yields very similar results as the other databases (WATEQ, old PSI TDB) discussed in Section 5. The largest differences are seen for pH – P_{CO2} conditions for the illite(Mg)-kaolinite variant. This difference can be attributed first of all to the different logK data for kaolinite. In the case of the PSI TDB, these are based on thermodynamic data proposed by Nordstrom et al. (1990) whereas in THERMOCHIMIE logK of kaolinite is derived from calorimetric data of Fialips et al. (2001) and Robie & Hemingway (1991). The latter data set yields a lower kaolinite solubility concentrations and thus lower Al concentrations compared to data obtained from the PSI TDB (compare Tab. 6-1 and Tab. 6-2). Looking second at the calculations at 50°°C with THERMOCHIMIE, one can observe similar trends for the different components as obtained with the PSI TDB. Thus, the shift in pH and P_{CO2} to lower and higher values, respectively, is very similar with both databases.

Tab. 6-2: Same calculations as shown in Tab. 6-1 but considering the THERMOCHIMIE database

Concentrations in mmol/kgw. Blue font: components showing significant changes with temperature.

	Ref. Model	Illite(Mg)/Clinochlore		Illite(Mg)/Kaolinite		Kaolinite/Clinochlore	
Temp. (°C)	25	25	50	25	50	25	50
pH (-)	7.06	7.01	6.47	7.82	7.37	7.10	6.57
pe (-)	-2.73	-2.68	-2.59	-3.60	-3.61	-2.78	-2.70
Cl	240.0	240.01	240.02	240.00	240.00	240.01	240.01
SO_4	23.38	23.32	23.33	23.32	23.33	23.32	23.33
Na	203.0	203.38	203.74	203.06	203.26	203.29	203.59
Ca	24.08	24.12	28.66	23.73	28.02	24.04	28.54
Mg	17.34	17.37	12.93	17.10	12.63	17.32	12.87
K	1.17	1.21	1.25	1.13	1.13	1.17	1.18
Sr	0.35	0.35	0.37	0.35	0.36	0.35	0.37
Fe	0.24	0.24	0.34	0.24	0.34	0.24	0.34
Si	0.18	0.18	0.35	0.18	0.35	0.18	0.35
Al	6.4E-6	1.9E-5	1.3E-4	1.4E-5	5.2E-5	6.2E-6	3.3E-5
$CO_{3,t}$	2.08	2.35	3.92	0.37	0.42	1.88	2.96
log P_{CO2} (bar)	-2.2	-2.10	-1.26	-3.71	-3.05	-2.29	-1.46
SI (gypsum)	-0.15	-0.15	-0.11	-0.16	-0.12	-0.15	-0.11
SI (anhydrite)	-0.32	-0.32	-0.04	-0.32	-0.05	-0.32	-0.05

The same set of calculations were carried out with the THERMODDEM database from BRGM (not shown) and yielded very similar results as those obtained from THERMOCHIMIE.

The trends with temperature within the range of 25 – 80°°C are illustrated in Fig. 6-1 to Fig. 6-3. Note that in these figures, the full lines reflect results from the PSI TDB whereas the dashed lines reflect data from THERMOCHIMIE. Regarding P_{CO2} and pH, a consistent trend is revealed for all three model variants (Fig. 6-1). Thus, for the two model variants including clinochlore similar curves as a function of temperature are obtained. The model variant with Mg-illite/kaolinite displays slightly flatter P_{CO2} – T and pH – T curves. Using the PSI TDB, the model simulations predict only small differences in pH – P_{CO2} over all the temperature range. Thus, the maximum pH difference between the three variants in this range is 0.25°pH units. Using THERMOCHIMIE, differences are larger, thus the Mg-illite/kaolinite model variant yields about 1°pH unit higher values than the other two variants. As mentioned above, the main reason for the larger spread is the different thermodynamic data used for kaolinite, manifested for example by the different Al concentrations.

The main cationic and anionic components (Na, Ca, Mg, Cl, SO_4) show only minor changes with temperature (Fig. 6-2). A slight decrease for Mg and increase for Ca, respectively, with temperature is noted which is more pronounced with THERMOCHIMIE. This difference is due to the different underlying calcite-dolomite data in the two databases. Sulphate shows a small

drop at higher temperatures which is related the retrograde solubility of Ca sulphates (anhydrite and gypsum). At lower temperatures, porewaters are undersaturated with repsect to these minerals but reach equilibrium with respect to anhydrite at about 70°C with the PSI TDB and about 55°C with THERMOCHIME (Fig. 6-3). This difference is again related to the different underlying thermodynamic data for this mineral (see Section 5.1).

Differences in the two databases are also revealed regarding the predicted iron concentrations, primarily because of different underlying thermodynamic data for siderite. Thus, using the PSI data, lower Fe concentrations and very little dependence with temperature is predicted in contrast to the data obtained from THERMOCHIMIE (compare Tab. 6-1 and Tab. 6-2). These differences, however, have only a small effect on the redox potential which is constrained by the SO_4 – pyrite – siderite equilibrium in the model.

The effect of pressure has been neglected in this modelling exercise. As shown by previous modellings (e.g., Wersin et al. 2020) this effect is expected to be very small for OPA porewaters at the relevant depths.

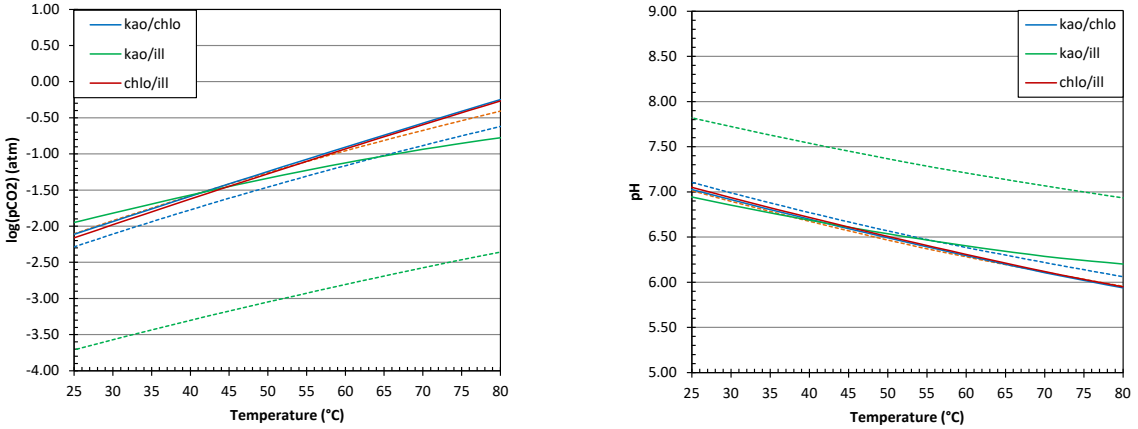

Fig. 6-1: P_{CO2} in log(bar) (left) and pH (right) vs. temperature for the model including clay mineral equilibria

Solid lines: PSI TDB, dashed lines: THERMOCHIMIE

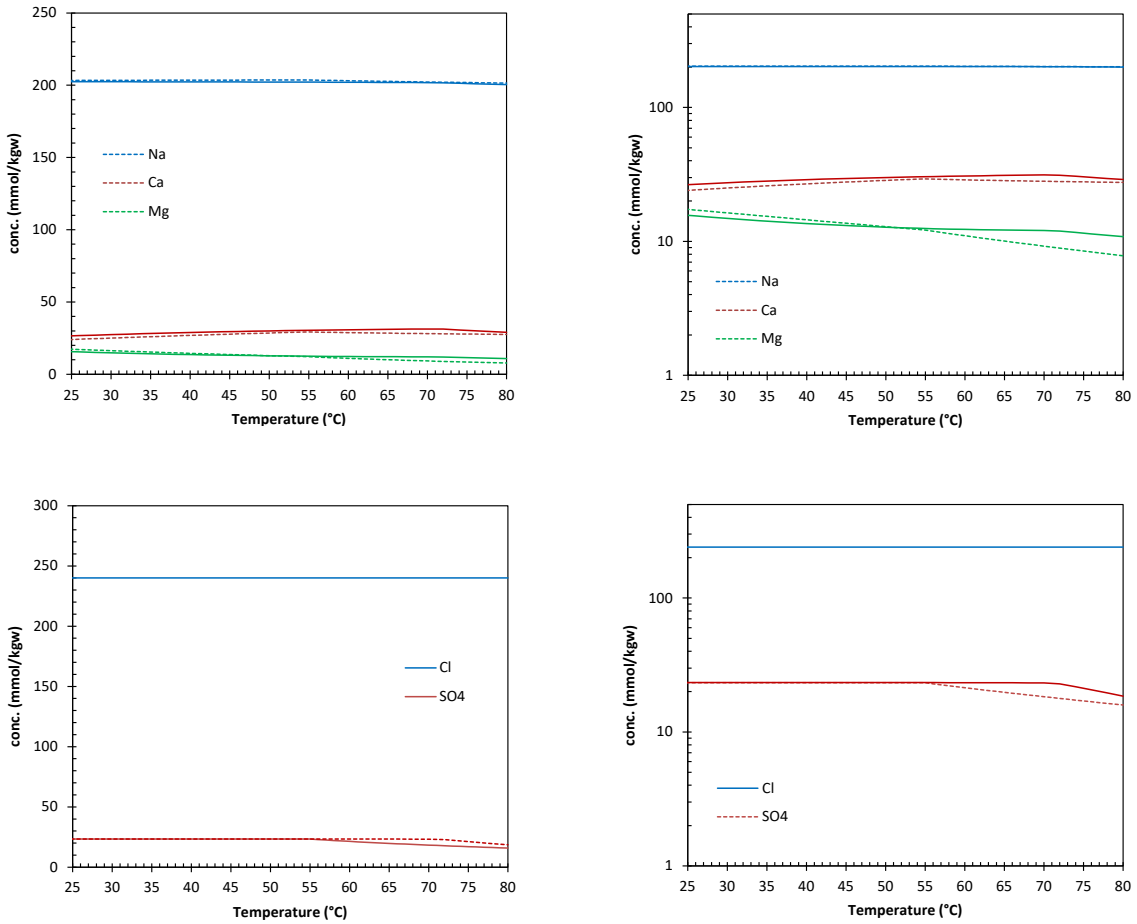

Fig. 6-2: Concentrations of main components for the model including clay mineral equilibria in linear (left) and logarithmic (right) scales vs. temperature

Solid lines: PSI TDB, dashed lines: THERMOCHIMIE

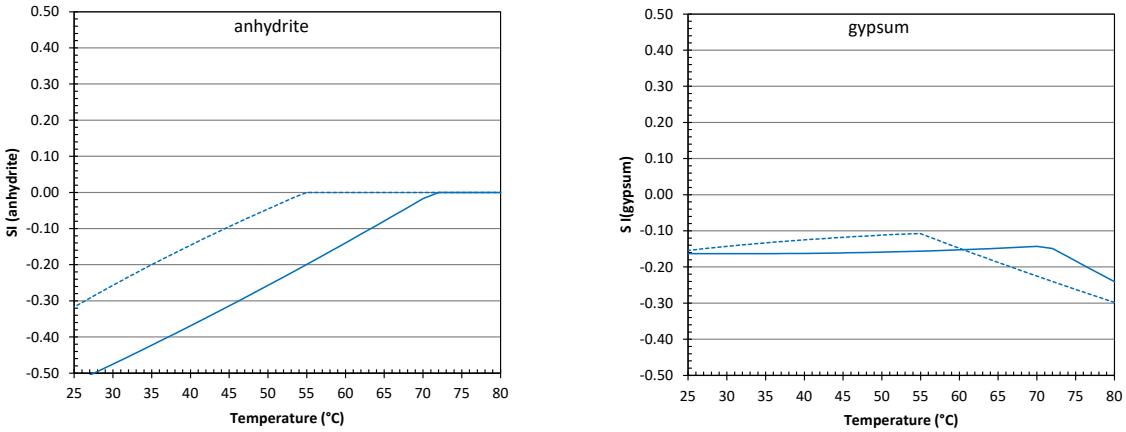

Fig. 6-3: Saturation indices (SI) for anhydrite (left) and gypsum (right) vs. temperature
Solid lines: PSI TDB, dashed lines: THERMOCHIMIE

In summary, the temperature calculations yield broadly consistent results for different model variants and different thermodynamic databases. In the range of in-situ temperatures (40 – 50°°C) and even beyond, changes in major ion composition relative to 25°°C are very minor. Regarding P_{CO2}, an increase of 0.6 to 0.9°log(bar) is predicted depending on the Al silicate assemblage considered. The corresponding shift in pH is 0.4 – 0.5°pH units (to lower values). These changes arise from the increased solubility of the silicate minerals together with change of solubility of CO_2 and of the ion dissociation constant of water. In a more general sense, this modelling exercise provides some confidence that the equilibrium model for OPA including clay mineral equilibria yields reasonable estimates of porewater composition over the temperature range of interest. Nevertheless, it should be pointed out that the inherent uncertainty related to clay mineral thermodynamics and the incomplete knowledge of the nature of clay mineral-chemistry in OPA remains.

7 Acknowledgements

The authors acknowledge support by Carmen Zwahlen, Mirjam Kiczka and Thomas Gimmi (all at University of Bern) for participating in discussions and for preparing many figures modified from Dossier VIII reports. Daniel Traber and Raphael Wüst (both at Nagra) provided helpful input and guidance at all stages of the project. Colleagues at PSI, Wolfgang Hummel and Dan Miron, discussed issues related to thermodynamic data. Enzo Curti (PSI) contributed with a thorough review to improve the clarity of arguments. Petra Blaser (petraconsult) expertly handled all editorial aspects and improved the consistency of presentation.

8 References

Appelo, C.A.J. & Postma, D. (2005): Geochemistry, Groundwater and Pollution (2nd edition). Balkema, Keiden (1st edition 1993).

Appelo, C.A.J. & Wersin, P. (2007): Multicomponent diffusion modeling in clay systems with application to the diffusion of tritium, iodide, and sodium in Opalinus Clay. Environmental Science and Technology 41, 5002-5007.

Appelo, C.A.J., Van Loon, L.R. & Wersin, P. (2009): Multicomponent diffusion of a suite of tracers (HTO, Cl, Br, I, Na, Sr, Cs) in a single sample of Opalinus Clay. Geochimica et Cosmochimica Acta 74, 1201-1219.

Aschwanden, L. & Wersin, P. (2020). Experimental study of sulphate in the Opalinus Clay: Results from extraction tests. Nagra Arbeitsbericht NAB 20-17.

Aschwanden, L., Camesi, L., Gaucher, E., Gimmi, T., Jenni, A., Kiczka, M., Mäder, U., Mazurek, M., Rufer, D., Waber, H.N., Wersin, P., Zwahlen, C. & Traber, D. (2021): TBO Trüllikon-1-1: Data report. Dossier VIII; Rock properties, porewater characterisation and natural tracer profiles. Nagra Arbeitsbericht NAB 20-09.

Aschwanden, L., Camesi, L., Gimmi, T., Jenni, A., Kiczka, M., Mäder, U., Mazurek, M., Rufer, D., Waber, H.N., Wersin, P., Zwahlen, C. & Traber, D. (2022): TBO Stadel-3-1: Data report. Dossier VIII: Rock properties, porewater characterisation and natural tracer profiles. Nagra Arbeitsbericht NAB 22-01.

Baeyens, B. & Fernandes, M.M. (2022): Determination of the cation exchange capacities and exchangeable cations of deep drilling core samples from the siting regions Jura Ost, Nördlich Lägern and Zürich Nordost. Nagra Arbeitsbericht NAB 21-01.

Beaucaire, C., Tertre, E., Ferrage, E., Grenut, B., Pronier, S. & Madé, B. (2012): A thermodynamic model for the prediction of pore water composition of clayey rock at 25 and 80 ºC – comparison with results from hydrothermal alteration experiments. Chemical Geology 334, 62-76.

Blanc, P., Lassin, A., Piantone, P., Azaroual, M., Jacquemet, N., Fabbri, A. & Gaucher, E.C. (2012): THERMODDEM: A geochemical database focused on low temperature water/rock interactions and waste materials. Applied Geochemistry 27, 2107-2116.

Bleyen, N., Smets, S., Small, J., Moors, H., Leys, N., Albrecht, A., De Canniere, P., Schwyn, B., Wittebroodt, C. & Valcke, E. (2017): Impact of the electron donor on in situ microbial nitrate reduction in Opalinus Clay: Results from the Mont Terri rock laboratory (Switzerland). Swiss Geoscience Journal 110, 355-374.

Bradbury, M.H. & Baeyens, B. (1997): Derivation of *in situ* Opalinus Clay porewater compositions from experimental and geochemical modelling studies, with Corrigendum. Nagra Technical Report NTB 97-07.

Bradbury, M.H., Baeyens, B. & Thoenen, T. (2008): Sorption data bases for generic Swiss argillaceous, crystalline and calcareous rock systems. Nagra Arbeitsbericht NAB 08-50.

Ceriotti, G., Porta, G., Geloni, C., Dalla Rosa, M. & Guadagnini, A. (2017): Quantification of CO_2 generation in sedimentary basins through carbonate/clays reactions with uncertain thermodynamic parameters. Geochimica et Cosmochimica Acta 213, 198-215.

Coudrain-Ribstein, A. & Gouze, P. (1993): Quantitative study of geochemical processes in the Dogger aquifer, Paris basin. Applied Geochemistry 8, 495-506.

Coudrain-Ribstein, A., Gouze, P. & de Marsily, G. (1998): Temperature – carbon dioxide partial pressure trends in confined aquifers. Chemical Geology 14, 73-89.

Curti, E., Thoenen, T., Kosakowski, G., Miron, D., Baeyens, B., Van Loon, L.R. & Leupin, O.X. (*in prep.*): The chemical near-field evolution within the HLW/SF repository. Nagra Technical Report NTB 23-02.

Egli, D, Mosar, J., Ibele, T. & Madritsch, H. (2017): The role of precursory structures on tertiary deformation in the Black Forest – Hegau region. International Journal of Earth Sciences 106, 2297-2318.

Fernández, A.M., Sánchez-Ledesma, D.M., Tournassat., C., Melón, A., Gaucher, E.C., Astudillo, J. & Vinsot, A. (2014): Applying the squeezing technique to highly consolidated clayrocks for porewater characterisation: Lessons learned from experiments at the Mont Terri Rock Laboratory. Applied Geochemistry 49, 2-21.

Fialips, C.-I., Navrotsky, A. & Petit, S. (2001): Crystal properties and energetics of synthetic kaolinite. American Mineralogist 86, 304-311.

Gaucher, E.C., Blanc, P., Bardot, F., Braibant, G., Buschaert, S., Crouzet, C., Gautier, A., Girard, J.-P., Jacquot, E. & Lassin, A. (2006): Modelling the porewater chemistry of the Callovian–Oxfordian formation at a regional scale. Comptes Rendus Géoscience 338, 917-930.

Gaucher, E.C., Tournassat, C., Pearson, F.J., Blanc, P., Crouzet, C., Lerouge, C. & Altmann, S. (2009): A robust model for pore-water chemistry of clayrock. Geochimica et Cosmochimica Acta 73, 6470-6487.

Gaucher, E., C., Lassin, A., Lerouge, C., Fléhoc, C., Marty, N., Henry, B., Tournassat, C., Altmann, S., Vinsot, A. & Buschaert, S. (2010): CO_2 partial pressure in clayrocks: A general model (2010). *In:* Water-Rock Interaction XIII – Water-Rock Interaction WRI-13, Mexico.

Gaucher, E., Aschwanden, L., Camesi, L., Gimmi, T., Jenni, A., Kiczka, M., Mäder, U., Mazurek, M., Rufer, D., Waber, H.N., Wersin, P., Zwahlen, C. & Traber, D. (*in prep.*): TBO Bachs-1-1: Data report. Dossier VIII: Rock properties, porewater characterisation and natural tracer profiles. Nagra Arbeitsbericht NAB 22-04.

Gailhanou, H., Lerouge, C., Debure, M., Gaboreau, S., Gaucher, E.C., Grangeon, S., Grenèche, J.-M., Kars, M., Madé, B. & Marty, N. (2017): Effects of a thermal perturbation on mineralogy and pore water composition in a clay-rock: An experimental and modeling study. Geochimica et Cosmochimica Acta 197, 193-214.

Gimmi, Th. & Waber, H.N. (2004): Modelling of tracer profiles in pore water of argillaceous rocks in the Benken borehole: stable water isotopes, chloride, and chlorine isotopes. Nagra Technical Report NTB 04-05.

Gimmi, T., Aschwanden, L., Camesi, L., Gaucher, E.C., Jenni, A., Kiczka, M., Mäder, U., Mazurek, M., Rufer, D., Waber, H.N., Wersin, P., Zwahlen, C. & Traber, D. (2022): TBO Bözberg-2-1: Data report. Dossier VIII: Rock properties, porewater characterisation and natural tracer profiles. Nagra Arbeitsbericht NAB 21-22.

Hummel, W., Berner, U., Curti, E., Pearson, F.J. & Thoenen, T. (2002): Nagra / PSI Chemical Thermodynamic Data Base 01/01. Nagra Technical Report NTB 02-16. Also issued by Universal Publishers, Parkland (FL), USA.

Hummel, W. & Thoenen, T. (2023): The PSI Chemical Thermodynamic Database 2020. Nagra Technical Report NTB 21-03.

Iannotta, J., Eichinger, F. & Traber D. (*in prep.*): TBO Rheinau-1-1: Data report. Dossier VIII: Rock properties and natural tracer profiles. Nagra Arbeitsbericht NAB 22-03.

Jenni, A., Aschwanden, P., Lanari, P., de Haller, A. & Wersin, P. (2019): Spectroscopic investigation of sulphur-containing minerals in Opalinus Clay. Nagra Arbeitsbericht NAB 19-23.

Langmuir, D. (1997): Aqueous Environmental Geochemistry. Prentice-Hall, Inc.

Lassin, A., Gaucher, E.C. & Crouzet, C. (2003): Dissolved carbon dioxide and hydrocarbon extraction. Annex 6 *in:* Pearson F.J. et al.: Geochemistry of water in the Opalinus Clay Formation at the Mont Terri Rock Laboratory. Geology Series. No.5. Swiss Federal Office for Water and Geology, Bern.

Lu, P., Luo, P., Zhang, G., Zhang, S. & Zhu, C. (2020): A mineral-water-gas interaction model of pCO_2 as a function of temperature in sedimentary basins. Chemical Geology 558, 119868.

Mäder, U. (2009): Reference pore water for the Oplainus Clay and 'Brown Dogger' for the provisional safety-analysis in the framework of the sectoral plan – interim results (SGT-ZE). Nagra Arbeitsbericht NAB 09-14.

Mäder, U. & Waber, H.-N. (2017): Results of advective displacement / multi-component transport experiments from claystone samples of the Schlattingen borehole. Nagra Arbeitsbericht NAB 17-16.

Mäder, U., Aschwanden, L., Camesi, L., Gimmi, T., Jenni, A., Kiczka, M., Mazurek, M., Rufer, D., Waber, H.N., Wersin, P., Zwahlen, C. & Traber, D. (2021): TBO Marthalen-1-1: Data report. Dossier VIII: Rock properties, porewater characterisation and natural tracer profiles. Nagra Arbeitsbericht NAB 21-20.

Madritsch, H. & Hammer, P. (2012): Characterisation of Cenozoic brittle deformation of potential geological siting regions for radioactive waste repositories in Northern Switzerland based on structural geological analysis of field outcrops. Nagra Arbeitsbericht NAB 12-14.

Matter, A., Peters, Tj., Isenschmid, Ch., Bläsi, H.-R. & Ziegler, H.-J. (1987): Sondierbohrung Riniken: Geologie, Textband. Nagra Technical Report NTB 86-02.

Matter, A., Peters, Tj., Bläsi, H.-R., Meyer, J., Ischi, H. & Meyer, Ch. (1988): Sondierbohrung Weiach: Geologie, Textband. Nagra Technical Report NTB 86-01.

Mazurek, M. & Aschwanden, L. (2020): Multi-scale petrographic and structural characterisation of Opalinus Clay. Nagra Arbeitsbericht NAB 19-44.

Mazurek, M., Alt-Epping, P., Bath, A., Gimmi, Th. & Waber, H.N. (2009): Natural tracer profiles across argillaceous formations: the CLAYTRAC project. OECD Nuclear Energy Agency, NEA No. 6253.

Mazurek, M., Oyama, T., Wersin, P. & Alt-Epping, P. (2015): Porewater squeezing from indurated shales. Chemical Geology 400, 106-121.

Mazurek, M., Al, T., Celejewski, M., Clark, I.D., Fernández, A.M., Jaeggi, D., Kennell-Morrison, L., Matray, J.M., Murseli, S., Oyama, T., Qiu, S., Rufer, D., St-Jean, G., Waber, H.N. & Yu, C. (2017): Mont Terri DB-A experiment: Comparison of porewater investigations conducted by several research groups on core materials from the BDB-1 borehole. Mont Terri Technical Report 17-01. Mont Terri Project, Switzerland.

Mazurek, M., Aschwanden, L., Camesi, L., Gimmi, T., Jenni, A., Kiczka, M., Mäder, U., Rufer, D., Waber, H.N., Wanner, P., Wersin, P. & Traber, D. (2021): TBO Bülach-1-1: Data Report. Dossier VIII: Rock properties, porewater characterisation and natural tracer profiles. Nagra Arbeitsbericht NAB 20-08.

Meier, D. & Mazurek, M. (2011): Ancillary rock and pore water studies on drillcores from northern Switzerland. Nagra Arbeitsbericht NAB 10-21.

Nagra (2001): Sondierbohrung Benken: Untersuchungsbericht. Nagra Technical Report NTB 00-01.

Nagra (2002): Projekt Opalinuston: Synthese der Geowissenschaftlichen Untersuchungsergebnisse. Entsorgungsnachweis für abgebrannte Brennelemente, verglaste hochaktive sowie langlebige mittelaktive Abfälle. Nagra Technical Report NTB 02-03.

Nagra (2008): Vorschlag geologischer Standortgebiete für das SMA und HAA-Lager. Geologische Grundlagen. Nagra Technical Report NTB 08-04.

Nagra (2014): Sicherheitstechnischer Vergleich und Vorschlag der in Etappe 3 weiter zu untersuchenden geologischen Standortgebiete. Nagra Technical Report NTB 14-01.

Nordstrom, D.K., Plummer, L.N., Langmuir, D., Busenberg, E., May, H.M., Jones, B.F. & Parkhurst, D.L. (1990): Revised chemical equilibrium data for major water-mineral reactions and their limitations. *In*: Melchior, D.C. & Bassett, R.L. (eds.): Chemical Modeling of Aqueous Systems II, Washington D.C. American Chemical Society ACS, Symposium Series 416, 398-413.

Parkhurst, D.L. & Appelo, C.A.J. (1999): User's guide to PHREEQC, a computer program for speciation, batch-reaction, one-dimensional transport, and inverse geochemical calculations. U.S. Geological Survey Water-Resources Investigation Report 99-4259 (v.2.15; 2008).

Parkhurst, D.L. & Appelo, C.A.J. (2013): Description of input and examples for PHREEQC Version 3 – A computer program for speciation, batch-reaction, one-dimensional transport, and inverse geochemical calculations. U.S. Geological Survey Techniques and Methods, Book 6, Chapter A43, 497 p. (available only at http://pubs.usgs.gov/tm/06/a43/).

Pearson, F.J. (2002): Benken. Reference water chemistry. Unpublished Nagra Internal Report.

Pearson, F.J., Arcos D., Bath, A., Boisson, J.Y., Fernandez, A.M., Gaebler, H.E., Gaucher, E.C., Gautschi, A., Griffault, L., Hernan, P. & Waber, H.N. (2003): Mont Terri Project – Geochemistry of Water in the Opalinus Clay Formation at the Mont Terri Rock Laboratory. Reports of the Federal Office of Water and Geology (FOWG), Geology Series No. 5.

Pearson, F.J., Tournassat, C. & Gaucher, E.C. (2011): Biogeochemical processes in a clay formation *in situ* experiment: Part E – equilibrium controls on chemistry of porewater from the Opalinus Claylinus Clay, Mont Terri underground research laboratory, Switzerland. Applied Geochemistry 26, 990-1008.

Robie, R.A. & Hemingway, B.S. (1991): Heat capacities of kaolinite from 7 to 380 K and of DMSO-intercalated kaolinite from 20 to 310 K. The entropy of kaolinite $Al_2Si_2O_5(OH)_4$. Clays and Clay Minerals 39, 362-368.

Rodriguez, J., Colàs, E., Gailhanou, H., Duro, L., Fuller, A.J. & Harvey, L. (2022): Track-changes and track-error document: From version 10d to version 11. ThermoChimie Technical Report TCIII-2022-06E-vs1.

Stumm, W. & Morgan, J.J. (1996): Aquatic Chemistry, 3rd edition. John Wiley & Sons, Inc.

Thoenen, T., Hummel, W., Berner, U. & Curti, E. (2014): The PSI/Nagra Chemical Thermodynamic Database 12/07. PSI Bericht Nr. 14-04. Nuclear Energy and Safety Research Department, Laboratory for Waste Management (LES). ISSN 1019-0643 (available from website http://www.psi.ch/les/database).

Tournassat, C., Gailhanou, H., Crouzet, C., Braibant, G., Gautier, A., Lassin, A., Blanc, P. & Gaucher, E.C. (2007): Two cation exchange models for direct and inverse modelling of solution major cation composition in equilibrium with illite surfaces. Geochimica et Cosmochimica Acta 71, 1098-1114.

Tournassat, C. & Steefel, C.I. (2019a): Modeling diffusion processes in the presence of a diffuse layer at charged mineral surfaces: a benchmark exercise. Computational Geosciences 25, 1319-1336.

Tournassat, C. & Steefel, C.I. (2019b): Reactive transport modeling of coupled processes in nanoporous media. Reviews in Mineralogy and Geochemistry 85, 75-109.

Van Loon, L., Glaus, M. & Wüst, R. (2023): Diffusion coefficients for HTO, ^{36}Cl and ^{22}Na in the lithologically heterogeneous Mesozoic cover of Northern Switzerland. Submitted to Applied Geochemistry.

Van Loon, L.R. & Glaus, M. A. (*in prep.*): Diffusion measurements of HTO, $^{36}Cl^-$ and $^{22}Na^+$ on rock samples of Opalinus Clay and confining geological units from deep boreholes at the potential siting regions for a deep geological repository for radioactive waste in Switzerland: Jura Ost, Nördlich Lägern and Zürich Nordost. Nagra Working Report NAB 23-26.Vinsot, A., Appelo, C.A.J., Cailteau, C., Wechner, S., Pironon, J., De Donato, P., De Cannière, P., Mettler, S., Wersin, P. & Gäbler, H.-E. (2008): CO_2 data on gas and porewater sampled in situ in the Opalinus Clay at the Mont Terri rock laobratory. Physics and Chemistry of the Earth 33, S54-S60.

Vinsot, A., Appelo, C.A.J., Lundy, M., Wechner, S., Lettry, Y., Lerouge, C., Fernández, A.M., Labat, M., Tournassat, C., De Cannière, P., Schwyn, B., McKelvie, J., Dewonck, S., Bossart, P. & Delay, J. (2014): In situ diffusion test of hydrogen gas in the Opalinus Clay. Geological Society, London, Special Publications 400.

Vinsot, A., Madé, B. & Lundy, M. (2015): Chimie des eaux du Callovo-Oxfordien au voisinage des alvéoles ha. ANDRA Document technique CG.NT.ASTR. 15.0016.

Waber, H.N., Pearson, F.J., Hobbs, M.Y. & Oyama, T. (2003): Sondierbohrung Benken: Characterisation of pore water from argillaceous rocks. Unpubl. Nagra Internal Report.

Waber, H.N. (ed.) (2020): SGT-E3 deep drilling campaign (TBO): Experiment procedures and analytical methods at RWI, University of Bern (Version 1.0, April 2020). Nagra Arbeitsbericht NAB 20-13.

Waber, H.N. & Traber, D. (2022): Die Tiefengrundwässer in der Nordschweiz und im angrenzenden Süddeutschland: Beschaffenheit, Herkunft und unterirdische Verweilzeit. Mit Beiträgen von: M. Heidinger und G. Lorenz. Nagra Technischer Bericht NTB 19-02.

Wersin, P., Gaucher, E.C., Gimmi, T., Leupin, O., Mäder, U., Thoenen, T. & Tournassat, C. (2009): Geochemistry of porewaters in Opalinus Clay at Mont Terri: Experimental data and modelling. Mont Terri Technical Report TR 08-06. Mont Terri Project, Switzerland.

Wersin, P., Mazurek, M., Waber, H.N., Mäder, U.K., Gimmi, T., Rufer, D. & de Haller, A. (2013): Rock and porewater characterisation on drillcores from the Schlattingen borehole. Nagra Arbeitsbericht NAB 12-54.

Wersin, P., Mazurek, M., Mäder, U.K., Gimmi, T., Rufer, D., Lerouge, C. & Traber, D. (2016): Constraining porewater chemistry in a 250 m thick argillaceous rock sequence. Chemical Geology 434, 43-61.

Wersin, P., Pekala, M., Mazurek, M., Gimmi, T., Mäder, U., Jenni, A., Rufer, D. & Aschwanden, L. (2020): Porewater chemistry of Opalinus Clay: Methods, data, modelling and buffering capacity. Nagra Technical Report NTB 18-01.

Wersin, P., Aschwanden, L., Camesi, L., Gaucher, E.C., Gimmi, T., Jenni, A., Kiczka, M., Mäder, U., Mazurek, M., Rufer, D., Waber, H.N., Zwahlen, C. & Traber, D. (2022a): TBO Bözberg-1-1: Data report. Dossier VIII: Rock properties, porewater characterisation and natural tracer profiles. Nagra Arbeitsbericht NAB 21-21.

Wersin, P., Mazurek, M. & Gimmi, T. (2022b): Porewater chemistry of Opalinus Clay revisited: Findings from 25 years of data collection at the Mont Terri rock laboratory. Applied Geochemistry 138, 105234.

Wigger, C. & Van Loon, R.C. (2017): Importance of interlayer equivalent pores for anion diffusion in clay-rich sedimentary rocks. Environmental Science and Technology 51, 1998-2006.

Zwahlen, C., Aschwanden, L., Camesi, L., Gimmi, T., Jenni, A., Kiczka, M., Mäder, U., Mazurek, M., Rufer, D., Waber, H.N., Wersin, P. & Traber, D. (*in prep.*): TBO Stadel-2-1: Data report. Dossier VIII: Rock properties, porewater characterisation and natural tracer profiles. Nagra Arbeitsbericht NAB 22-02.

App. A Full speciation output for the reference porewater for ZNO-NL

The following is a copy of the full speciation output of the PHREEQC model of the base case of the reference porewater for ZNO-NL, as generated by the PHREEQC input file shown in Section 5.6. The output has been transferred by copy-paste, only some line breaks were inserted for extra-long lines for better readability.

```
-----------------------------Exchange composition-----------------------------

X                1.470e-01 mol

                                        Equiv-    Equivalent      Log
       Species             Moles       alents      Fraction     Gamma

       NaX               6.465e-02   6.465e-02   4.398e-01    -0.000
       CaX2              2.714e-02   5.428e-02   3.693e-01    -0.000
       MgX2              1.051e-02   2.103e-02   1.430e-01    -0.000
       KX                5.844e-03   5.844e-03   3.976e-02    -0.000
       SrX2              5.011e-04   1.002e-03   6.817e-03    -0.000
       MnX2              5.648e-05   1.130e-04   7.684e-04    -0.000
       FeX2              4.204e-05   8.407e-05   5.719e-04    -0.000
       BaX2              2.089e-07   4.178e-07   2.842e-06    -0.000

-----------------------------Solution composition-----------------------------

       Elements           Molality       Moles

       Al                1.998e-08   1.998e-08
       Ba                1.614e-07   1.614e-07
       C                 2.105e-03   2.105e-03
       Ca                2.648e-02   2.648e-02
       Cl                2.400e-01   2.400e-01
       F                 1.592e-04   1.592e-04
       Fe                1.022e-04   1.022e-04
       K                 1.156e-03   1.156e-03
       Mg                1.560e-02   1.560e-02
       Mn                9.772e-05   9.772e-05
       Na                2.024e-01   2.024e-01
       S                 2.338e-02   2.338e-02
       Si                1.743e-04   1.743e-04
       Sr                3.809e-04   3.809e-04

----------------------------Description of solution----------------------------

                                       pH  =   7.071      Charge balance
                                       pe  =  -2.756         Adjusted to redox
equilibrium
                          Activity of water  =   0.992
                 Ionic strength (mol/kgw)  =   3.243e-01
                       Mass of water (kg)  =   1.000e+00
                 Total alkalinity (eq/kg)  =   1.909e-03
                       Total CO2 (mol/kg)  =   2.105e-03
                         Temperature (°C)  =  25.00
                  Electrical balance (eq)  =  -5.374e-12
 Percent error, 100*(Cat-|An|)/(Cat+|An|)  =  -0.00
                                Iterations  =  40
                           Gamma iterations  =  11
                      Osmotic coefficient  =   0.89394
                                  Total H  = 1.110186e+02
                                  Total O  = 5.560834e+01
```

----------Distribution of species----------

Species	Molality	Activity	Log Molality	Log Activity	Log Gamma	mole V cm³/mol
OH-	1.644e-07	1.167e-07	-6.784	-6.933	-0.149	(0)
H+	1.141e-07	8.500e-08	-6.943	-7.071	-0.128	0.00
H2O	5.551e+01	9.919e-01	1.744	-0.004	0.000	18.07
Al	1.998e-08					
Al(OH)2F	9.183e-09	9.183e-09	-8.037	-8.037	0.000	(0)
Al(OH)4-	6.143e-09	4.186e-09	-8.212	-8.378	-0.167	(0)
Al(OH)3	2.983e-09	2.983e-09	-8.525	-8.525	0.000	(0)
AlF2+	8.256e-10	5.918e-10	-9.083	-9.228	-0.145	(0)
AlF3	5.146e-10	5.146e-10	-9.289	-9.289	0.000	(0)
Al(OH)2F2-	1.489e-10	1.015e-10	-9.827	-9.994	-0.167	(0)
Al(OH)2+	8.171e-11	5.856e-11	-10.088	-10.232	-0.145	(0)
AlF+2	6.658e-11	1.709e-11	-10.177	-10.767	-0.591	(0)
AlF4-	1.894e-11	1.291e-11	-10.723	-10.889	-0.167	(0)
AlOH+2	8.732e-12	2.242e-12	-11.059	-11.649	-0.591	(0)
AlSiO(OH)3+2	7.098e-13	1.822e-13	-12.149	-12.739	-0.591	(0)
Al+3	3.927e-13	1.834e-14	-12.406	-13.737	-1.331	(0)
AlSO4+	2.955e-13	2.118e-13	-12.529	-12.674	-0.145	(0)
Al(SO4)2-	7.672e-14	5.228e-14	-13.115	-13.282	-0.167	(0)
AlF5-2	4.432e-14	1.000e-14	-13.353	-14.000	-0.646	(0)
AlOHF2	1.518e-15	1.518e-15	-14.819	-14.819	0.000	(0)
AlF6-3	2.134e-17	7.754e-19	-16.671	-18.110	-1.440	(0)
Al2(OH)2+4	2.890e-19	1.099e-21	-18.539	-20.959	-2.420	(0)
SiAlO3(OH)4-3	8.178e-21	2.972e-22	-20.087	-21.527	-1.440	(0)
Al3(OH)4+5	8.961e-24	1.441e-27	-23.048	-26.841	-3.794	(0)
Al13(OH)32+7	0.000e+00	0.000e+00	-45.073	-52.458	-7.385	(0)
Ba	1.614e-07					
Ba+2	1.404e-07	3.448e-08	-6.853	-7.462	-0.610	(0)
BaSO4	2.042e-08	2.042e-08	-7.690	-7.690	0.000	(0)
BaHCO3+	5.240e-10	3.755e-10	-9.281	-9.425	-0.145	(0)
BaF+	1.744e-11	1.250e-11	-10.758	-10.903	-0.145	(0)
BaCO3	1.015e-11	1.015e-11	-10.994	-10.994	0.000	(0)
BaOH+	2.687e-14	1.926e-14	-13.571	-13.715	-0.145	(0)
C(-4)	2.089e-17					
CH4	2.089e-17	2.089e-17	-16.680	-16.680	0.000	(0)
C(4)	2.105e-03					
HCO3-	1.599e-03	1.115e-03	-2.796	-2.953	-0.157	(0)
CO2	2.148e-04	2.148e-04	-3.668	-3.668	0.000	(0)
CaHCO3+	1.054e-04	7.558e-05	-3.977	-4.122	-0.145	(0)
NaHCO3	1.017e-04	1.017e-04	-3.993	-3.993	0.000	(0)
MgHCO3+	6.473e-05	4.640e-05	-4.189	-4.334	-0.145	(0)
CaCO3	6.026e-06	6.026e-06	-5.220	-5.220	0.000	(0)
FeCO3	4.560e-06	4.560e-06	-5.341	-5.341	0.000	(0)
CO3-2	2.699e-06	6.147e-07	-5.569	-6.211	-0.642	(0)
MgCO3	2.080e-06	2.080e-06	-5.682	-5.682	0.000	(0)
SrHCO3+	1.947e-06	1.395e-06	-5.711	-5.855	-0.145	(0)
NaCO3-	1.275e-06	8.688e-07	-5.894	-6.061	-0.167	(0)
MnHCO3+	6.100e-07	4.750e-07	-6.215	-6.323	-0.109	(0)
MnCO3	5.601e-07	5.601e-07	-6.252	-6.252	0.000	(0)
KHCO3	4.013e-07	4.013e-07	-6.397	-6.397	0.000	(0)
SrCO3	3.135e-08	3.135e-08	-7.504	-7.504	0.000	(0)
KCO3-	5.645e-09	3.847e-09	-8.248	-8.415	-0.167	(0)
Fe(OH)CO3	1.153e-09	1.153e-09	-8.938	-8.938	0.000	(0)
Fe(CO3)2-2	7.132e-10	1.647e-10	-9.147	-9.783	-0.637	(0)
BaHCO3+	5.240e-10	3.755e-10	-9.281	-9.425	-0.145	(0)
BaCO3	1.015e-11	1.015e-11	-10.994	-10.994	0.000	(0)
Fe(CO3)3-3	2.127e-14	7.452e-16	-13.672	-15.128	-1.456	(0)
Ca	2.648e-02					
Ca+2	2.261e-02	5.772e-03	-1.646	-2.239	-0.593	(0)
CaSO4	3.747e-03	3.747e-03	-2.426	-2.426	0.000	(0)
CaHCO3+	1.054e-04	7.558e-05	-3.977	-4.122	-0.145	(0)

CaF+	1.298e-05	9.564e-06	-4.887	-5.019	-0.133	(0)
CaCO3	6.026e-06	6.026e-06	-5.220	-5.220	0.000	(0)
CaSiO(OH)3+	3.829e-08	2.744e-08	-7.417	-7.562	-0.145	(0)
CaOH+	2.530e-08	1.813e-08	-7.597	-7.742	-0.145	(0)
CaSiO2(OH)2	3.229e-11	3.229e-11	-10.491	-10.491	0.000	(0)
Cl	2.400e-01					
Cl-	2.400e-01	1.696e-01	-0.620	-0.771	-0.151	(0)
MnCl+	5.618e-06	4.886e-06	-5.250	-5.311	-0.061	(0)
FeCl+	4.560e-07	3.473e-07	-6.341	-6.459	-0.118	(0)
FeCl+2	5.352e-20	1.801e-20	-19.271	-19.744	-0.473	(0)
FeCl2+	1.573e-20	1.462e-20	-19.803	-19.835	-0.032	(0)
FeCl3	1.564e-22	1.564e-22	-21.806	-21.806	0.000	(0)
FeCl4-	3.894e-25	2.653e-25	-24.410	-24.576	-0.167	(0)
MnCl+2	5.159e-33	1.521e-33	-32.287	-32.818	-0.531	(0)
ClO4-	0.000e+00	0.000e+00	-153.787	-153.944	-0.157	(0)
F	1.592e-04					
F-	1.102e-04	7.751e-05	-3.958	-4.111	-0.153	(0)
MgF+	3.021e-05	2.083e-05	-4.520	-4.681	-0.161	(0)
CaF+	1.298e-05	9.564e-06	-4.887	-5.019	-0.133	(0)
NaF	5.618e-06	5.618e-06	-5.250	-5.250	0.000	(0)
FeF+	1.110e-07	7.955e-08	-6.955	-7.099	-0.145	(0)
SrF+	7.440e-08	5.332e-08	-7.128	-7.273	-0.145	(0)
MnF+	5.016e-08	3.971e-08	-7.300	-7.401	-0.101	(0)
HF	9.880e-09	9.880e-09	-8.005	-8.005	0.000	(0)
Al(OH)2F	9.183e-09	9.183e-09	-8.037	-8.037	0.000	(0)
AlF2+	8.256e-10	5.918e-10	-9.083	-9.228	-0.145	(0)
AlF3	5.146e-10	5.146e-10	-9.289	-9.289	0.000	(0)
Al(OH)2F2-	1.489e-10	1.015e-10	-9.827	-9.994	-0.167	(0)
AlF+2	6.658e-11	1.709e-11	-10.177	-10.767	-0.591	(0)
AlF4-	1.894e-11	1.291e-11	-10.723	-10.889	-0.167	(0)
BaF+	1.744e-11	1.250e-11	-10.758	-10.903	-0.145	(0)
HF2-	3.211e-12	2.129e-12	-11.493	-11.672	-0.179	(0)
AlF5-2	4.432e-14	1.000e-14	-13.353	-14.000	-0.646	(0)
AlOHF2	1.518e-15	1.518e-15	-14.819	-14.819	0.000	(0)
AlF6-3	2.134e-17	7.754e-19	-16.671	-18.110	-1.440	(0)
FeF+2	1.004e-18	3.059e-19	-17.998	-18.514	-0.516	(0)
FeF2+	6.722e-19	4.953e-19	-18.172	-18.305	-0.133	(0)
MnOHF+	3.294e-23	2.565e-23	-22.482	-22.591	-0.109	(0)
MnF2+	8.709e-30	6.781e-30	-29.060	-29.169	-0.109	(0)
MnF+2	1.488e-30	4.385e-31	-29.827	-30.358	-0.531	(0)
MnF3	1.320e-30	1.320e-30	-29.879	-29.879	0.000	(0)
Fe(2)	1.022e-04					
Fe+2	7.890e-05	2.048e-05	-4.103	-4.689	-0.586	(0)
FeSO4	1.794e-05	1.794e-05	-4.746	-4.746	0.000	(0)
FeCO3	4.560e-06	4.560e-06	-5.341	-5.341	0.000	(0)
FeCl+	4.560e-07	3.473e-07	-6.341	-6.459	-0.118	(0)
FeOH+	1.239e-07	8.880e-08	-6.907	-7.052	-0.145	(0)
FeF+	1.110e-07	7.955e-08	-6.955	-7.099	-0.145	(0)
Fe(SO4)2-2	9.175e-08	2.071e-08	-7.037	-7.684	-0.646	(0)
Fe(CO3)2-2	7.132e-10	1.647e-10	-9.147	-9.783	-0.637	(0)
FeS	1.555e-10	1.555e-10	-9.808	-9.808	0.000	(0)
FeHSO4+	9.032e-12	6.473e-12	-11.044	-11.189	-0.145	(0)
Fe(OH)2	8.423e-12	8.423e-12	-11.075	-11.075	0.000	(0)
Fe(OH)3-	9.981e-17	6.801e-17	-16.001	-16.167	-0.167	(0)
Fe(3)	1.157e-09					
Fe(OH)CO3	1.153e-09	1.153e-09	-8.938	-8.938	0.000	(0)
Fe(OH)3	2.802e-12	2.802e-12	-11.553	-11.553	0.000	(0)
Fe(OH)2+	9.634e-13	8.518e-13	-12.016	-12.070	-0.053	(0)
Fe(OH)4-	2.193e-14	1.495e-14	-13.659	-13.825	-0.167	(0)
Fe(CO3)3-3	2.127e-14	7.452e-16	-13.672	-15.128	-1.456	(0)
FeOH+2	8.610e-16	2.362e-16	-15.065	-15.627	-0.562	(0)
FeSiO(OH)3+2	2.090e-17	5.050e-18	-16.680	-17.297	-0.617	(0)
FeF+2	1.004e-18	3.059e-19	-17.998	-18.514	-0.516	(0)
FeF2+	6.722e-19	4.953e-19	-18.172	-18.305	-0.133	(0)
FeSO4+	2.086e-19	1.814e-19	-18.681	-18.741	-0.061	(0)

Fe(SO4)2-	6.917e-20	5.383e-20	-19.160	-19.269	-0.109	(0)
Fe+3	5.414e-20	3.208e-21	-19.266	-20.494	-1.227	(0)
FeCl+2	5.352e-20	1.801e-20	-19.271	-19.744	-0.473	(0)
FeCl2+	1.573e-20	1.462e-20	-19.803	-19.835	-0.032	(0)
FeCl3	1.564e-22	1.564e-22	-21.806	-21.806	0.000	(0)
FeCl4-	3.894e-25	2.653e-25	-24.410	-24.576	-0.167	(0)
FeHSO4+2	1.391e-26	4.529e-27	-25.857	-26.344	-0.487	(0)
Fe2(OH)2+4	3.183e-28	1.724e-30	-27.497	-29.763	-2.266	(0)
Fe3(OH)4+5	1.455e-36	3.068e-40	-35.837	-39.513	-3.676	(0)
H(0)	3.690e-12					
H2	1.845e-12	1.845e-12	-11.734	-11.734	0.000	(0)
K	1.156e-03					
K+	1.130e-03	7.878e-04	-2.947	-3.104	-0.157	(0)
KSO4-	2.543e-05	1.733e-05	-4.595	-4.761	-0.167	(0)
KHCO3	4.013e-07	4.013e-07	-6.397	-6.397	0.000	(0)
KCO3-	5.645e-09	3.847e-09	-8.248	-8.415	-0.167	(0)
KOH	2.907e-11	2.907e-11	-10.537	-10.537	0.000	(0)
Mg	1.560e-02					
Mg+2	1.350e-02	3.543e-03	-1.870	-2.451	-0.581	(0)
MgSO4	2.004e-03	2.004e-03	-2.698	-2.698	0.000	(0)
MgHCO3+	6.473e-05	4.640e-05	-4.189	-4.334	-0.145	(0)
MgF+	3.021e-05	2.083e-05	-4.520	-4.681	-0.161	(0)
MgCO3	2.080e-06	2.080e-06	-5.682	-5.682	0.000	(0)
MgOH+	1.151e-07	8.251e-08	-6.939	-7.084	-0.145	(0)
MgSiO(OH)3+	3.640e-08	2.609e-08	-7.439	-7.583	-0.145	(0)
MgSiO2(OH)2	2.075e-10	2.075e-10	-9.683	-9.683	0.000	(0)
Mn(2)	9.772e-05					
Mn+2	7.851e-05	2.289e-05	-4.105	-4.640	-0.535	(0)
MnSO4	1.236e-05	1.236e-05	-4.908	-4.908	0.000	(0)
MnCl+	5.618e-06	4.886e-06	-5.250	-5.311	-0.061	(0)
MnHCO3+	6.100e-07	4.750e-07	-6.215	-6.323	-0.109	(0)
MnCO3	5.601e-07	5.601e-07	-6.252	-6.252	0.000	(0)
MnF+	5.016e-08	3.971e-08	-7.300	-7.401	-0.101	(0)
MnOH+	9.022e-09	7.025e-09	-8.045	-8.153	-0.109	(0)
Mn(OH)2	2.059e-13	2.059e-13	-12.686	-12.686	0.000	(0)
Mn(OH)3-	2.440e-18	1.663e-18	-17.613	-17.779	-0.167	(0)
Mn(OH)4-2	9.872e-25	2.228e-25	-24.006	-24.652	-0.646	(0)
Mn(3)	7.860e-18					
Mn(OH)2+	7.860e-18	6.121e-18	-17.105	-17.213	-0.109	(0)
MnOHF+	3.294e-23	2.565e-23	-22.482	-22.591	-0.109	(0)
MnOH+2	8.918e-25	2.628e-25	-24.050	-24.580	-0.531	(0)
MnF2+	8.709e-30	6.781e-30	-29.060	-29.169	-0.109	(0)
MnF+2	1.488e-30	4.385e-31	-29.827	-30.358	-0.531	(0)
MnF3	1.320e-30	1.320e-30	-29.879	-29.879	0.000	(0)
Mn+3	2.620e-32	1.421e-33	-31.582	-32.847	-1.266	(0)
MnCl+2	5.159e-33	1.521e-33	-32.287	-32.818	-0.531	(0)
Na	2.024e-01					
Na+	1.989e-01	1.381e-01	-0.701	-0.860	-0.159	(0)
NaSO4-	3.306e-03	2.252e-03	-2.481	-2.647	-0.167	(0)
NaHCO3	1.017e-04	1.017e-04	-3.993	-3.993	0.000	(0)
NaF	5.618e-06	5.618e-06	-5.250	-5.250	0.000	(0)
NaCO3-	1.275e-06	8.688e-07	-5.894	-6.061	-0.167	(0)
NaOH	6.417e-09	6.417e-09	-8.193	-8.193	0.000	(0)
O(0)	0.000e+00					
O2	0.000e+00	0.000e+00	-68.733	-68.733	0.000	(0)
S(-2)	2.468e-10					
FeS	1.555e-10	1.555e-10	-9.808	-9.808	0.000	(0)
HS-	5.762e-11	4.167e-11	-10.239	-10.380	-0.141	(0)
H2S	3.366e-11	3.461e-11	-10.473	-10.461	0.012	(0)
S-2	2.172e-22	4.903e-23	-21.663	-22.310	-0.646	(0)
S(0)	4.730e-14					
S	4.730e-14	4.730e-14	-13.325	-13.325	0.000	(0)
S(2)	2.102e-15					
S2O3-2	1.051e-15	2.394e-16	-14.978	-15.621	-0.642	(0)
S(4)	1.951e-14					

```
   SO3-2           1.326e-14   3.019e-15   -13.878   -14.520    -0.642     (0)
   HSO3-           6.251e-15   4.259e-15   -14.204   -14.371    -0.167     (0)
S(6)          2.338e-02
   SO4-2           1.422e-02   3.180e-03    -1.847    -2.498    -0.650     (0)
   CaSO4           3.747e-03   3.747e-03    -2.426    -2.426     0.000     (0)
   NaSO4-          3.306e-03   2.252e-03    -2.481    -2.647    -0.167     (0)
   MgSO4           2.004e-03   2.004e-03    -2.698    -2.698     0.000     (0)
   SrSO4           5.129e-05   5.129e-05    -4.290    -4.290     0.000     (0)
   KSO4-           2.543e-05   1.733e-05    -4.595    -4.761    -0.167     (0)
   FeSO4           1.794e-05   1.794e-05    -4.746    -4.746     0.000     (0)
   MnSO4           1.236e-05   1.236e-05    -4.908    -4.908     0.000     (0)
   Fe(SO4)2-2      9.175e-08   2.071e-08    -7.037    -7.684    -0.646     (0)
   HSO4-           3.788e-08   2.629e-08    -7.422    -7.580    -0.159     (0)
   BaSO4           2.042e-08   2.042e-08    -7.690    -7.690     0.000     (0)
   FeHSO4+         9.032e-12   6.473e-12   -11.044   -11.189    -0.145     (0)
   AlSO4+          2.955e-13   2.118e-13   -12.529   -12.674    -0.145     (0)
   Al(SO4)2-       7.672e-14   5.228e-14   -13.115   -13.282    -0.167     (0)
   FeSO4+          2.086e-19   1.814e-19   -18.681   -18.741    -0.061     (0)
   Fe(SO4)2-       6.917e-20   5.383e-20   -19.160   -19.269    -0.109     (0)
   FeHSO4+2        1.391e-26   4.529e-27   -25.857   -26.344    -0.487     (0)
Si            1.743e-04
   Si(OH)4         1.737e-04   1.764e-04    -3.760    -3.754     0.007     (0)
   SiO(OH)3-       4.717e-07   3.214e-07    -6.326    -6.493    -0.167     (0)
   CaSiO(OH)3+     3.829e-08   2.744e-08    -7.417    -7.562    -0.145     (0)
   MgSiO(OH)3+     3.640e-08   2.609e-08    -7.439    -7.583    -0.145     (0)
   MgSiO2(OH)2     2.075e-10   2.075e-10    -9.683    -9.683     0.000     (0)
   CaSiO2(OH)2     3.229e-11   3.229e-11   -10.491   -10.491     0.000     (0)
   SiO2(OH)2-2     7.730e-13   1.769e-13   -12.112   -12.752    -0.640     (0)
   AlSiO(OH)3+2    7.098e-13   1.822e-13   -12.149   -12.739    -0.591     (0)
   FeSiO(OH)3+2    2.090e-17   5.050e-18   -16.680   -17.297    -0.617     (0)
   SiAlO3(OH)4-3   8.178e-21   2.972e-22   -20.087   -21.527    -1.440     (0)
   Si4O8(OH)4-4    3.226e-21   1.006e-23   -20.491   -22.998    -2.506     (0)
Sr            3.809e-04
   Sr+2            3.276e-04   8.271e-05    -3.485    -4.082    -0.598     (0)
   SrSO4           5.129e-05   5.129e-05    -4.290    -4.290     0.000     (0)
   SrHCO3+         1.947e-06   1.395e-06    -5.711    -5.855    -0.145     (0)
   SrF+            7.440e-08   5.332e-08    -7.128    -7.273    -0.145     (0)
   SrCO3           3.135e-08   3.135e-08    -7.504    -7.504     0.000     (0)
   SrOH+           9.535e-11   6.834e-11   -10.021   -10.165    -0.145     (0)

-----------------------------Saturation indices-------------------------------

  Phase               SI** log IAP   log K(298 K,   1 atm)

  2-line-ferrihydrite  -2.79      0.71    3.50  Fe(OH)3
  4C-pyrrhotite    -2.86    -11.36   -8.50  Fe0.625Fe0.25S
  5C-pyrrhotite    -3.09    -10.69   -7.60  Fe0.7Fe0.2S
  Analcime         -8.84     12.37   21.21  Na2Al2Si4O12(H2O)2
  Anhydrite        -0.53     -4.74   -4.21  CaSO4
  Aragonite        -0.13      1.88    2.01  CaCO3
  Barite            0.00     -9.96   -9.96  BaSO4
  Beidellite(Ca)    0.22      5.79    5.56  Ca0.17Al2.34Si3.66O10(OH)2
  Beidellite(K)     0.72      5.11    4.39  K0.34Al2.34Si3.66O10(OH)2
  Beidellite(Mg)    0.73      5.75    5.02  Mg0.17Al2.34Si3.66O10(OH)2
  Beidellite(Na)    2.74      5.88    3.14  Na0.34Al2.34Si3.66O10(OH)2
  Beidellite_SBld-1 -0.31     7.07    7.38
      (Ca0.185K0.104)(Si3.574Al0.426)(Al1.812Mg0.090Fe0.112)O10(OH)2
  Berthierine(FeII)  -4.36     30.08   34.44  (Fe2Al)(SiAl)O5(OH)4
  Berthierine(FeIII)  -4.05     24.71   28.76
      (Fe2.34Fe0.33Al0.33)(Si1.34Al0.66)O5(OH)4
  Berthierine_ISGS  -4.95     22.85   27.80
      (Si1.332Al0.668)(Al0.976Fe0.182Fe1.44Mg0.157)O5(OH)4
  Bixbyite        -22.47    -23.28   -0.81  Mn2O3
  Boehmite         -1.93      7.47    9.40  AlOOH
  Brucite          -5.43     11.68   17.11  Mg(OH)2
```

Calcite	0.00	1.88	1.88	CaCO3
Celestite	0.00	-6.58	-6.58	SrSO4
CH4(g)	-13.82	-16.68	-2.86	CH4
Chabazite-Ca	-4.68	11.83	16.51	CaAl2Si4O12(H2O)6
Chabazite-Na	-3.73	12.35	16.08	Na2Al2Si4O12(H2O)6
Clinoptilolite	-6.69	-4.64	2.06	Ca0.52Al1.04Si4.96O12(H2O)3.1
CO2(g)	-2.20	-10.02	-7.82	CO2
Cronstedtite	0.46	16.57	16.11	(Fe2Fe)(SiFe)O5(OH)4
Dawsonite	-1.36	3.66	5.02	NaAlCO3(OH)2
Dolomite	-0.00	3.55	3.55	CaMg(CO3)2
Faujasite-X	-7.72	17.97	25.69	Na2Al2Si2.5O9(H2O)6.2
Faujasite-Y	-6.12	12.34	18.46	Na2Al2Si4O12(H2O)8
Fe(OH)2(s)	-2.81	9.45	12.26	Fe(OH)2
Fe-hibbingite	-6.15	11.05	17.20	Fe2Cl(OH)3
Fe4(OH)8Cl:nH2O(s)	-5.44	21.21	26.65	Fe3Fe(OH)8Cl
Fe6(OH)12CO3:nH2O(s)	-7.45	29.18	36.63	Fe2Fe4(OH)12CO3
Fe6(OH)12SO4:nH2O(s)	-6.54	22.57	29.10	Fe4Fe2(OH)12SO4
Fluorite	0.00	-10.46	-10.46	CaF2
Gibbsite	-0.29	7.46	7.75	Al(OH)3
Glauconite	-2.94	-1.17	1.77	K0.75(Mg0.25Fe0.25Fe1.25Al0.25)(Al0.25Si3.75)O10(OH)2
Goethite	0.38	0.71	0.33	FeOOH
Graphite	-5.45	-27.27	-21.82	C
Greigite	-17.77	-58.91	-41.14	Fe3S4
Gypsum	-0.16	-4.74	-4.58	CaSO4(H2O)2
H2(g)	-8.63	-11.73	-3.11	H2
H2S(g)	-9.44	-17.45	-8.01	H2S
Hausmannite	-24.36	-13.78	10.58	Mn3O4
Hematite	0.71	1.43	0.72	Fe2O3
Heulandite_1	-8.62	3.00	11.62	Ca1.07Al2.14Si6.86O18(H2O)4.4
Heulandite_2	-9.69	3.00	12.69	Ca1.07Al2.14Si6.86O18(H2O)4.5
Hydrosodalite	-33.30	72.00	105.30	Na8Al6Si6O24(OH)2(H2O)2
Illite(Al)	0.08	12.86	12.78	K0.85Al2.85Si3.15O10(OH)2
Illite(FeII)	1.29	10.55	9.25	K0.85Fe0.25Al2.35Si3.4O10(OH)2
Illite(FeIII)	-0.97	11.17	12.14	K0.85Fe0.25Al2.6Si3.15O10(OH)2
Illite(Mg)	0.30	11.11	10.80	K0.85Mg0.25Al2.35Si3.4O10(OH)2
Illite_IMt-2	-5.06	9.66	14.72	(K0.762Na0.044)(Si3.387Al0.613)(Al1.427Fe0.292Mg0.241Fe0.084)O10(OH)2
Iron(alpha)	-15.07	0.82	15.89	Fe
Kaolinite	0.00	7.44	7.44	Al2Si2O5(OH)4
Lepidocrocite	-1.15	0.71	1.86	FeOOH
Linda_type_A	-9.30	19.50	28.80	Na1.98Al1.98Si2.02O8(H2O)5.31
Low-silica_P-Ca	-4.62	19.33	23.95	CaAl2Si2O8(H2O)4.5
Low-silica_P-Na	-8.02	19.85	27.87	Na2Al2Si2O8(H2O)3.8
Mackinawite	-4.81	-8.00	-3.19	FeS
Maghemite	-1.79	1.43	3.22	Fe2O3
Magnesite	-1.00	1.67	2.67	MgCO3
Magnetite	1.66	10.87	9.21	Fe3O4
Manganite	-11.56	-11.64	-0.08	MnOOH
Manganosite	-8.46	9.50	17.96	MnO
Marcasite	-0.68	-21.32	-20.64	FeS2
Molecular_sieve_4Ã…	-7.12	19.85	26.97	Na2Al2Si2O8(H2O)4.5
Montmorillonite(HcCa)	-0.70	6.05	6.75	Ca0.3Mg0.6Al1.4Si4O10(OH)2
Montmorillonite(HcK)	0.57	4.86	4.29	K0.6Mg0.6Al1.4Si4O10(OH)2
Montmorillonite(HcMg)	0.15	5.99	5.84	Mg0.3Mg0.6Al1.4Si4O10(OH)2
Montmorillonite(HcNa)	0.89	6.21	5.31	Na0.6Mg0.6Al1.4Si4O10(OH)2
Montmorillonite(MgCa)	-0.64	3.41	4.05	Ca0.17Mg0.34Al1.66Si4O10(OH)2
Montmorillonite(MgK)	0.08	2.73	2.65	K0.34Mg0.34Al1.66Si4O10(OH)2
Montmorillonite(MgMg)	-0.16	3.37	3.53	Mg0.17Mg0.34Al1.66Si4O10(OH)2
Montmorillonite(MgNa)	0.26	3.50	3.23	Na0.34Mg0.34Al1.66Si4O10(OH)2
Mordenite-Ca	-6.51	-10.82	-4.31	Ca0.34Al0.68Si5.32O12(H2O)2.9
Mordenite-Na	-5.72	-9.94	-4.22	Na0.72Al0.72Si5.28O12(H2O)2.71
Natrolite	-5.04	16.11	21.15	Na2Al2Si3O10(H2O)2
Nontronite(Ca)	-2.56	-5.50	-2.94	Ca0.17Fe1.67Al0.67Si3.66O10(OH)2
Nontronite(K)	-2.06	-6.17	-4.11	K0.34Fe1.67Al0.67Si3.66O10(OH)2

```
  Nontronite(Mg)    -2.05     -5.53    -3.48  Mg0.17Fe1.67Al0.67Si3.66O10(OH)2
  Nontronite(Na)    -1.80     -5.41    -3.61  Na0.34Fe1.67Al0.67Si3.66O10(OH)2
  Nontronite_Nau-1  -3.04     -1.83     1.21
     (Ca0.247K0.020)(Si3.458Al0.542)(Fe1.688Al0.276Mg0.068)O10(OH)2
  O2(g)           -65.84    -68.73    -2.89  O2
  Phillipsite-Na    -7.17     13.57    20.75  Na2.5Al2.5Si5.5O16(H2O)5
  Phillipsite-NaK   -8.91     11.33    20.25  Na1.5KAl2.5Si5.5O16(H2O)5
  Portlandite      -10.85     11.90    22.75  Ca(OH)2
  Pyrite            -0.00    -21.32   -21.32  FeS2
  Pyrochroite       -5.70      9.49    15.19  Mn(OH)2
  Pyrolusite       -23.49     18.12    41.61  MnO2
  Quartz            -0.00     -3.75    -3.75  SiO2
  Rhodochrosite      0.00     -0.52    -0.52  MnCO3
  Ripidolite_Cca-2  -0.90     59.74    60.65
     (Si2.633Al1.367)(Al1.116Fe0.215Mg2.952Fe1.712Mn0.012)(Ca0.011)O10(OH)8
  S(orth)           -6.68    -13.33    -6.65  S
  Saponite(Ca)      -3.38     25.91    29.28  Ca0.17Mg3Al0.34Si3.66O10(OH)2
  Saponite(FeCa)    -2.85     23.67    26.52  Ca0.17Mg2FeAl0.34Si3.66O10(OH)2
  Saponite(FeK)     -2.35     23.00    25.35  K0.34Mg2FeAl0.34Si3.66O10(OH)2
  Saponite(FeMg)    -2.34     23.63    25.97  Mg0.17Mg2FeAl0.34Si3.66O10(OH)2
  Saponite(FeNa)    -1.91     23.76    25.67  Na0.34Mg2FeAl0.34Si3.66O10(OH)2
  Saponite(K)       -2.88     25.23    28.12  K0.34Mg3Al0.34Si3.66O10(OH)2
  Saponite(Mg)      -2.87     25.87    28.74  Mg0.17Mg3Al0.34Si3.66O10(OH)2
  Saponite(Na)      -2.62     26.00    28.61  Na0.34Mg3Al0.34Si3.66O10(OH)2
  Saponite_SapCa-2  -4.14     27.26    31.40
     (Na0.394K0.021Ca0.038)(Si3.569Al0.397)(Mg2.949Fe0.034Fe0.021)O10(OH)2
  Scolecite         -7.43     15.59    23.02  CaAl2Si3O10(H2O)3
  Siderite           0.00     -0.57    -0.57  FeCO3
  Silica(am)        -1.03     -3.75    -2.71  SiO2
  Smectite_MX80      0.50      5.58     5.09
 (Na0.409K0.024Ca0.009)(Si3.738Al0.262)(Al1.598Mg0.214Fe0.173Fe0.035)O10(OH)2
  Sodalite         -16.77     56.33    73.10  Na8Al6Si6O24Cl2
  Stilbite          -9.05      4.37    13.42  Ca1.11Al2.22Si6.78O18(H2O)6.8
  Strontianite      -1.02      0.04     1.06  SrCO3
  Troilite          -4.01     -8.00    -3.99  FeS
  Vaterite          -0.54      1.88     2.42  CaCO3
  Vermiculite(Ca)   -4.62     34.83    39.46  Ca0.43Mg3Al0.86Si3.14O10(OH)2
  Vermiculite(K)    -4.23     33.13    37.35  K0.86Mg3Al0.86Si3.14O10(OH)2
  Vermiculite(Mg)   -3.21     34.74    37.95  Mg0.43Mg3Al0.86Si3.14O10(OH)2
  Vermiculite(Na)   -3.24     35.06    38.30  Na0.86Mg3Al0.86Si3.14O10(OH)2
  Witherite         -5.10     -3.34     1.76  BaCO3

**For a gas, SI = log10(fugacity). Fugacity = pressure * phi / 1 atm.
  For ideal gases, phi = 1.
```

App. B Full speciation output for the reference porewater for JO

The following is a copy of the full speciation output of the PHREEQC model of the base case of the reference porewater for JO, as generated by the PHREEQC input file shown in Section 5.7. The output has been transferred by copy-paste, only some line breaks were inserted for extra-long lines for better readability.

```
-----------------------------Exchange composition-----------------------------

X               1.486e-01 mol

                                      Equiv-    Equivalent      Log
       Species             Moles      alents      Fraction     Gamma

       NaX               5.878e-02   5.878e-02   3.956e-01    -0.131
       CaX2              2.943e-02   5.886e-02   3.961e-01    -0.500
       MgX2              1.129e-02   2.258e-02   1.519e-01    -0.496
       KX                6.204e-03   6.204e-03   4.175e-02    -0.128
       SrX2              9.855e-04   1.971e-03   1.326e-02    -0.502
       MnX2              5.843e-05   1.169e-04   7.864e-04    -0.479
       FeX2              4.531e-05   9.062e-05   6.098e-04    -0.497
       BaX2              4.149e-07   8.297e-07   5.584e-06    -0.506

-----------------------------Solution composition-----------------------------

       Elements           Molality       Moles

       Al                2.411e-08   2.411e-08
       Ba                7.847e-08   7.847e-08
       C                 3.238e-03   3.237e-03
       Ca                7.398e-03   7.398e-03
       Cl                8.500e-02   8.500e-02
       F                 2.213e-04   2.213e-04
       Fe                3.328e-05   3.328e-05
       K                 7.956e-04   7.956e-04
       Mg                4.355e-03   4.355e-03
       Mn                2.831e-05   2.831e-05
       Na                1.182e-01   1.182e-01
       S                 2.738e-02   2.738e-02
       Si                1.775e-04   1.775e-04
       Sr                1.899e-04   1.899e-04

----------------------------Description of solution----------------------------

                                       pH  =   7.340      Charge balance
                                       pe  =  -3.063        Adjusted to redox
equilibrium
                          Activity of water  =   0.996
                 Ionic strength (mol/kgw)  =   1.617e-01
                       Mass of water (kg)  =   1.000e+00
                 Total alkalinity (eq/kg)  =   3.047e-03
                       Total CO2 (mol/kg)  =   3.238e-03
                         Temperature (°C)  =  25.00
                  Electrical balance (eq)  =   8.385e-13
 Percent error, 100*(Cat-|An|)/(Cat+|An|)  =   0.00
                                Iterations  =  46
                           Gamma iterations  =  10
                      Osmotic coefficient  =   0.89539
                                  Total H  = 1.110186e+02
                                  Total O  = 5.562715e+01
```

----------Distribution of species----------

Species	Molality	Activity	Log Molality	Log Activity	Log Gamma	mole V cm³/mol
OH-	2.894e-07	2.179e-07	-6.538	-6.662	-0.123	(0)
H+	5.996e-08	4.572e-08	-7.222	-7.340	-0.118	0.00
H2O	5.551e+01	9.961e-01	1.744	-0.002	0.000	18.07
Al	2.411e-08					
Al(OH)4-	1.065e-08	7.831e-09	-7.973	-8.106	-0.134	(0)
Al(OH)2F	9.183e-09	9.183e-09	-8.037	-8.037	0.000	(0)
Al(OH)3	2.990e-09	2.990e-09	-8.524	-8.524	0.000	(0)
AlF3	5.125e-10	5.125e-10	-9.290	-9.290	0.000	(0)
AlF2+	4.205e-10	3.163e-10	-9.376	-9.500	-0.124	(0)
Al(OH)2F2-	2.571e-10	1.890e-10	-9.590	-9.723	-0.134	(0)
Al(OH)2+	4.179e-11	3.144e-11	-10.379	-10.503	-0.124	(0)
AlF4-	3.257e-11	2.394e-11	-10.487	-10.621	-0.134	(0)
AlF+2	1.547e-11	4.904e-12	-10.810	-11.309	-0.499	(0)
AlOH+2	2.033e-12	6.445e-13	-11.692	-12.191	-0.499	(0)
AlSiO(OH)3+2	1.660e-13	5.261e-14	-12.780	-13.279	-0.499	(0)
AlF5-2	1.153e-13	3.457e-14	-12.938	-13.461	-0.523	(0)
AlSO4+	8.329e-14	6.265e-14	-13.079	-13.203	-0.124	(0)
Al(SO4)2-	4.041e-14	2.970e-14	-13.394	-13.527	-0.134	(0)
Al+3	3.753e-14	2.825e-15	-13.426	-14.549	-1.123	(0)
AlOHF2	1.515e-15	1.515e-15	-14.820	-14.820	0.000	(0)
AlF6-3	7.360e-17	4.992e-18	-16.133	-17.302	-1.169	(0)
SiAlO3(OH)4-3	2.845e-20	1.930e-21	-19.546	-20.715	-1.169	(0)
Al2(OH)2+4	9.437e-21	9.088e-23	-20.025	-22.042	-2.016	(0)
Al3(OH)4+5	9.140e-26	6.396e-29	-25.039	-28.194	-3.155	(0)
Al13(OH)32+7	0.000e+00	0.000e+00	-48.178	-54.344	-6.166	(0)
Ba	7.847e-08					
Ba+2	5.753e-08	1.795e-08	-7.240	-7.746	-0.506	(0)
BaSO4	2.042e-08	2.042e-08	-7.690	-7.690	0.000	(0)
BaHCO3+	4.853e-10	3.650e-10	-9.314	-9.438	-0.124	(0)
BaCO3	1.833e-11	1.833e-11	-10.737	-10.737	0.000	(0)
BaF+	1.612e-11	1.212e-11	-10.793	-10.916	-0.124	(0)
BaOH+	2.489e-14	1.872e-14	-13.604	-13.728	-0.124	(0)
C(-4)	4.143e-17					
CH4	4.143e-17	4.143e-17	-16.383	-16.383	0.000	(0)
C(4)	3.238e-03					
HCO3-	2.793e-03	2.081e-03	-2.554	-2.682	-0.128	(0)
CO2	2.148e-04	2.148e-04	-3.668	-3.668	0.000	(0)
NaHCO3	1.165e-04	1.165e-04	-3.934	-3.934	0.000	(0)
CaHCO3+	5.405e-05	4.066e-05	-4.267	-4.391	-0.124	(0)
MgHCO3+	3.318e-05	2.496e-05	-4.479	-4.603	-0.124	(0)
CO3-2	7.079e-06	2.133e-06	-5.150	-5.671	-0.521	(0)
CaCO3	6.026e-06	6.026e-06	-5.220	-5.220	0.000	(0)
FeCO3	4.560e-06	4.560e-06	-5.341	-5.341	0.000	(0)
NaCO3-	2.517e-06	1.850e-06	-5.599	-5.733	-0.134	(0)
MgCO3	2.080e-06	2.080e-06	-5.682	-5.682	0.000	(0)
SrHCO3+	1.803e-06	1.356e-06	-5.744	-5.868	-0.124	(0)
MnCO3	5.601e-07	5.601e-07	-6.252	-6.252	0.000	(0)
KHCO3	5.401e-07	5.401e-07	-6.268	-6.268	0.000	(0)
MnHCO3+	3.299e-07	2.555e-07	-6.482	-6.593	-0.111	(0)
SrCO3	5.665e-08	5.665e-08	-7.247	-7.247	0.000	(0)
KCO3-	1.309e-08	9.623e-09	-7.883	-8.017	-0.134	(0)
Fe(CO3)2-2	1.882e-09	5.716e-10	-8.725	-9.243	-0.517	(0)
Fe(OH)CO3	1.062e-09	1.062e-09	-8.974	-8.974	0.000	(0)
BaHCO3+	4.853e-10	3.650e-10	-9.314	-9.438	-0.124	(0)
BaCO3	1.833e-11	1.833e-11	-10.737	-10.737	0.000	(0)
Fe(CO3)3-3	6.666e-14	4.427e-15	-13.176	-14.354	-1.178	(0)
Ca	7.398e-03					
Ca+2	5.257e-03	1.663e-03	-2.279	-2.779	-0.500	(0)
CaSO4	2.074e-03	2.074e-03	-2.683	-2.683	0.000	(0)
CaHCO3+	5.405e-05	4.066e-05	-4.267	-4.391	-0.124	(0)

CaF+	6.759e-06	5.134e-06	-5.170	-5.290	-0.119	(0)
CaCO3	6.026e-06	6.026e-06	-5.220	-5.220	0.000	(0)
CaSiO(OH)3+	1.971e-08	1.482e-08	-7.705	-7.829	-0.124	(0)
CaOH+	1.297e-08	9.753e-09	-7.887	-8.011	-0.124	(0)
CaSiO2(OH)2	3.242e-11	3.242e-11	-10.489	-10.489	0.000	(0)
Cl	8.500e-02					
Cl-	8.500e-02	6.351e-02	-1.071	-1.197	-0.127	(0)
MnCl+	6.546e-07	5.273e-07	-6.184	-6.278	-0.094	(0)
FeCl+	4.877e-08	3.748e-08	-7.312	-7.426	-0.114	(0)
FeCl+2	2.748e-21	9.589e-22	-20.561	-21.018	-0.457	(0)
FeCl2+	3.535e-22	2.915e-22	-21.452	-21.535	-0.084	(0)
FeCl3	1.168e-24	1.168e-24	-23.933	-23.933	0.000	(0)
FeCl4-	1.009e-27	7.419e-28	-26.996	-27.130	-0.134	(0)
MnCl+2	2.432e-34	8.095e-35	-33.614	-34.092	-0.478	(0)
ClO4-	0.000e+00	0.000e+00	-154.536	-154.664	-0.128	(0)
F	2.213e-04					
F-	1.928e-04	1.444e-04	-3.715	-3.840	-0.126	(0)
MgF+	1.507e-05	1.118e-05	-4.822	-4.951	-0.130	(0)
CaF+	6.759e-06	5.134e-06	-5.170	-5.290	-0.119	(0)
NaF	6.423e-06	6.423e-06	-5.192	-5.192	0.000	(0)
SrF+	6.876e-08	5.172e-08	-7.163	-7.286	-0.124	(0)
FeF+	5.677e-08	4.270e-08	-7.246	-7.370	-0.124	(0)
MnF+	2.736e-08	2.132e-08	-7.563	-7.671	-0.108	(0)
HF	9.901e-09	9.901e-09	-8.004	-8.004	0.000	(0)
Al(OH)2F	9.183e-09	9.183e-09	-8.037	-8.037	0.000	(0)
AlF3	5.125e-10	5.125e-10	-9.290	-9.290	0.000	(0)
AlF2+	4.205e-10	3.163e-10	-9.376	-9.500	-0.124	(0)
Al(OH)2F2-	2.571e-10	1.890e-10	-9.590	-9.723	-0.134	(0)
AlF4-	3.257e-11	2.394e-11	-10.487	-10.621	-0.134	(0)
BaF+	1.612e-11	1.212e-11	-10.793	-10.916	-0.124	(0)
AlF+2	1.547e-11	4.904e-12	-10.810	-11.309	-0.499	(0)
HF2-	5.492e-12	3.974e-12	-11.260	-11.401	-0.141	(0)
AlF5-2	1.153e-13	3.457e-14	-12.938	-13.461	-0.523	(0)
AlOHF2	1.515e-15	1.515e-15	-14.820	-14.820	0.000	(0)
AlF6-3	7.360e-17	4.992e-18	-16.133	-17.302	-1.169	(0)
FeF2+	3.217e-19	2.443e-19	-18.493	-18.612	-0.119	(0)
FeF+2	2.405e-19	8.099e-20	-18.619	-19.092	-0.473	(0)
MnOHF+	1.637e-23	1.268e-23	-22.786	-22.897	-0.111	(0)
MnF2+	4.319e-30	3.345e-30	-29.365	-29.476	-0.111	(0)
MnF3	1.213e-30	1.213e-30	-29.916	-29.916	0.000	(0)
MnF+2	3.488e-31	1.161e-31	-30.457	-30.935	-0.478	(0)
Fe(2)	3.328e-05					
Fe+2	1.854e-05	5.901e-06	-4.732	-5.229	-0.497	(0)
FeSO4	9.927e-06	9.927e-06	-5.003	-5.003	0.000	(0)
FeCO3	4.560e-06	4.560e-06	-5.341	-5.341	0.000	(0)
Fe(SO4)2-2	7.343e-08	2.201e-08	-7.134	-7.657	-0.523	(0)
FeOH+	6.350e-08	4.777e-08	-7.197	-7.321	-0.124	(0)
FeF+	5.677e-08	4.270e-08	-7.246	-7.370	-0.124	(0)
FeCl+	4.877e-08	3.748e-08	-7.312	-7.426	-0.114	(0)
Fe(CO3)2-2	1.882e-09	5.716e-10	-8.725	-9.243	-0.517	(0)
FeS	1.692e-10	1.692e-10	-9.772	-9.772	0.000	(0)
Fe(OH)2	8.459e-12	8.459e-12	-11.073	-11.073	0.000	(0)
FeHSO4+	2.562e-12	1.927e-12	-11.591	-11.715	-0.124	(0)
Fe(OH)3-	1.735e-16	1.275e-16	-15.761	-15.894	-0.134	(0)
Fe(3)	1.065e-09					
Fe(OH)CO3	1.062e-09	1.062e-09	-8.974	-8.974	0.000	(0)
Fe(OH)3	2.591e-12	2.591e-12	-11.587	-11.587	0.000	(0)
Fe(OH)2+	5.208e-13	4.220e-13	-12.283	-12.375	-0.091	(0)
Fe(CO3)3-3	6.666e-14	4.427e-15	-13.176	-14.354	-1.178	(0)
Fe(OH)4-	3.510e-14	2.580e-14	-13.455	-13.588	-0.134	(0)
FeOH+2	1.931e-16	6.267e-17	-15.714	-16.203	-0.489	(0)
FeSiO(OH)3+2	4.338e-18	1.346e-18	-17.363	-17.871	-0.508	(0)
FeF2+	3.217e-19	2.443e-19	-18.493	-18.612	-0.119	(0)
FeF+2	2.405e-19	8.099e-20	-18.619	-19.092	-0.473	(0)
FeSO4+	6.147e-20	4.952e-20	-19.211	-19.305	-0.094	(0)

Fe(SO4)2-	3.557e-20	2.823e-20	-19.449	-19.549	-0.100	(0)
Fe+3	5.568e-21	4.559e-22	-20.254	-21.341	-1.087	(0)
FeCl+2	2.748e-21	9.589e-22	-20.561	-21.018	-0.457	(0)
FeCl2+	3.535e-22	2.915e-22	-21.452	-21.535	-0.084	(0)
FeCl3	1.168e-24	1.168e-24	-23.933	-23.933	0.000	(0)
FeHSO4+2	1.929e-27	6.651e-28	-26.715	-27.177	-0.462	(0)
FeCl4-	1.009e-27	7.419e-28	-26.996	-27.130	-0.134	(0)
Fe2(OH)2+4	1.112e-29	1.214e-31	-28.954	-30.916	-1.962	(0)
Fe3(OH)4+5	1.389e-38	0.000e+00	-37.857	-40.971	-3.113	(0)
H(0)	4.388e-12					
H2	2.194e-12	2.194e-12	-11.659	-11.659	0.000	(0)
K	7.956e-04					
K+	7.624e-04	5.679e-04	-3.118	-3.246	-0.128	(0)
KSO4-	3.264e-05	2.400e-05	-4.486	-4.620	-0.134	(0)
KHCO3	5.401e-07	5.401e-07	-6.268	-6.268	0.000	(0)
KCO3-	1.309e-08	9.623e-09	-7.883	-8.017	-0.134	(0)
KOH	3.912e-11	3.912e-11	-10.408	-10.408	0.000	(0)
Mg	4.355e-03					
Mg+2	3.196e-03	1.021e-03	-2.495	-2.991	-0.496	(0)
MgSO4	1.109e-03	1.109e-03	-2.955	-2.955	0.000	(0)
MgHCO3+	3.318e-05	2.496e-05	-4.479	-4.603	-0.124	(0)
MgF+	1.507e-05	1.118e-05	-4.822	-4.951	-0.130	(0)
MgCO3	2.080e-06	2.080e-06	-5.682	-5.682	0.000	(0)
MgOH+	5.901e-08	4.438e-08	-7.229	-7.353	-0.124	(0)
MgSiO(OH)3+	1.874e-08	1.409e-08	-7.727	-7.851	-0.124	(0)
MgSiO2(OH)2	2.084e-10	2.084e-10	-9.681	-9.681	0.000	(0)
Mn(2)	2.831e-05					
Mn+2	1.989e-05	6.595e-06	-4.701	-5.181	-0.479	(0)
MnSO4	6.840e-06	6.840e-06	-5.165	-5.165	0.000	(0)
MnCl+	6.546e-07	5.273e-07	-6.184	-6.278	-0.094	(0)
MnCO3	5.601e-07	5.601e-07	-6.252	-6.252	0.000	(0)
MnHCO3+	3.299e-07	2.555e-07	-6.482	-6.593	-0.111	(0)
MnF+	2.736e-08	2.132e-08	-7.563	-7.671	-0.108	(0)
MnOH+	4.879e-09	3.779e-09	-8.312	-8.423	-0.111	(0)
Mn(OH)2	2.068e-13	2.068e-13	-12.684	-12.684	0.000	(0)
Mn(OH)3-	4.241e-18	3.117e-18	-17.373	-17.506	-0.134	(0)
Mn(OH)4-2	2.601e-24	7.798e-25	-23.585	-24.108	-0.523	(0)
Mn(3)	3.914e-18					
Mn(OH)2+	3.914e-18	3.032e-18	-17.407	-17.518	-0.111	(0)
MnOHF+	1.637e-23	1.268e-23	-22.786	-22.897	-0.111	(0)
MnOH+2	2.095e-25	6.975e-26	-24.679	-25.156	-0.478	(0)
MnF2+	4.319e-30	3.345e-30	-29.365	-29.476	-0.111	(0)
MnF3	1.213e-30	1.213e-30	-29.916	-29.916	0.000	(0)
MnF+2	3.488e-31	1.161e-31	-30.457	-30.935	-0.478	(0)
Mn+3	2.545e-33	2.020e-34	-32.594	-33.695	-1.100	(0)
MnCl+2	2.432e-34	8.095e-35	-33.614	-34.092	-0.478	(0)
Na	1.182e-01					
Na+	1.145e-01	8.476e-02	-0.941	-1.072	-0.131	(0)
NaSO4-	3.612e-03	2.655e-03	-2.442	-2.576	-0.134	(0)
NaHCO3	1.165e-04	1.165e-04	-3.934	-3.934	0.000	(0)
NaF	6.423e-06	6.423e-06	-5.192	-5.192	0.000	(0)
NaCO3-	2.517e-06	1.850e-06	-5.599	-5.733	-0.134	(0)
NaOH	7.351e-09	7.351e-09	-8.134	-8.134	0.000	(0)
O(0)	0.000e+00					
O2	0.000e+00	0.000e+00	-68.880	-68.880	0.000	(0)
S(-2)	3.179e-10					
FeS	1.692e-10	1.692e-10	-9.772	-9.772	0.000	(0)
HS-	1.113e-10	8.466e-11	-9.954	-10.072	-0.119	(0)
H2S	3.735e-11	3.782e-11	-10.428	-10.422	0.005	(0)
S-2	6.176e-22	1.852e-22	-21.209	-21.732	-0.523	(0)
S(0)	4.346e-14					
S	4.346e-14	4.346e-14	-13.362	-13.362	0.000	(0)
S(2)	3.321e-15					
S2O3-2	1.660e-15	5.004e-16	-14.780	-15.301	-0.521	(0)

```
S(4)          2.988e-14
   SO3-2           2.279e-14   6.867e-15   -13.642   -14.163    -0.521      (0)
   HSO3-           7.089e-15   5.211e-15   -14.149   -14.283    -0.134      (0)
S(6)          2.738e-02
   SO4-2           2.048e-02   6.108e-03    -1.689    -2.214    -0.525      (0)
   NaSO4-          3.612e-03   2.655e-03    -2.442    -2.576    -0.134      (0)
   CaSO4           2.074e-03   2.074e-03    -2.683    -2.683     0.000      (0)
   MgSO4           1.109e-03   1.109e-03    -2.955    -2.955     0.000      (0)
   SrSO4           5.129e-05   5.129e-05    -4.290    -4.290     0.000      (0)
   KSO4-           3.264e-05   2.400e-05    -4.486    -4.620    -0.134      (0)
   FeSO4           9.927e-06   9.927e-06    -5.003    -5.003     0.000      (0)
   MnSO4           6.840e-06   6.840e-06    -5.165    -5.165     0.000      (0)
   Fe(SO4)2-2      7.343e-08   2.201e-08    -7.134    -7.657    -0.523      (0)
   HSO4-           3.657e-08   2.716e-08    -7.437    -7.566    -0.129      (0)
   BaSO4           2.042e-08   2.042e-08    -7.690    -7.690     0.000      (0)
   FeHSO4+         2.562e-12   1.927e-12   -11.591   -11.715    -0.124      (0)
   AlSO4+          8.329e-14   6.265e-14   -13.079   -13.203    -0.124      (0)
   Al(SO4)2-       4.041e-14   2.970e-14   -13.394   -13.527    -0.134      (0)
   FeSO4+          6.147e-20   4.952e-20   -19.211   -19.305    -0.094      (0)
   Fe(SO4)2-       3.557e-20   2.823e-20   -19.449   -19.549    -0.100      (0)
   FeHSO4+2        1.929e-27   6.651e-28   -26.715   -27.177    -0.462      (0)
Si            1.775e-04
   Si(OH)4         1.767e-04   1.779e-04    -3.753    -3.750     0.003      (0)
   SiO(OH)3-       8.198e-07   6.026e-07    -6.086    -6.220    -0.134      (0)
   CaSiO(OH)3+     1.971e-08   1.482e-08    -7.705    -7.829    -0.124      (0)
   MgSiO(OH)3+     1.874e-08   1.409e-08    -7.727    -7.851    -0.124      (0)
   MgSiO2(OH)2     2.084e-10   2.084e-10    -9.681    -9.681     0.000      (0)
   CaSiO2(OH)2     3.242e-11   3.242e-11   -10.489   -10.489     0.000      (0)
   SiO2(OH)2-2     2.040e-12   6.165e-13   -11.690   -12.210    -0.520      (0)
   AlSiO(OH)3+2    1.660e-13   5.261e-14   -12.780   -13.279    -0.499      (0)
   FeSiO(OH)3+2    4.338e-18   1.346e-18   -17.363   -17.871    -0.508      (0)
   SiAlO3(OH)4-3   2.845e-20   1.930e-21   -19.546   -20.715    -1.169      (0)
   Si4O8(OH)4-4    1.361e-20   1.221e-22   -19.866   -21.913    -2.047      (0)
Sr            1.899e-04
   Sr+2            1.367e-04   4.306e-05    -3.864    -4.366    -0.502      (0)
   SrSO4           5.129e-05   5.129e-05    -4.290    -4.290     0.000      (0)
   SrHCO3+         1.803e-06   1.356e-06    -5.744    -5.868    -0.124      (0)
   SrF+            6.876e-08   5.172e-08    -7.163    -7.286    -0.124      (0)
   SrCO3           5.665e-08   5.665e-08    -7.247    -7.247     0.000      (0)
   SrOH+           8.831e-11   6.642e-11   -10.054   -10.178    -0.124      (0)

-----------------------------Saturation indices-------------------------------

  Phase               SI** log IAP   log K(298 K,   1 atm)

  2-line-ferrihydrite  -2.83      0.67    3.50  Fe(OH)3
  4C-pyrrhotite    -2.84    -11.34   -8.50  Fe0.625Fe0.25S
  5C-pyrrhotite    -3.06    -10.66   -7.60  Fe0.7Fe0.2S
  Analcime         -8.73     12.48   21.21  Na2Al2Si4O12(H2O)2
  Anhydrite        -0.78     -4.99   -4.21  CaSO4
  Aragonite        -0.13      1.88    2.01  CaCO3
  Barite            0.00     -9.96   -9.96  BaSO4
  Beidellite(Ca)    0.22      5.78    5.56  Ca0.17Al2.34Si3.66O10(OH)2
  Beidellite(K)     0.76      5.15    4.39  K0.34Al2.34Si3.66O10(OH)2
  Beidellite(Mg)    0.73      5.75    5.02  Mg0.17Al2.34Si3.66O10(OH)2
  Beidellite(Na)    2.75      5.89    3.14  Na0.34Al2.34Si3.66O10(OH)2
  Beidellite_SBld-1        -0.30                          7.08              7.38
(Ca0.185K0.104)(Si3.574Al0.426)(Al1.812Mg0.090Fe0.112)O10(OH)2
  Berthierine(FeII)  -4.36     30.08   34.44  (Fe2Al)(SiAl)O5(OH)4
  Berthierine(FeIII)         -4.06                         24.70             28.76
(Fe2.34Fe0.33Al0.33)(Si1.34Al0.66)O5(OH)4
  Berthierine_ISGS          -4.95                          22.85             27.80
(Si1.332Al0.668)(Al0.976Fe0.182Fe1.44Mg0.157)O5(OH)4
  Bixbyite        -22.54    -23.36   -0.81  Mn2O3
  Boehmite         -1.93      7.47    9.40  AlOOH
```

Brucite	-5.42	11.69	17.11	Mg(OH)2
Calcite	0.00	1.88	1.88	CaCO3
Celestite	0.00	-6.58	-6.58	SrSO4
CH4(g)	-13.53	-16.38	-2.86	CH4
Chabazite-Ca	-4.67	11.84	16.51	CaAl2Si4O12(H2O)6
Chabazite-Na	-3.61	12.47	16.08	Na2Al2Si4O12(H2O)6
Clinoptilolite	-6.69	-4.63	2.06	Ca0.52Al1.04Si4.96O12(H2O)3.1
CO2(g)	-2.20	-10.02	-7.82	CO2
Cronstedtite	0.39	16.50	16.11	(Fe2Fe)(SiFe)O5(OH)4
Dawsonite	-1.31	3.71	5.02	NaAlCO3(OH)2
Dolomite	-0.00	3.55	3.55	CaMg(CO3)2
Faujasite-X	-7.59	18.09	25.69	Na2Al2Si2.5O9(H2O)6.2
Faujasite-Y	-5.99	12.47	18.46	Na2Al2Si4O12(H2O)8
Fe(OH)2(s)	-2.81	9.45	12.26	Fe(OH)2
Fe-hibbingite	-6.84	10.36	17.20	Fe2Cl(OH)3
Fe4(OH)8Cl:nH2O(s)	-6.17	20.48	26.65	Fe3Fe(OH)8Cl
Fe6(OH)12CO3:nH2O(s)	-7.51	29.12	36.63	Fe2Fe4(OH)12CO3
Fe6(OH)12SO4:nH2O(s)	-6.86	22.25	29.10	Fe4Fe2(OH)12SO4
Fluorite	0.00	-10.46	-10.46	CaF2
Gibbsite	-0.28	7.47	7.75	Al(OH)3
Glauconite	-2.89	-1.12	1.77	K0.75(Mg0.25Fe0.25Fe1.25Al0.25)(Al0.25Si3.75)O10(OH)2
Goethite	0.35	0.68	0.33	FeOOH
Graphite	-5.31	-27.12	-21.82	C
Greigite	-17.70	-58.84	-41.14	Fe3S4
Gypsum	-0.42	-5.00	-4.58	CaSO4(H2O)2
H2(g)	-8.55	-11.66	-3.11	H2
H2S(g)	-9.40	-17.41	-8.01	H2S
Hausmannite	-24.43	-13.86	10.58	Mn3O4
Hematite	0.63	1.35	0.72	Fe2O3
Heulandite_1	-8.61	3.01	11.62	Ca1.07Al2.14Si6.86O18(H2O)4.4
Heulandite_2	-9.69	3.01	12.69	Ca1.07Al2.14Si6.86O18(H2O)4.5
Hydrosodalite	-32.84	72.46	105.30	Na8Al6Si6O24(OH)2(H2O)2
Illite(Al)	0.18	12.96	12.78	K0.85Al2.85Si3.15O10(OH)2
Illite(FeII)	1.40	10.65	9.25	K0.85Fe0.25Al2.35Si3.4O10(OH)2
Illite(FeIII)	-0.87	11.26	12.14	K0.85Fe0.25Al2.6Si3.15O10(OH)2
Illite(Mg)	0.41	11.21	10.80	K0.85Mg0.25Al2.35Si3.4O10(OH)2
Illite_IMt-2	-4.97	9.75	14.72	(K0.762Na0.044)(Si3.387Al0.613)(Al1.427Fe0.292Mg0.241Fe0.084)O10(OH)2
Iron(alpha)	-15.00	0.90	15.89	Fe
Kaolinite	0.00	7.44	7.44	Al2Si2O5(OH)4
Lepidocrocite	-1.18	0.68	1.86	FeOOH
Linda_type_A	-9.18	19.62	28.80	Na1.98Al1.98Si2.02O8(H2O)5.31
Low-silica_P-Ca	-4.61	19.33	23.95	CaAl2Si2O8(H2O)4.5
Low-silica_P-Na	-7.90	19.97	27.87	Na2Al2Si2O8(H2O)3.8
Mackinawite	-4.77	-7.96	-3.19	FeS
Maghemite	-1.87	1.35	3.22	Fe2O3
Magnesite	-1.00	1.67	2.67	MgCO3
Magnetite	1.59	10.80	9.21	Fe3O4
Manganite	-11.60	-11.68	-0.08	MnOOH
Manganosite	-8.46	9.50	17.96	MnO
Marcasite	-0.68	-21.32	-20.64	FeS2
Molecular_sieve_4Ã…	-7.00	19.97	26.97	Na2Al2Si2O8(H2O)4.5
Montmorillonite(HcCa)	-0.70	6.05	6.75	Ca0.3Mg0.6Al1.4Si4O10(OH)2
Montmorillonite(HcK)	0.64	4.94	4.29	K0.6Mg0.6Al1.4Si4O10(OH)2
Montmorillonite(HcMg)	0.15	5.99	5.84	Mg0.3Mg0.6Al1.4Si4O10(OH)2
Montmorillonite(HcNa)	0.93	6.24	5.31	Na0.6Mg0.6Al1.4Si4O10(OH)2
Montmorillonite(MgCa)	-0.64	3.41	4.05	Ca0.17Mg0.34Al1.66Si4O10(OH)2
Montmorillonite(MgK)	0.12	2.77	2.65	K0.34Mg0.34Al1.66Si4O10(OH)2
Montmorillonite(MgMg)	-0.16	3.37	3.53	Mg0.17Mg0.34Al1.66Si4O10(OH)2
Montmorillonite(MgNa)	0.28	3.51	3.23	Na0.34Mg0.34Al1.66Si4O10(OH)2
Mordenite-Ca	-6.51	-10.81	-4.31	Ca0.34Al0.68Si5.32O12(H2O)2.9
Mordenite-Na	-5.67	-9.90	-4.22	Na0.72Al0.72Si5.28O12(H2O)2.71
Natrolite	-4.92	16.23	21.15	Na2Al2Si3O10(H2O)2
Nontronite(Ca)	-2.62	-5.56	-2.94	Ca0.17Fe1.67Al0.67Si3.66O10(OH)2

```
  Nontronite(K)     -2.08     -6.19    -4.11  K0.34Fe1.67Al0.67Si3.66O10(OH)2
  Nontronite(Mg)    -2.11     -5.59    -3.48  Mg0.17Fe1.67Al0.67Si3.66O10(OH)2
  Nontronite(Na)    -1.84     -5.45    -3.61  Na0.34Fe1.67Al0.67Si3.66O10(OH)2
  Nontronite_Nau-1  -3.10     -1.89     1.21
     (Ca0.247K0.020)(Si3.458Al0.542)(Fe1.688Al0.276Mg0.068)O10(OH)2
  O2(g)           -65.99    -68.88    -2.89  O2
  Phillipsite-Na    -7.02     13.72    20.75  Na2.5Al2.5Si5.5O16(H2O)5
  Phillipsite-NaK   -8.69     11.55    20.25  Na1.5KAl2.5Si5.5O16(H2O)5
  Portlandite      -10.85     11.90    22.75  Ca(OH)2
  Pyrite            -0.00    -21.32   -21.32  FeS2
  Pyrochroite       -5.69      9.50    15.19  Mn(OH)2
  Pyrolusite       -23.56     18.05    41.61  MnO2
  Quartz             0.00     -3.75    -3.75  SiO2
  Rhodochrosite      0.00     -0.52    -0.52  MnCO3
  Ripidolite_Cca-2  -0.91     59.74    60.65
     (Si2.633Al1.367)(Al1.116Fe0.215Mg2.952Fe1.712Mn0.012)(Ca0.011)O10(OH)8
  S(orth)           -6.71    -13.36    -6.65  S
  Saponite(Ca)      -3.37     25.91    29.28  Ca0.17Mg3Al0.34Si3.66O10(OH)2
  Saponite(FeCa)    -2.85     23.67    26.52  Ca0.17Mg2FeAl0.34Si3.66O10(OH)2
  Saponite(FeK)     -2.31     23.04    25.35  K0.34Mg2FeAl0.34Si3.66O10(OH)2
  Saponite(FeMg)    -2.34     23.64    25.97  Mg0.17Mg2FeAl0.34Si3.66O10(OH)2
  Saponite(FeNa)    -1.89     23.78    25.67  Na0.34Mg2FeAl0.34Si3.66O10(OH)2
  Saponite(K)       -2.84     25.28    28.12  K0.34Mg3Al0.34Si3.66O10(OH)2
  Saponite(Mg)      -2.87     25.87    28.74  Mg0.17Mg3Al0.34Si3.66O10(OH)2
  Saponite(Na)      -2.60     26.02    28.61  Na0.34Mg3Al0.34Si3.66O10(OH)2
  Saponite_SapCa-2  -4.11     27.29    31.40
     (Na0.394K0.021Ca0.038)(Si3.569Al0.397)(Mg2.949Fe0.034Fe0.021)O10(OH)2
  Scolecite         -7.43     15.59    23.02  CaAl2Si3O10(H2O)3
  Siderite           0.00     -0.57    -0.57  FeCO3
  Silica(am)        -1.03     -3.75    -2.71  SiO2
  Smectite_MX80      0.52      5.60     5.09
 (Na0.409K0.024Ca0.009)(Si3.738Al0.262)(Al1.598Mg0.214Fe0.173Fe0.035)O10(OH)2
  Sodalite         -17.71     55.40    73.10  Na8Al6Si6O24Cl2
  Stilbite          -9.04      4.37    13.42  Ca1.11Al2.22Si6.78O18(H2O)6.8
  Strontianite      -0.77      0.29     1.06  SrCO3
  Troilite          -3.97     -7.96    -3.99  FeS
  Vaterite          -0.54      1.88     2.42  CaCO3
  Vermiculite(Ca)   -4.62     34.83    39.46  Ca0.43Mg3Al0.86Si3.14O10(OH)2
  Vermiculite(K)    -4.12     33.24    37.35  K0.86Mg3Al0.86Si3.14O10(OH)2
  Vermiculite(Mg)   -3.21     34.74    37.95  Mg0.43Mg3Al0.86Si3.14O10(OH)2
  Vermiculite(Na)   -3.19     35.11    38.30  Na0.86Mg3Al0.86Si3.14O10(OH)2
  Witherite         -4.85     -3.09     1.76  BaCO3

**For a gas, SI = log10(fugacity). Fugacity = pressure * phi / 1 atm.
  For ideal gases, phi = 1.
```